R/V HEINCKE
Cruise Report HE449

Microbial Methane Oxidation in Fjords and Offshore Svalbard

HE449
Trondheim – Tromsø
01 August – 22 August, 2015

Cruise sponsored by Deutsche Forschungsgemeinschaft (DFG)

Edited by
Dr. Susan Mau
With contributions of cruise participants

The cruise was performed by
MARUM – Center for Marine Environmental Sciences

marum

Universität Bremen

R/V HEINCKE Cruise Report HE449

Table of Contents

1 Preface

The R/V HEINCKE cruise HE449 indented to investigate the removal of the greenhouse gas methane by microbial oxidation in the Svalbard region. As isotope tracers are essential for this research, the isotope container of R/V METEOR was transferred to R/V HEINCKE. We are thankful for all who helped with the organization: the Control Station German Research Vessels in Hamburg and the Alfred Wegener Institute in Bremerhaven (AWI).

The cruise is linked to the German Research Foundation (DFG) project "Limitations of Marine Methane Oxidation" and was coordinated and carried out by MARUM. The cruise was financed by a MARUM incentive fund proposal "Marine Methane Oxidation off Svalbard" with additions by the DFG-project mentioned above. Technical support during the cruise was provided by the shipping operator Reederei Briese Schiffahrts GmbH & Co KG and the AWI Bremerhaven. Especially, we like to acknowledge the master of the vessel Werner Riederer and his crew for their continuous assistance aboard R/V HEINCKE.

Fig. 1: Scientific crew aboard R/V HEINCKE HE449

Personel aboard R/V HEINCKE

Table 1: Scientific crew

Name	Discipline	Affiliation
Susan Mau	Chief scientist	GeoB
Miriam Römer	Hydroacoustics	MARUM
Anna Lichtschlag	Geochemistry	NOC
Eva Falck	Geochemistry	UNIS
Ingeborg Bussmann	Geochemistry	AWI, Helgoland
Torben Gentz	Geochemistry	AWI, BHV
Stefanie Buchheister	Geochemistry	MARUM
Mirko Lange	Geochemistry	MARUM

Nils Brueckner	Hydroacoustics	MARUM
Stefanie Gaide	Hydroacoustics	MARUM
Nadine Goldenstein	Geochemistry	MARUM
Anne-Christin Melcher	Geochemistry	MARUM

AWI	Alfred Wegener Institute, Helmholtz Zentrum für Polar- und Meeresforschung, Kurpromenade, Biosciences, 27498 Helgoland, **Germany**
AWI	Alfred-Wegener-Institute, Helmholtz Zentrum für Polar- und Meeresforschung, Geosciences, Bussestr. 27, 27570 Bremerhaven, **Germany**
GeoB	Department of Geosciences, University of Bremen, Klagenfurter Str., 28359 Bremen, **Germany**
MARUM	Center for Marine and Environmental Sciences, DFG Research Center and Cluster of Excellence, University of Bremen, Postfach 330440, 28334 Bremen, **Germany**
NOC	National Oceanographic Centre, Science of the Environment, University of Southampton, Waterfront Campus, European Way, Southampton SO14 3ZH, **UK**
UNIS	University of Svalbard, Arctic Geophysics, Pb. 156, 9171 Longyearbyen, **Norway**

Table 2: Crew members onboard

Name	**Discipline**
Werner Riederer	Master
Remo Franke	Chief officer
Marvin v. Aswegen	2nd officer
Klaus-Dieter Klinder	Chief engineer
Abu Hackmann	Electrician
Heiko Baron	Bosun
Martin Drager	Seaman
Derk Heeren	Seaman
Steffen De Vries	Seaman
Stefan Trautmann	Seaman
Marius Kruse	Seaman
Ronald Klafack	Cook

Shipping operator: Briese Schiffahrts GmbH & Co KG, Abteilung Forschungsschifffahrt, Hafenstr. 12, 26789 Leer, **Germany**

2 Introduction

2.1 Objectives, Background and Research Program

(S. Mau)

The cruise was designed to investigate the pathways of the greenhouse gas methane in the water column off Svalbard. Methane is either emitted from sediments or is generated in the water column. The dissolved fraction of the gas in the water column is available for methanotrophic bacteria, who are specialized to break the methane molecule and oxidize it to CO_2. This process is thought to be the only sink of methane in the water column (Reeburgh, 2007) limiting the release of the greenhouse gas to the atmosphere. However, if the dissolved methane is transported into the mixed layer of the ocean, the gas can be transferred into the atmosphere, where it has a global warming potential that is 23 times higher than that of CO_2 over a 100-year timescale (IPCC, 2007). The target of the cruise was to investigate especially the microbial oxidation.

The key organisms, who aerobically oxidize methane, are bacteria, which have been categorized as methane-assimilating bacteria (methanotrophs) (Holmes et al., 1999). Methanotrophic bacteria are capable of using methane as their sole source of carbon and energy to support cellular activity. Although significant effort has been undertaken to characterize and culture methanotrophs, the study of methanotrophs in the marine environment remains limited. Especially, the active pelagic methanotrophic populations continue to be largely unknown, and it remains uncertain that existing isolates (Lidstrom, 1988; Sieburth et al., 1987) truly represent the natural community. Novel sequences continue to be found, which are similar to the one of the enzyme methane monooxygenase (Elsaied et al., 2004; Tavormina et al., 2008; Wasmund et al., 2009), a specific enzyme of aerobic methanotrophs catalyzing the oxidation of methane to methanol. However, it is not known if these genes are actually expressed (Valentine, 2011). Evidently, the role of methanotrophs in the marine environment need further study.

Therefore, the prime aim of the cruise was to investigate the abundance and activity of methanotrophic micro-organisms in different water masses and to identify any limitations reducing or increasing the growths and/or activity of these micro-organisms in these waters. The Svalbard region with its fjords holds different water masses, some are locally formed due to ice development during winter and others originate from the open ocean. Moreover, these water masses contain significant concentrations of methane; often concentrations are above the atmospheric equilibrium concentrations of 3-4 nM. Elevated methane concentrations were reported around Svalbard related to phytoplankton blooms (Damm et al., 2005) and to bubble emission sites offshore Prins Karls Forland (Sahling et al., 2014). Therefore, waters around Svalbard are a “natural laboratory” to study methanotrophic micro-organisms.

Factors influencing the activity of methane oxidizing bacteria are suggested to be substrate supply and removal, light, the history of the water mass, and the regional setting. For example, wind speed influences the transfer of methane from the ocean to the atmosphere removing the substrate for the bacteria (Mau et al., 2011; Mau et al., 2007). Lower oxygen concentrations were found to be favorable to reduce methane in a small eutrophic Canadian shield lake as reported by Rudd and Hamilton (1975). Inhibition of both growth and methanotrophic activity of an enriched culture from a reservoir in French Guiana by light illumination over 150 $\mu E\ m^{-2}\ s^{-1}$ was illustrated by Dumestre et al.(1999). Depending on where the water mass originates, it transports more or less seeds of methane-oxidizing bacteria as proposed by Heintz et al. (2012). Regions such as estuaries (Moussard et al., 2009), enclosed waters (Ward et al., 1989), areas of high primary production, and seeps typically hold elevated methane levels

and are thought to sustain methane oxidizing bacteria. All these influencing factors have been derived at different sites and under different conditions in the laboratory and in freshwater systems, but only few studies were done in the ocean.

Fig. 2: Research tools used during cruise HE449. R/V HEINCKE in the port of Trondheim, Norway (above left); CTD-water sampler on the working deck during the launching (above right); conventional multi-corer comes back from the seafloor (below left) and the underwater mass-spectrometer (UWMS) deployed from the vessel (below right).

As methane in the water column is readily dispersed by ocean currents, we also aimed to evaluate this dispersion and the likelihood of methane transfer to the atmosphere. Methane generated in the water column occurs dissolved in the water whereas methane from sea floor seeps can either be emitted dissolved in fluids or, in the case of over-saturation, in the form of gas bubbles. When methane is emitted as bubbles, a fraction of the gas dissolves during the bubbles' transit through the water column; its quantity depends on release depth, volume of the bubbles, but also on the buoyancy force of the plume (Greinert and McGinnis, 2009). Bubble dissolution creates patches of dissolved methane (Clark et al., 2003), which in cases where methane emissions are persistent and of sufficient magnitude can form large continuous plumes (e.g. at COP seep field). Such methane plumes disperse in the water, where dispersion is a combination of transport of methane (advection) and spreading of the gas (turbulent diffusion) (Largier, 2003). If this dissolved methane is transported in the mixed layer it can be transferred to the atmosphere via sea-air gas exchange depending mainly on wind speed (e.g. Mau et al., 2007). We indented to quantify the partitioning between the microbial sink and the gas transfer sink during the cruise. In the case of the gas transfer, current measurements in relation with methane concentration measurements illustrate the dispersion and the sea-air flux can be evaluated using wind speeds measured by the ship. For measuring methane concentrations, we used two recent approaches: an integrated cavity output spectrometer (ICOS, Wankel et al., 2013) to analyze discrete water samples and an underwater mass-spectrometer (UWMS, Gentz and Schlüter, 2012), which records methane concentration in the water while being towed by the ship (Fig. 2).

According to these objectives, we planned to collect water and surface sediments with a CTD-water sampler, in situ pumps, an under-water mass spectrometer (UWMS), and a multi-corer (MUC) during the day (Fig. 2). Acoustic surveys were designed to identify gas emission sites and were planned to be conducted during the night. Moreover, the acoustic Doppler current profiler (ADCP) was arranged to record current speed and direction during most of the cruise. We indented to sample the water column along transects crossing the fjords and shelf regions and to use in situ pumps and the MUC in addition to CTD-water sampler at locations of observed gas flares and in front of and after the sills of the fjords to compare the water masses in- and outside of the fjords. The UWMS, which has a detection limit of 16 nM, was indented to be deployed in areas of flare clusters to derive a better spatial resolution of methane concentrations. The grab sampler was planned to identify if the sediments were suitable for deployment of the MUC.

2.2 Setting of Svalbard

Geology

The geological record of Svalbard can be separated into three broad divisions (Elvevold et al., 2007). The first is the basement, which consists mainly of igneous and metamorphic rocks that have been folded and altered and were formed during Precambrian to Silurian times (Fig. 3). The second unit contains unaltered sedimentary rocks formed in Late Palaeozic to Cenozoic times. Beds of this age form a trough-shaped structure from the Isfjorden area to the south, with youngest beds in the core and the oldest on the flanks. The last division consists of unconsolidated surficial deposits from the Quaternary period formed during and after the last ice age. These deposits are moraines, fluvial and beach deposits, talus and scree.

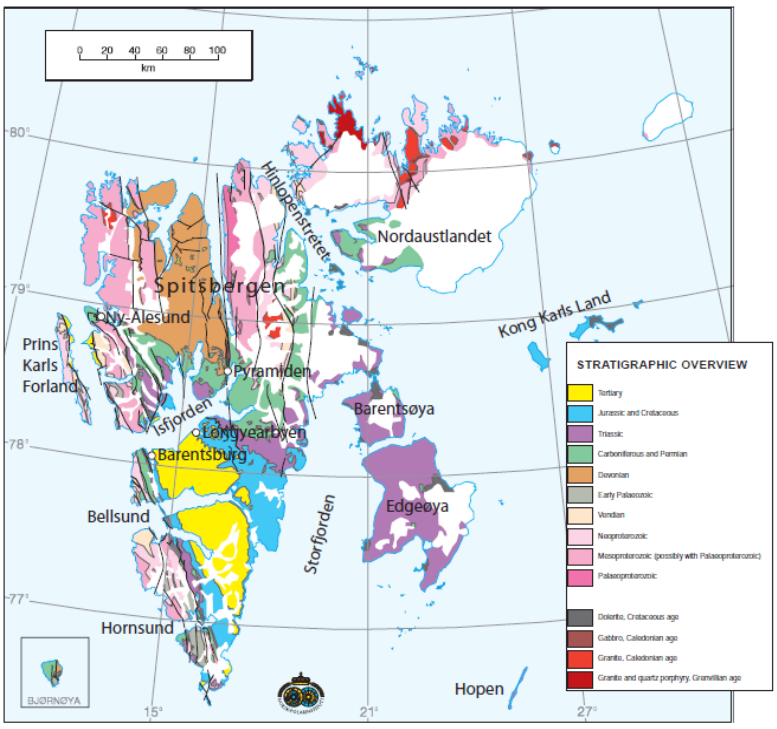

Fig. 3: The geological units of Svalbard as presented by Elvevold et al. (2007).

Svalbard is also known for its coal deposits and oil accumulations have been found there, too. The lowermost Carboniferous sandstones contain coal seams (Elvevold et al., 2007). This coal was only

successfully mined by the Russian in Pyramiden over a longer period of time. The mine was abandoned in 1998. Additional deposits were discovered in the central Tertiary Basin containing abundant plant fossils. This unit hosts the majority of coal deposits that are worked on in Longyearbyen, Grumantbyen, Ny-Ålesund, Sveagruva, and Barentsburg. Permian and Mesozoic rocks are potential source rocks for hydrocarbons, which can potentially be trapped in the structural framework of Svalbard. Although oil accumulations are not economically profitable, hydrocarbon seepage might be linked to the high concentration of pockmarks found over Jurassic–Cretaceous and the Triassic–Lower Jurassic bedrock (Roy et al., 2015).

Oceanography

Two source waters dominate the conditions west of Spitsbergen (Fig. 4). On the shelf, there is a relatively cold and fresh current named South Cape Current, which is a prolongation of the East Spitsbergen Current transporting cold and relatively fresh Arctic Water (ArW, S < 34.8) from the Barents Sea into the area. Along the upper slope, the West Spitsbergen Current, which is an extension of the Norwegian Atlantic Current, is carrying relatively warm and saline Atlantic Water (AW, S > 34.9). The two currents are separated by a front, the Arctic Front, which is located near the shelf break between the warm and saline AW and the colder and fresher Arctic Water (ArW) on the shelf. Saloranta and Svendsen (2001) observed that the Arctic Front can be divided into two vertically fronts: a surface front (about 0-50 m) as a rather strong density front between the slope AW and the shelf ArW and a subsurface front (about 50-100 m) as a TS front between the two water masses with no clear density front.

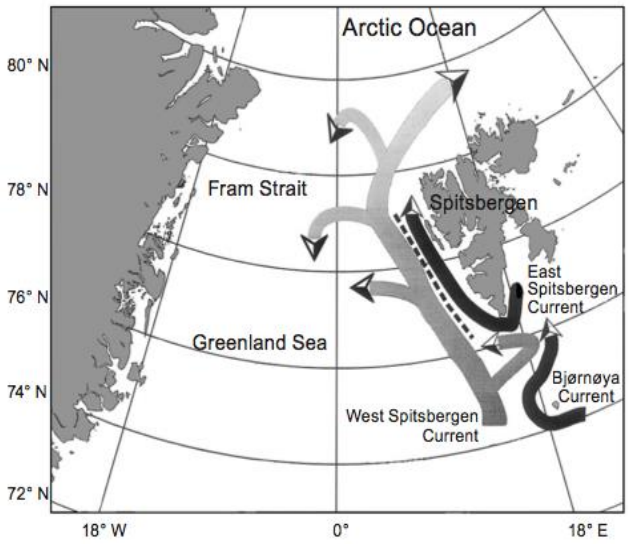

Fig. 4: Schematic illustration of the currents west of Svalbard. The dotted line indicates the Arctic Front between the West Spitsbergen Current (thick light grey arrow) and the colder South Cape Current (dark black arrow along the west coast) originating from the East Spitsbergen Current.

Due to the presence of the South Cape Current, it is difficult for AW to penetrate into the fjords on the west coast of Spitsbergen, but under certain conditions (northerly winds along the coast) it may upwell onto the shelf and continue into the fjords. During summer the fjords have generally a three layer structure. The water in the surface layer are named Surface Water (SW), and contains the fresh water from melting of sea ice and river runoff/glacial melt, it therefore has a reduced salinity. An intermediate layer is found below the surface layer consisting of water that generally is a mixture of the SW and what is found in the deeper parts of the fjord. Depending on whether the fjord has a sill or

not, the deepest parts will be filled with either Winter Water (produced by winter cooling and sea ice formation, T < 0°C) if a sill is present or waters from outside the fjord (ArW or AW, or a mixture of these two called Transformed Atlantic Water, TAW) if there is no sill. Of the fjords visited during the cruise Van Mijenfjorden is blocked at the mouth by Akseløya, and only two narrow and shallow (12 m and 34 m) passages on each side lead into the fjord. Because of this AW is not found inside the fjord and remnants of Winter Water are typically found in the deeper parts of the fjord each summer. Isfjorden does not have a sill at the mouth and during summer all or much of the Winter Water has been flushed out of the fjord and been replaced by waters from the shelf (ArW and/or TAW, AW). The innermost part of Isfjorden is named Billefjorden and a sill, 50 m deep, separates Billefjorden from the Isfjorden proper. Also in Billefjorden the water found below sill depth in summer is typically Winter Water.

3 Cruise Narrative

(S. Mau)

R/V HEINCKE had arrived in Trondheim on Thursday, the 30th of July, and we went on board in the morning of the following day to load our equipment on the ship. The isotope container borrowed from R/V METEOR was already on board as the transfer of the container from one ship to the other was done before HEINCKE left Bremerhaven. HE449 started on Saturday, the 1st of August, at 8 am with nice and sunny weather. After we left the fjords of Trondheim, we went along the Norwegian coast to the north, to Svalbard (Fig. 5). Our first target area was Storfjorden located between the islands Spitsbergen, Barentsøya, and Edgeøya.

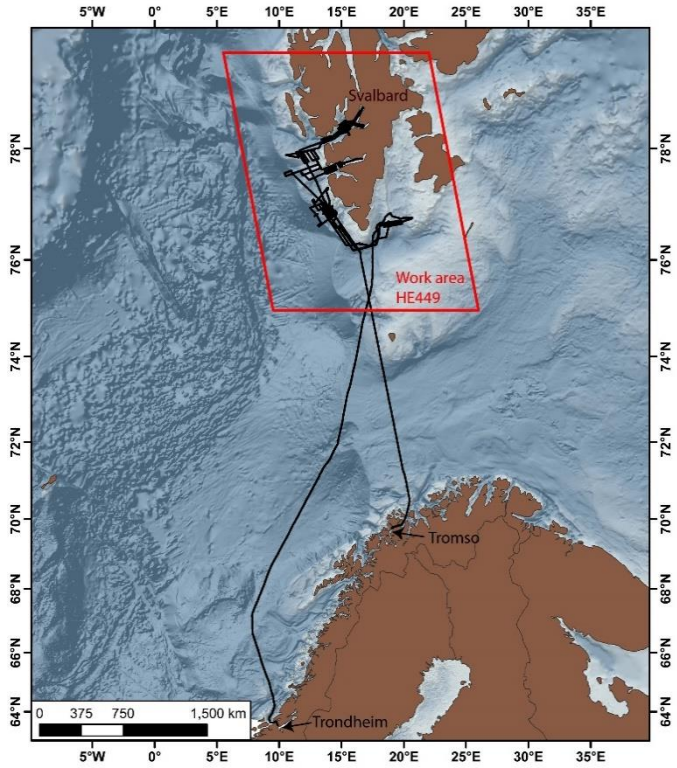

Fig. 5: Cruise track of R/V HEINCKE cruise 449 with harbour stops in Trondheim and Tromsø; area of research is shown in the box.

Sunday, the 2nd of August, we continued to set up the laboratories and steamed farther to the north with fine weather. On Monday we reached the scientifically well investigated Håkon Mosby Mud Volcano at 8 pm. The structure was crossed to test EK60 and the Multibeam settings and, as expected, we observed gas flares above the mud volcano.

Further flares were observed while continuing our way north on the 4th of August. These observations were not recorded as we still had not reached our permitted research area (Fig. 5). As soon as we entered the area, we planned a CTD-station to test our water sampling procedure and to obtain a profile of regional background water, i.e., a profile without methane seepage influence.

An ADCP-transect crossing the mouth of the fjord was planned for the first night in Storfjorden. However, the bridge called at 2 am to tell that ice blocked the way into the fjord. As we had no information about ice cover in the fjord, we slowly moved along the ice front northward, but could not

even reach 77°N (Fig. 5). In addition, the good visibility decreased and the weather turned to be very foggy. To observe the extent of the drift ice, we moved eastward, but larger and larger sheets of ice forced us to turn south. As soon as we were out of the ice, we went to the east to reach Storfjordbanken and started sampling water along a transect crossing the ice-free mouth of the fjord from east to west (Fig. 6). Flares were observed on the N-S trending ridge on the western side of Storfjorden.

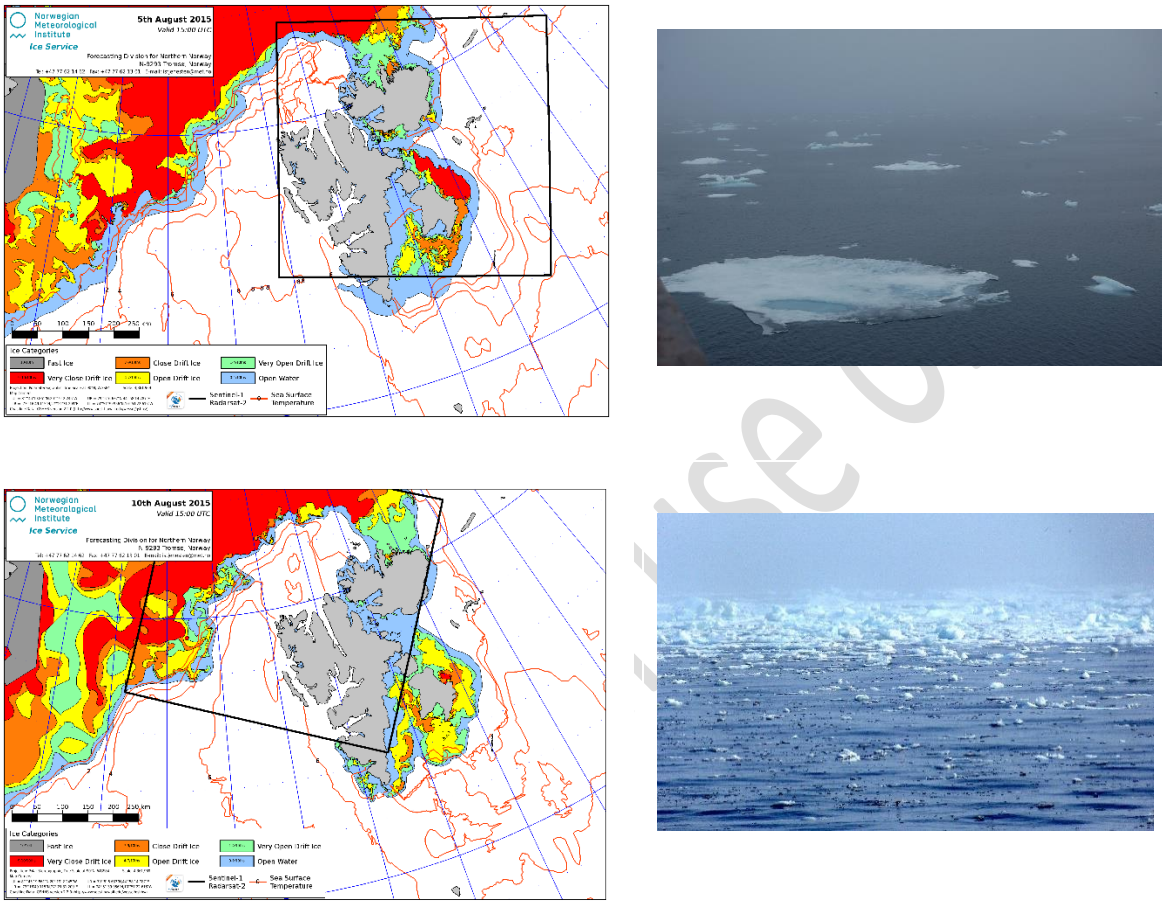

Fig. 6: Map of ice cover on 5th and 10th of August and pictures of the ice taken by S. Mau and N. Brückner.

After being able to download an ice-cover map from http://polarview.met.no/ and observing that drift ice did not leave a passage into Storfjorden, we decided to move to the western shelf of Spitsbergen. Hornsund, the southernmost fjord, was also closed by ice. Therefore, we started to sample water crossing the Hornsund shelf area. The first CTD-station was taken above a small basin structure, where we also deployed the MUC for the first time of the cruise. Two additional CTD-stations were located farther to the west where hard ground was expected. Several flare clusters were observed above the Hornsund shelf, which explained the methane concentrations >100 nM in the water column. In the evening, the in situ pumps (ISP) were deployed and recovered after 6 hours.

On the 7th of August, the CTD-transect, which crosses the Hornsund shelf, was completed. A quick survey of a deep basin located north of the Hornsund shelf revealed no flares in the basin, but on the ridges south and north of it. In this deep basin, we sampled water for incubations with ^{14}C-leucine and ^{14}C-DIC in addition to deploying the ISPs.

To complement the water sampling program of the previous day, we recovered sediment from the deep basin using the MUC. Due to the intense work load of the last days and as results from the Storfjorden area indicate seepage on the ridge, where we had not been sampling before, we returned to this area.

On the 9th of August, we started on the westernmost CTD-station in Storfjorden (Fig. 7). Here, we intended to collect surface sediments. We first tested the hardness of the ground by deploying the grab sampler before deploying the MUC. After successful sediment sampling, we went to the N-S-ridge, where flares had been observed. At this new station of the Storfjorden transect, we first sampled the water using the CTD-rosette and then deployed the Under Water Mass-Spectrometer (UWMS) above the detected flares. An UWMS survey was done below and one above the pycnocline in each a 500 x 400 m area. Recorded methane concentrations were investigated uniform on both planes. At these two depths, ISPs were deployed for 4.5 hours. The following morning, we wanted to complete our sampling schema by collecting surface sediments on the Storfjorden ridge site. We used the grab sampler and found a layer of small rock-pebbles above softer sediments, which prohibited MUC coring. We moved back to the westernmost station in Storfjorden and deployed a CTD-rosette to collect water for detailed methane oxidation rate measurements and ISPs at two different depths and in the phytoplankton bloom. The bloom had been sampled the night before at the ridge location, but the pump stopped working due to the amount of the suspended material, which quickly blocked the filter. After recovery of the pumps, we steamed back to the Hornsund area.

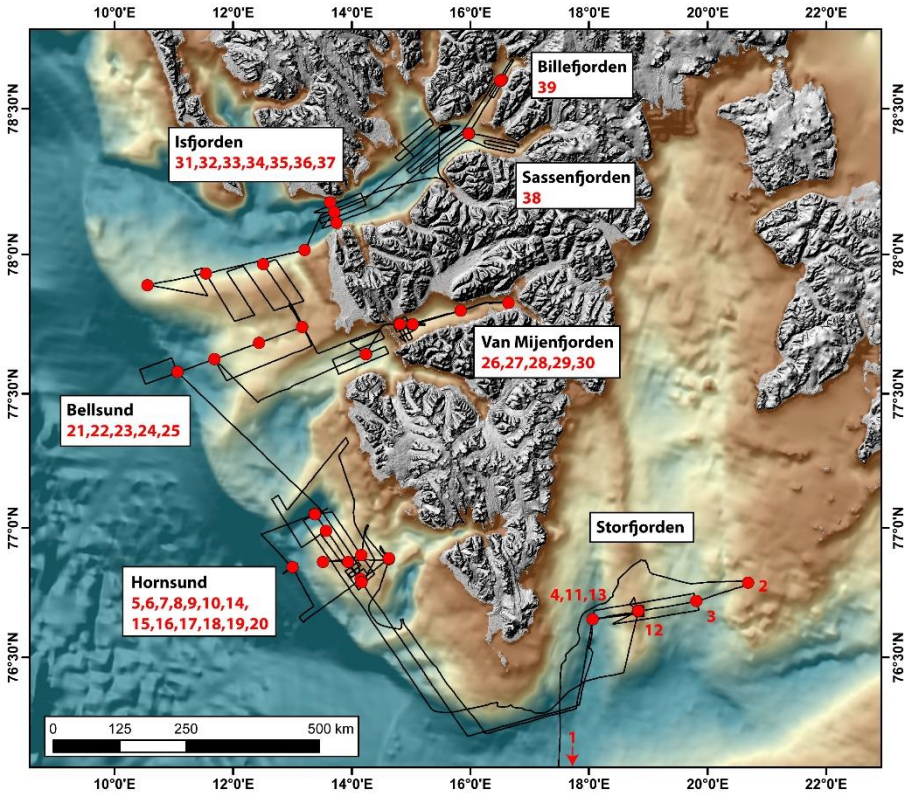

Fig. 7: Overview of the working area and the sampled stations.

On the 11th August, the mass spectrometer was used to map methane concentrations by crossing the flares of Hornsund. The weather was cold, foggy and the wind speed increased, which partly was the cause of recovering the mass spectrometer damaged. The program was changed as the UWMS had

to be repaired. We took a hydrocast and a sediment grab right at one of the observed flare clusters, but the latter recovered only gravel. Therefore, we changed slightly the position to try sediment sampling at a location with low backscatter. The sediment grab recovered soft sulfidic sediment and also the MUC could be successfully deployed at this location. Our original plan was to use the mass spectrometer to do transects perpendicular to the current while moving down-current of the flares to identify the methane plume broadening and diluting. As, unfortunately, the UWMS had to be fixed, we chose positions from the map instead from UWMS data to collect water for mainly methane oxidation rate measurements at two locations down-current of the Hornsund flares.

On the next day, we repeated the UWMS-transect, but instead of recording methane concentrations ~20 m above ground, we recorded the concentrations in 25-30 m water depth. Then, we wanted to replicate the transect ~20 m above ground, but the instrument failed. As otherwise our work in the Hornsund areas was completed, we moved farther north to Bellsund. There we sampled water on the edge of the shelf, a location, which should be complemented by three other stations crossing the Bellsund shelf on the following day. Meanwhile, we noticed that the tracer for methane oxidation rate analysis was running out and, thus, contacted Helgoland to send additional tracer. During the night from the 12th to the 13th of August, a few flares were observed on the Bellsund shelf. As intended, we finished the CTD-transect across the shelf on 13th of August and continued to a location in front of the entrance to Van Mijenfjorden. There we deployed the CTD-rosette and ISPs. Meanwhile we enjoyed the fine weather and saw a polar bear swimming towards our vessel and then turning (Fig. 8). After this exciting view and as we were close to land, some of us found that mobil phone contact was available and, thus, called their friends and families.

Fig. 8: The sighted polar bear, pictures by N. Brückner.

On the 14th of August, we first sampled sediments at the station in front of Van Mijenfjorden and then went into the fjord. There, we collected water at three stations from east to west through the fjord, before returning to the station right after the entrance to the fjord and deploying ISPs. The

weather had turned foggy, but we saw again a swimming polar bear. On the following day, we finished our work in Van Mijenfjorden. First we collected water for another incubation experiment with ^{14}C-leucine and ^{14}C-DIC at the CTD-ISP-station near the fjord's entrance before we sampled sediments at this location. As some small flares were detected right near the fjords entrance, not far away from the already sampled site, we took another hydrocast and MUC at this flare site situated on the edge of the fjord's basin. We had a nice view when leaving the fjord and went farther north to Isfjorden. There we sampled water at a station, which we planned to be part of a transect across the shelf south of Isfjordrenna.

On the 16th of August, we collected water at three more stations to finish the transect across the shelf south of Isfjordrenna. Afterwards we steamed to Longyearbyen to receive the ordered tracer for methane oxidation rate analysis. As it was Sunday, a personal transfer from the airport to the harbor had to be organized and caused some delay. With the help of Eva Falck and her daughter, we were able to clarify the situation and to collect the parcel using the small raft on-board of HEINCKE.

On the 17th of August, we started to collect water along a transect that crosses the mouth of Isfjorden to determine, how much methane is in the water that leaves the fjord. All three CTD-stations are located behind the sill, mainly because we intended to sample water from the basin situated behind the sill. After we finished our work at the mouth of Isfjorden, we went through the entire fjord to reach Billefjorden. There, we planned a similar approach as in Van Mijenfjorden, to sample the water and surface sediments in front of and behind the fjord's sill. We deployed the CTD and ISPs at a station in front of Billefjorden's sill. As the wind speed increased during ISPs deployment, we decided to recover the pumps half an hour earlier than planned. On the next morning, we deployed the MUC at the same station and went in rainy and windy weather into the fjord. In Billefjorden, we started sampling water using the CTD-rosette and ISPs at a station near the ghost-town Pyramides, the remnants of Russian coal mining. The ISPs were deployed for four hours, which left sufficient time to deploy a MUC to sample the surface sediments of this location. After finishing work at the last planned station, we had a goodbye party for Eva Falck and Torben Gentz, who left the ship in Longyearbyen on the 19th of August.

For the 19th of August an acoustic survey was planned before we stopped at Longyearbyen. Although the captain asked for a place at the pier, there was not sufficient room for R/V HEINCKE, thus, the captain organized transfer to the land by using the small raft on-board. All scientists and most members of the crew took the opportunity to explore Longyearbyen and its surrounding. At 7 pm, we left the harbor and started steaming to Tromsø. The wind strengthened during our passage of the Isfjorden's entrance, but quietened again on the next day. This transit day, we used for packing and starting to write the cruise report. As it was Anne-Christin's birthday, we had a celebration in the evening. We finalized the packing and sorting, what remains on board for the following cruise and what will be transferred back to Bremen University on the last day onboard, the 21th of August.

4 Water Column Analyses

4.1 CTD Measurements and Sampling

(E. Falck)

Hydrographic measurements were carried out using the ship-based Sea Bird SBE911 plus CTD (Conductivity, Temperature, Depth). The accuracy for this instrument is given to be 0.0003 S m^{-1} for conductivity, 0.001°C for temperature, and 0.015 % of full scale for pressure. The CTD was also equipped with a dissolved oxygen sensor (SBE 43), a fluorometer (Wetlabs ECO FL), and a transmissometer (Wetlabs C-Star). 12 Niskin bottles (5 L) were attached to the rosette for water sampling at different depths. In total 39 CTD stations were taken during the HE449 cruise, the position of the stations is shown in Figure 9. Before showing the results from the CTD measurements some input on the general hydrography of the area is given below.

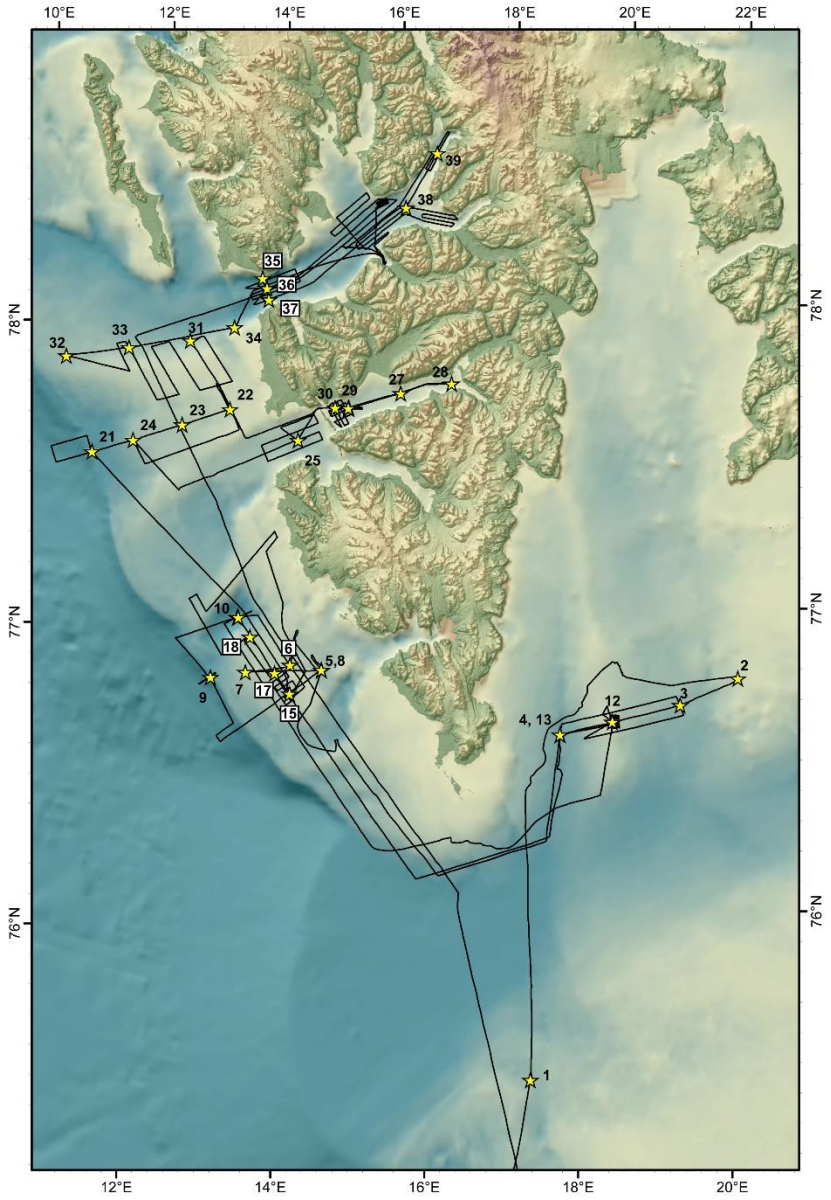

Fig. 9: CTD-stations conducted during HE449. The black line shows the cruise track. Some stations were sampled twice and, thus, have two different station numbers. White squares under some station numbers are only for better visibility.

A T-S diagram with all the stations is shown in Figure 10 together with the dissolved oxygen concentrations (in colour). Few stations show temperatures below 0°C, mainly the temperature lies between 0 and 8°C. The salinities measured varied between 30 and 35.2, with the exception of a few surface values having lower salinities. The dissolved oxygen values varied between 6 and 9 ml L^{-1}, the lowest found behind the sill in Billefjorden and the highest in the mouth of Storfjorden. Except for the deepest water in Billefjorden, Atlantic Water (AW) has the lowest dissolved oxygen values, shown as dark blue in the figure.

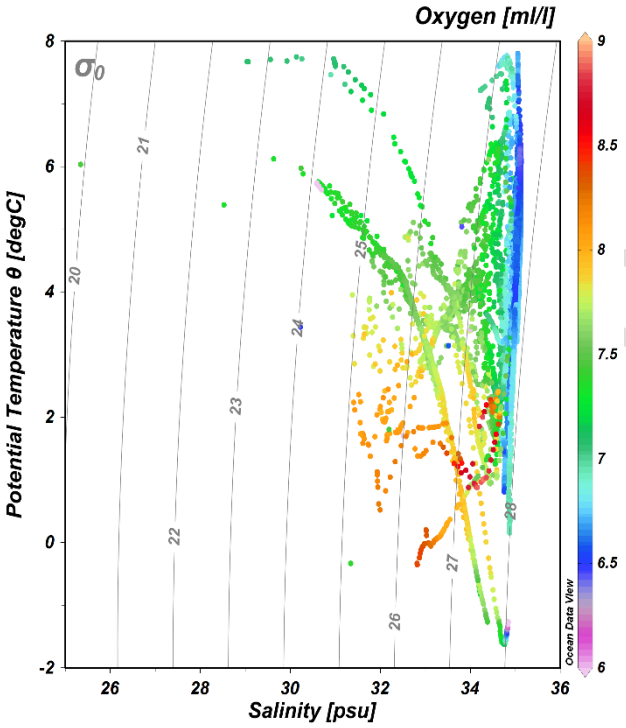

Fig. 10: Temperature-Salinity diagram of all the CTD data, the colour bar gives dissolved oxygen concentrations.

Storfjorden

The first area visited during the cruise was Storfjorden. Unfortunately, due to ice conditions, it was not possible to enter the fjord, but three CTD stations (2-4) were taken outside of Storfjorden (see Fig. 9). The vertical distribution of the different parameters along this transect is shown in Figure 11.

The easternmost station (St 2) has the coldest water at the surface, slightly below 0°C, while the two more western stations have surface values between 1 and 2°C. The surface layer down to 50 m is relatively cold and fresh and is of Arctic origin. From about 50 to about 150 m at Stations 3 and 4 there is a clear intrusion of Atlantic Water (T > 3°C, S > 34.9), while the deepest layer has temperatures close to 0°C and a salinity slightly below 34.9. This deeper water may be water exiting from Storfjorden or some mixture between AW and ArW. The upper 20 m is a layer with low salinities (S = 31-32) and has probably entered the area with the drifting ice. The highest oxygen concentrations measured during the cruise was found just below this fresher surface layer (nearly 9 ml L^{-1}), which also coincided with the highest percent oxygen saturation (>110 %) and fluorescence. The transmission was between 82 % and 94 %, and lowest at the surface in the eastern part (St. 2).

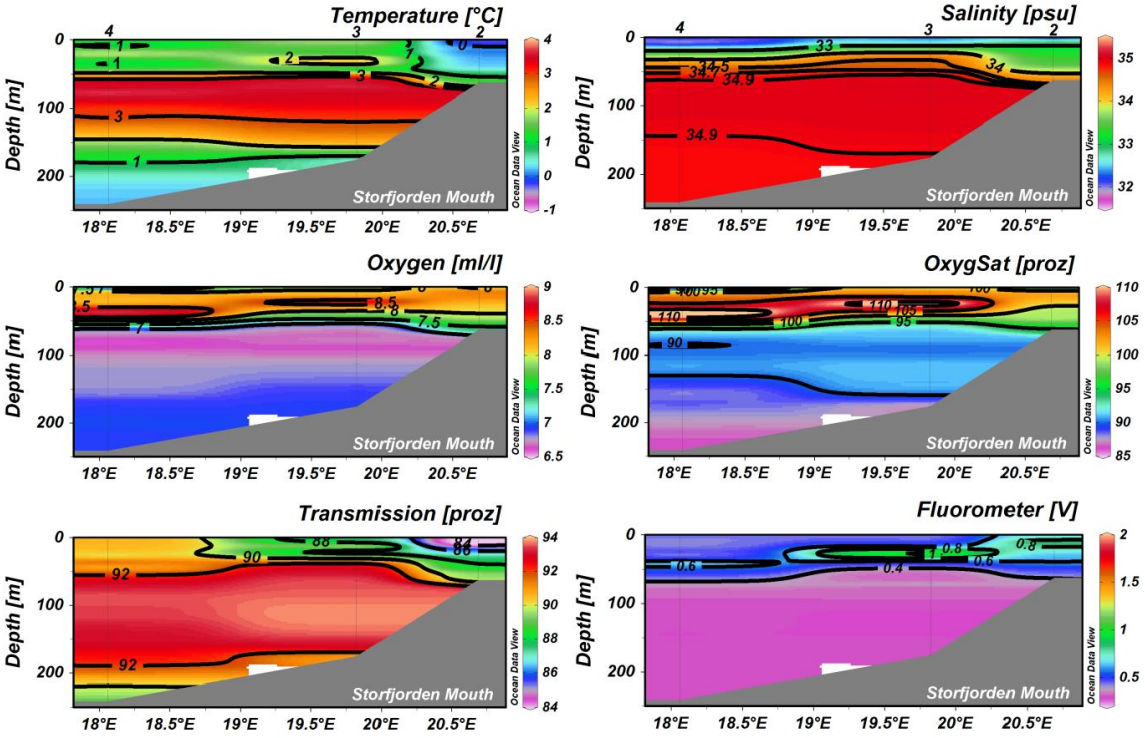

Fig. 11: Vertical distribution of temperature, salinity, dissolved oxygen, percent oxygen saturation, transmission, and fluorescence from stations taken across the Storfjorden Mouth. CTD station numbers are shown above the upper two panels.

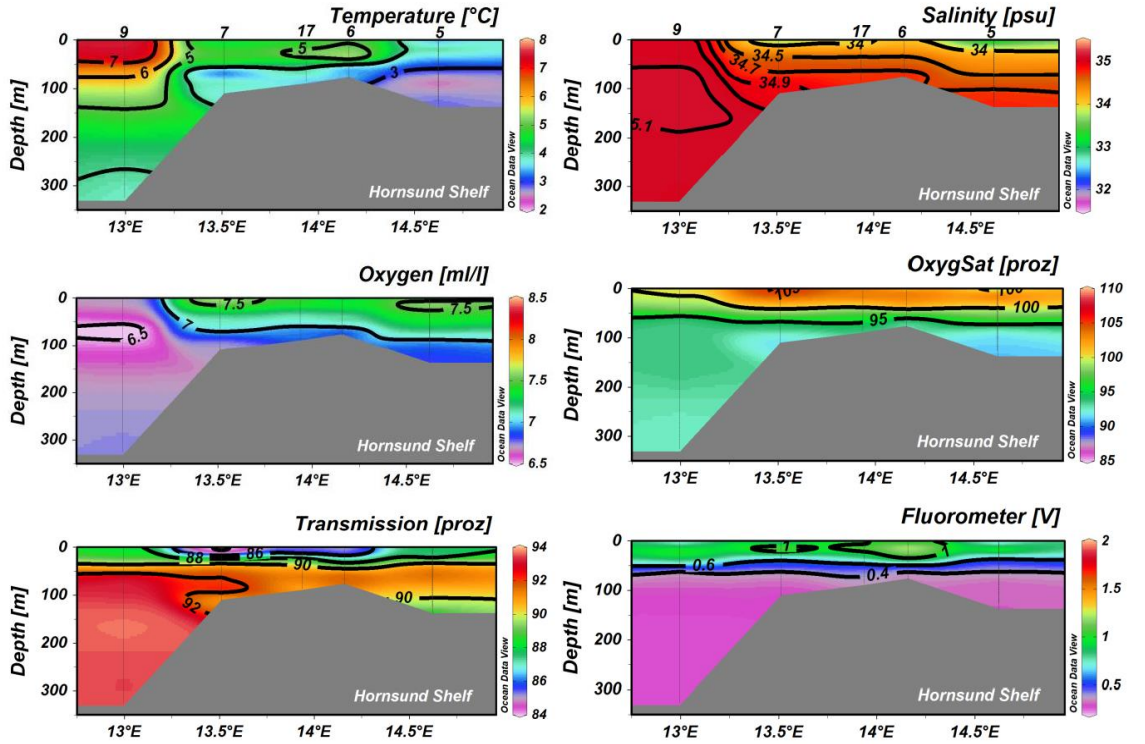

Fig. 12: Vertical distribution of temperature, salinity, dissolved oxygen, percent oxygen saturation, transmission, and fluorescence from stations taken across the Hornsund shelf. CTD station numbers are shown above the upper two panels.

Hornsund Shelf

The conditions on the shelf outside Hornsund are shown in Figure 12. CTD stations 5 to 9 were taken on the 6. August (CTD-5 and CTD-8 are taken at the same place) while CTD-17 was taken a few days later, but was also included in Figure 12.

The front separating ArW from AW is clearly seen between St 7 and St 9. Only AW is present at St 9, since the salinity is above 35 in the whole water column. Highest surface temperature was also found in the AW (> 7°C). The water on the shelf has lower temperatures and salinities, but higher oxygen concentrations (> 7 ml L^{-1}). Also the layer with percent oxygen saturation above 100 % is much deeper over the shelf than out in the AW. The percent transmission also here varied between 82 % and 94 % and highest fluorescence was found close to the surface.

Bellsund Shelf

Going further north on the shelf, a transect across the shelf outside Van Mijenfjorden was taken on the 12.-13. August. The CTD stations 21-24 are shown in Figure 13. Again, the Arctic Front is clearly visible between Stations 22 and 24. Much warmer and saltier water is seen on the western side of the front.

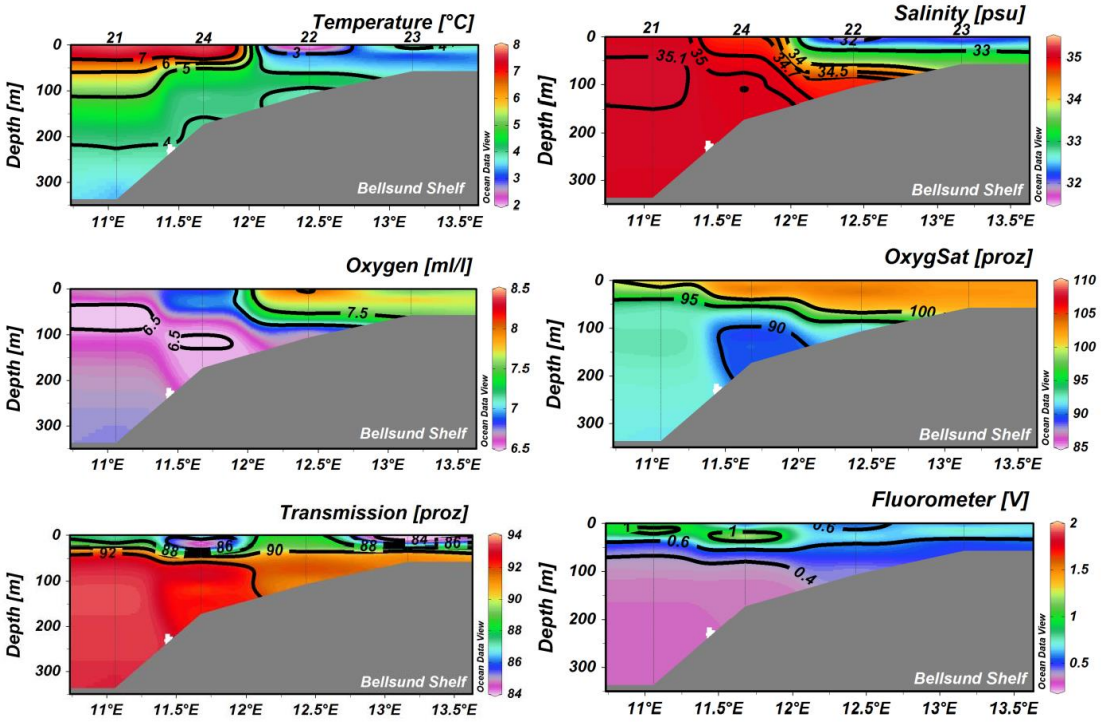

Fig. 13: Vertical distribution of temperature, salinity, dissolved oxygen, percent oxygen saturation, transmission, and fluorescence from stations taken across the Bellsund Shelf. CTD station numbers are shown above the upper two panels.

Van Mijenfjorden

Due to the shallow and narrow entrance to Van Mijenfjorden, the water inside the fjord is generally different than the water outside on the shelf. Five CTD stations (26-30) were taken during the 14.-15. August (Fig. 14). The temperature at the surface is relatively warm, around 6°C, but decreases with depth to below 0°C at the bottom were remnants of Winter Water can be seen. The freshest water (S

= 25.34) is found at the surface at St 28 in the innermost part of the fjord. There is a big river, Kjellstrømelva, which enters the fjord at its head that can explain this low salinity. The highest salinity found in the fjord is 34.4 (close to the bottom), so no AW is present inside the fjord. Dissolved oxygen varies between 7 and 8 ml L^{-1} and much of the water column has percent oxygen saturation values above 100 %. What is worth noticing is the quite lower percent transmission found inside the fjord compared to what was found elsewhere during the cruise. At St 28 the transmission was actually as low as 5 % at 6-7 m, and nowhere was it above 90 %.

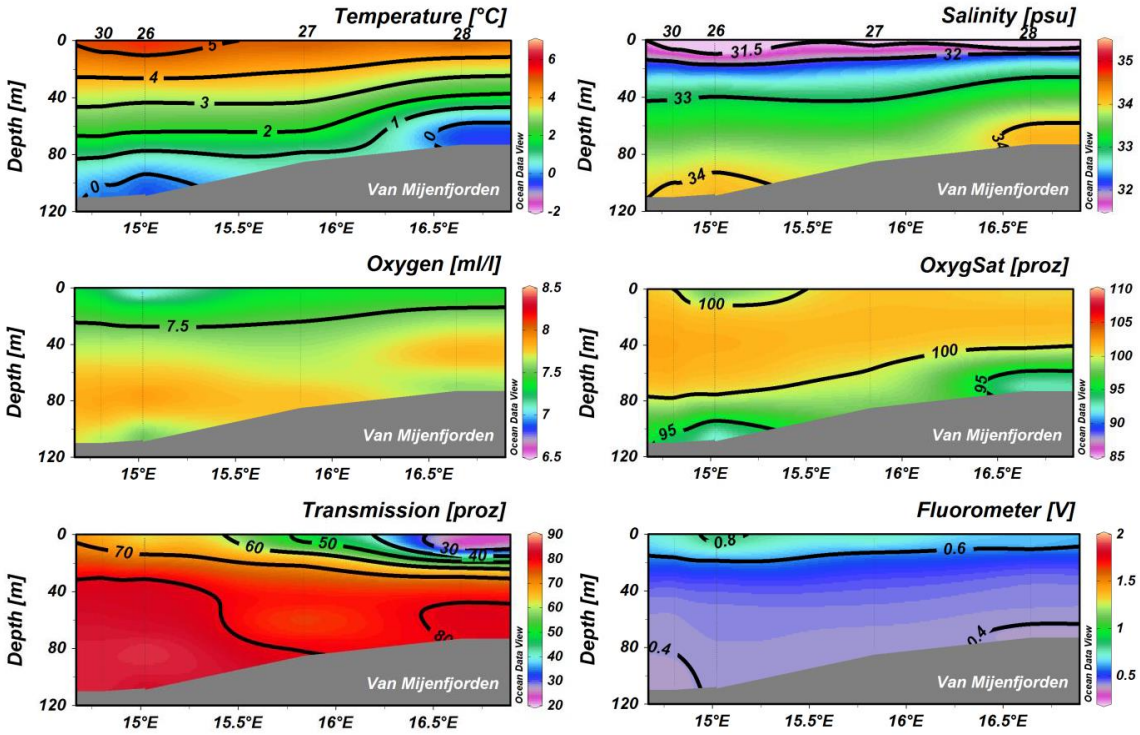

Fig. 14: Vertical distribution of temperature, salinity, dissolved oxygen, percent oxygen saturation, transmission, and fluorescence from stations taken in Van Mijenfjorden. CTD station numbers are shown above the upper two panels.

Isfjorden Shelf

Four CTD stations (31-34) were taken on the shelf outside Isfjorden on the 15.-16. August. The data are shown in Figure 15. Here the Artic Front is between Stations 31 and 34 (in the deeper part), but not so well defined at the surface since some lower salinity water can be seen on top of the AW on St 31-33. This is due to some wind effect, blowing the surface layer towards the west.

Isfjorden Mouth

Across the entrance to Isfjorden, three CTD stations (35-37) were taken on the 17. August (Fig. 16). The water column at the mouth can be divided into two, with a fresher (S < 34.5) layer in the upper 130 m and a saltier (S > 34.7) below. The lower layer consists of TAW with an intrusion of AW between 190 and 260 m at St 36 and along the bottom at St 37. The temperatures in the surface layer are between 2 and 4°C, the lowest temperature around 100 m. The temperature in the AW is between 3 and 4°C, while in the deep depression in the middle the temperature decreases to just below 1°C.

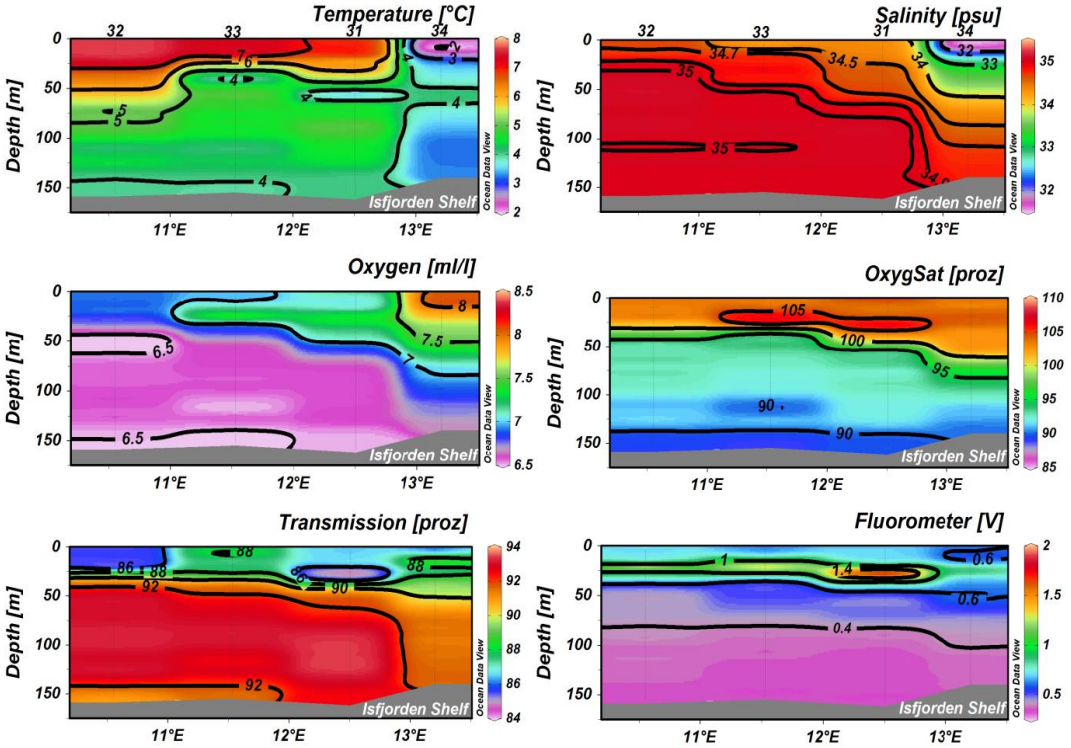

Fig. 15: Vertical distribution of temperature, salinity, dissolved oxygen, percent oxygen saturation, transmission, and fluorescence from stations taken across the Isfjorden Shelf. CTD station numbers are shown above the upper two panels.

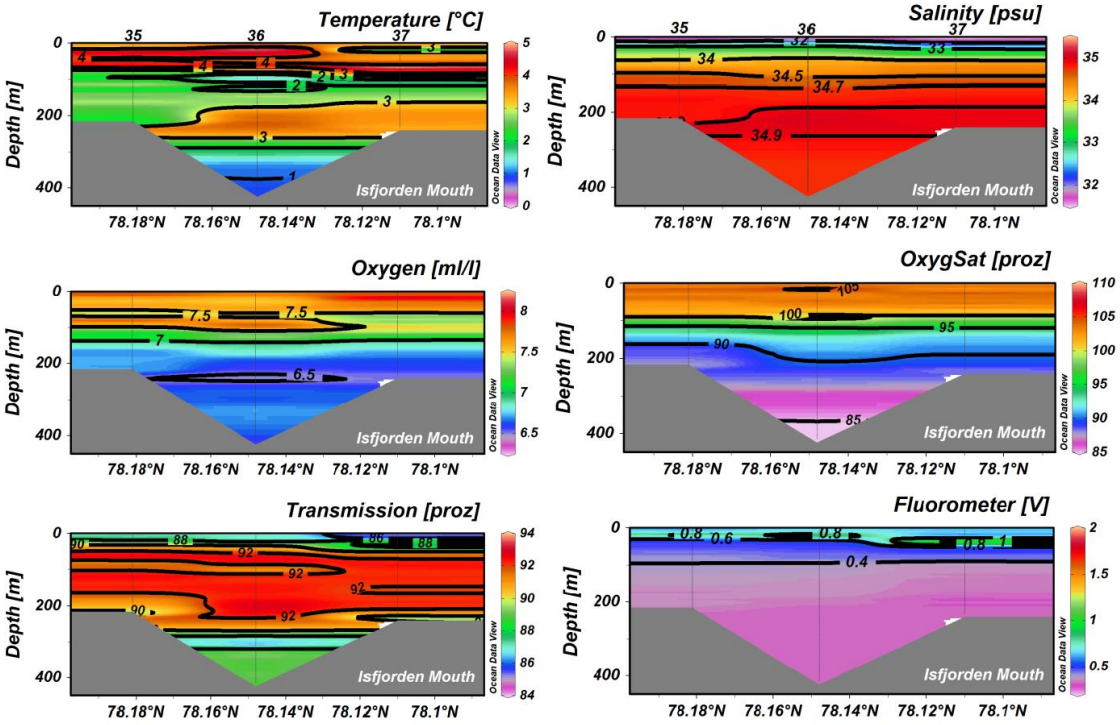

Fig. 16: Vertical distribution of temperature, salinity, dissolved oxygen, percent oxygen saturation, transmission, and fluorescence from stations taken across the Isfjorden Mouth. CTD station numbers are shown above the upper two panels.

The inner part of Isfjorden/Billefjorden

Two CTD stations were taken in the inner part of Isfjorden, Station 38 before the entrance to Billefjorden and Station 39 inside Billefjorden (Fig. 17). Billefjorden has a sill at the entrance with a depth of about 50 m, which means that water below this level cannot enter into Billefjorden from outside. Hence, the two profiles are quite different from each other below 50 m.

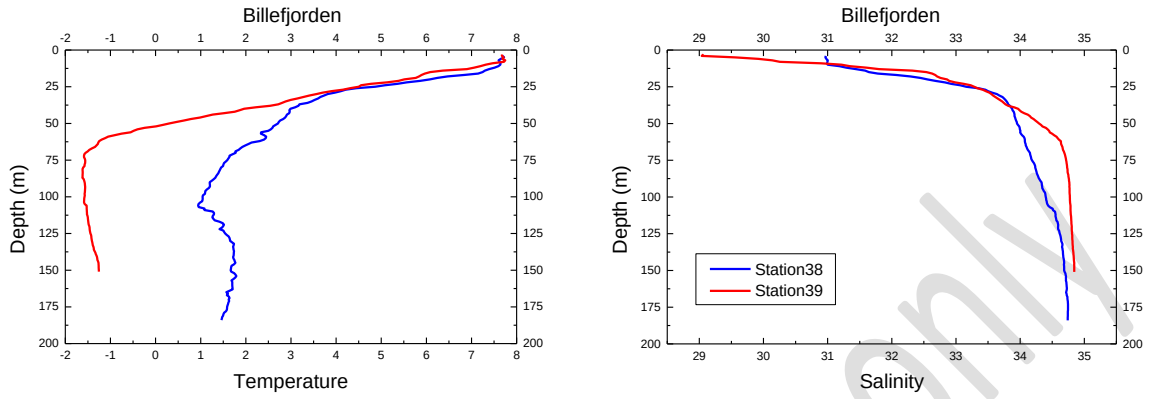

Fig. 17: CTD profiles of temperature (left panel) and salinity (right panel) from outside (blue) and inside (red) Billefjorden.

The temperature at the surface is the highest measured during the cruise, around 8°C, at both stations. Inside Billefjorden, Winter Water with temperatures below 0°C can be found from sill depth and all the way to the bottom. The coldest temperature, -1.62°C, was found at 81 m. This is close to freezing temperature and shows approximately how deep the winter convection was last winter at this point in the fjord. Below sill depth, Station 39 also show decreasing oxygen concentrations and percent oxygen saturation, at 50 m 7.85 ml L^{-1} and 99 %, while at bottom at 150 m 5.57 ml L^{-1} and 67%, respectively, indicative of quite old water behind the sill. Inside Billefjorden the surface water is fresher then farther out.

Dissolved Oxygen

To see if the dissolved oxygen sensor (SBE 43) gave correct concentrations of dissolved oxygen, water samples were taken for Winkler titration of dissolved oxygen from the three first CTD stations (CTD-stations 1-3). The results from the titrations of the water samples showed that the difference between those and the sensor (Fig. 18) only varied between 0.00 ml L^{-1} to ± 0.10 ml L^{-1}.

The mean difference of all the samples was 0.03 ml L^{-1}, which implies that the data from the dissolved oxygen sensor can be used as they are, with the exception of some surface values (mainly at 3 m) that are too low and unrealistic and needs be removed (some can be seen in Fig. 19).

All the dissolved oxygen profiles are plotted in Figure 19, showing concentrations between 6.3 ml L^{-1} and 8 ml L^{-1} in the upper 100 m for most stations, the values above 8 ml L^{-1} are mainly from the Storfjorden area. Below 150 m all values are below 7 ml L^{-1}, but noticeable is the higher oxygen concentration in the deeper water in the Storfjorden area (St 4) compared to the other deep profiles. The deeper part of Billefjorden stands out as having quite low oxygen concentrations (5.6 ml L^{-1} at the bottom).

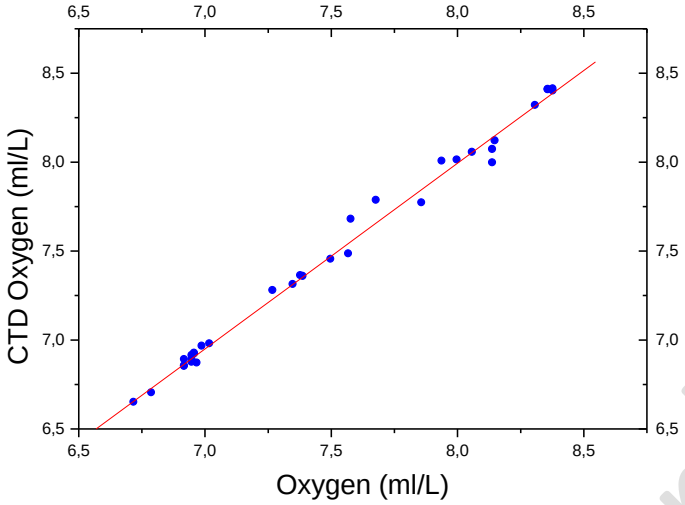

Fig. 18: Dissolved oxygen measured by Winkler titration (Oxygen) versus dissolved oxygen measured by the CTD (CTD Oxygen).

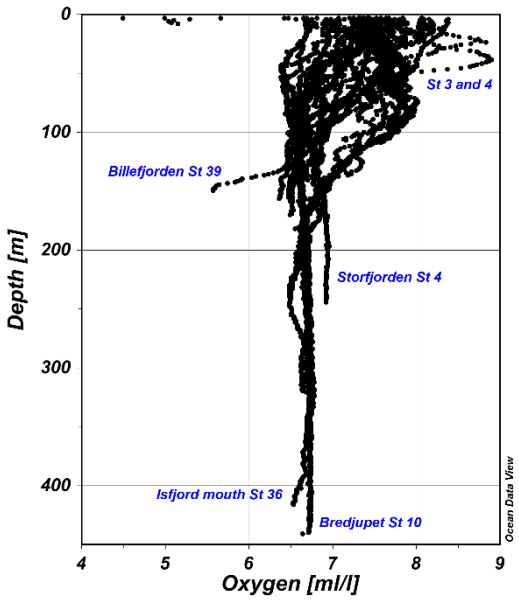

Fig. 19: Dissolved oxygen concentration versus depth from all the CTDs.

4.2 Methane Concentration Analyses

4.2.1 ICOS Measurements and Vacuum Extraction

(M. Lange, A.-C. Melcher, S. Mau)

ICOS Measurements

The concentration of methane in water samples was measured using the off-axis integrated cavity output spectroscopy (ICOS). This spectroscopy combines two highly specific infrared band lasers and a set of strongly reflective mirrors to obtain an effective laser path length of several kilometers. The ICOS System was installed on the 31th of July 2015 in the dry laboratory on the R/V HEINCKE and was

calibrated with standard gasses from 0.1 ppm to 100 ppm. During the scientific program precision of the instrument was daily checked with a 2.5 ppm methane standard.

Water samples were taken throughout the water column during the up-cast of the CTD/rosette system. Immediately upon recovery on deck, 3 x 100 ml of the water from each Niskin bottle was transferred into three plastic syringes; two syringes are sufficient for ICOS-analysis, the third one is used as backup. After collecting the samples, they were carried into the dry laboratory and measured. Forty ml of Zero Air was added to each of the two syringes and the syringes were vigorously shaken for two minutes in order to transfer the dissolved methane from the water into the added headspace. Each of the 40 ml headspace in the two syringes is collected into a third water free syringe. These 80 ml of sampling air and additional 60 ml of Zero Air were injected into the ICOS cell and measured. The screen connected to the ICOS displayed the measured methane concentration, which was written in a note book as well as it is automatically saved by the instrument. The data was copied onto an USB Stick after all samples of one hydrocast were measured and the final dissolved methane concentration was derived by taking water temperature, air pressure, salinity, dilution and a calibration factor into account. During the cruise methane concentrations from 4 nM to 793 nM were measured.

Vacuum Extraction

The dissolved gas of a water sample is extracted by putting the water sample in contact to vacuum. The gas extracted can be quantified and analyzed for methane and other gas concentrations. The method was performed on water sampled from 3-4 Niskin bottles, i.e., 3-4 different water depth, per CTD station. The extracted gas was then analyzed for methane concentration by an onboard gas chromatograph and will be analyzed for stable carbon isotopes in the home laboratory.

The extraction of the gas was conducted with slight modifications as described by Lammers & Suess (1994), Rehder et al. (1999), and Schmitt et al. (1991). Briefly, 650-750 ml water were collected in pre-evacuated (3.0 x 10^{-3} mbar) 1 L gas-tight bottles by avoiding air being sucked into the bottles. The extraction of dissolved gases was performed on a high-grade vacuum system (4.3-5.3x10^{-1} mbar) within 2 hours of collection (Fig. 20).

Fig. 20: Setup of the vacuum extraction on the cruise.

First the water sample is installed in the extraction setup. The inlet is connected to a bottle filled with saturated NaCl-solution and the outlet is connected to a burette which helps to quantify the amount of gas extracted from the water sample. The whole system has to be evacuated including the burette in order to transfer the gas sample from the sample bottle into the burette. The saturated solution is used as a medium to fill the sample bottles and trap the gas sample into the burette. Pre-evacuated and saturated saltwater is used as medium to minimize the chance of air to get into the sample. The amount of gas extracted from the sample is measured and the gas transferred through a septum port to two 20 ml vials pre-filled with saturated NaCl-solution with a gas tight syringe. Methane concentrations can be analyzed onboard if a gas chromatograph is available, otherwise, the vials are suitable for long-term storage.

Methane concentration results

The concentration data shown and discussed below was measured using the ICOS-system. Data derived by vacuum extraction do not deviate much and these samples will be used for characterization of the stable carbon isotope ratio of methane.

Storfjorden: Methane concentration is generally enriched at the wide entrance to Storfjorden (Fig. 21). All concentrations were oversaturated with respect to the atmospheric equilibrium concentration of 3.2–3.6 nM (at the relevant T /S conditions and an atmospheric methane concentration of 1.78 ppm, Wiesenburg and Guinasso, 1979). Three possible sources could lead to this enrichment of methane. Gas emissions were hydro-acoustically detected on the N/S trending ridge (CTD 12) in 40-60 m water depth where methane concentrations of 35 nM were measured. Fluctuating methane concentrations at station 4, which was sampled 3 days later again (station 13), might further support the influence of gas seepage. Currents possibly transported more or less methane from the ridge towards this location as we found first methane concentrations of 20 nM and 3 days later >40 nM. At station 3 and 4 methane concentrations increased towards the seafloor indicating possible additional sources from the seafloor-sediments. Finally, a lot of phytoplankton was visually observed by attaching a camera to the UWMS-frame, which points to sufficient organic matter, which can be degraded to methane.

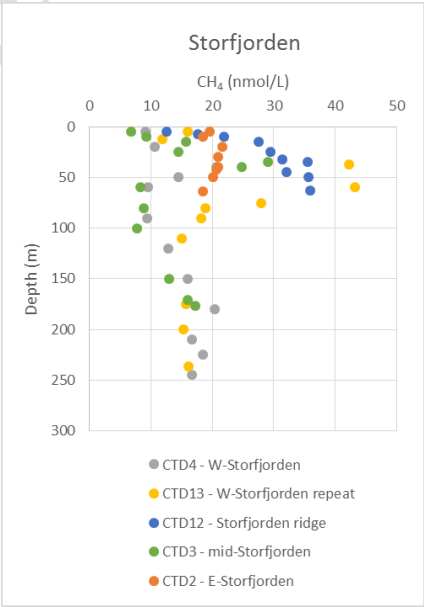

Fig. 21: Methane concentrations in the water at the southern end of Storfjorden.

Hornsund: Highest methane concentrations of all investigated areas were detected at the Hornsund shelf due to several clusters of gas emissions. We sampled water along a section perpendicular to the northward flowing currents and another section in direction of the current. The first is shown in Figure 22a with depth profiles named from west to east: shelf break, W-Hornsund, down current seeps, shallow Hornsund and E-Hornsund and the down-current section is shown in Figure 22b. Here, we followed the plume from the center of one flare cluster down current to stop and sample 10 km (down current 1) and 26 km (down current 2) from the source. Highest methane concentrations of 793 nM were measured in samples taken right above the flare cluster. Concentrations decreased rapidly to 235 nM and 90 nM at 10 km and 26 km down-current, respectively. Similarly methane concentrations decreased perpendicular to the northward current, spreading across the shelf but not as far as the shelf break.

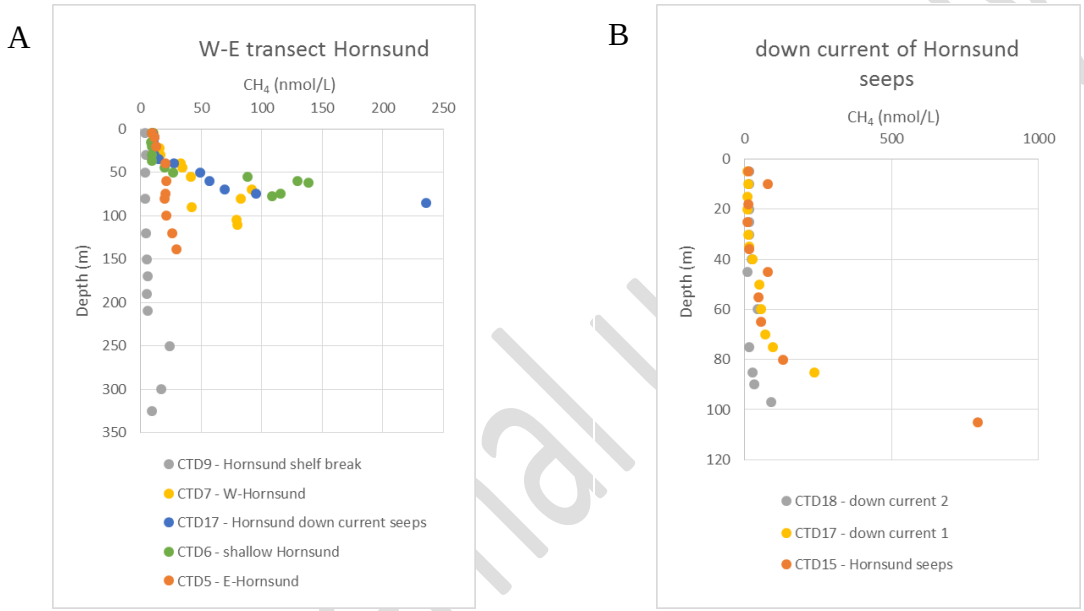

Fig. 22: Methane concentrations in the water above the shelf of Hornsund. The left plot shows depth profiles taken from west to east across the shelf (A) and the right plot shows profiles sampled down-current of the Hornsund seeps (B).

Bellsundet and Van Mijenfjorden: As in the other areas, even the lowermost methane concentrations at Bellsundet and Van Mijenfjorden were above the atmospheric equilibrium concentration. Less than 10 nM were only found at the outer shelf, in the fjord and on the landward part of the shelf methane concentrations were typically > 10 nM (Fig. 23). The enrichment of methane on the shelf at station 23 appears to be connected to seepage as a few flares were detected in the vicinity of the station. We speculate that widespread seepage on the shelf caused the methane plume in 50-150 m water depth, which reached almost all the way to the shelf break. Flares were also observed just behind the entrance of the fjord and appear to be the reason for the increasing methane concentration to the seafloor in the fjord. This plume near the fjord's ground extends to the mid of the fjord, but not all the way to its eastern end. In the eastern part of the fjord (CTD 28) an increase of methane in 20-50 m water depth was measured, which might be linked to a phytoplankton bloom. This plume in 20-50 m water depth is also apparent in the middle of the fjord, but not at the entrance of the fjord. In the basin outside of the fjord, methane concentrations indicate additional input from the sediment.

Isfjorden: Our intention was to observe how much methane originates from Isfjorden and from the shelf that is transported into the seepage area off Prins Karls Forland. Therefore, we collected samples across the shelf, just south of Isfjordrenna, and across the entrance of Isfjorden (Fig. 24). The westernmost and easternmost of the shelf stations (CTD32 and CTD34) show a two layer pattern with lower methane concentrations in water < 70 m and higher concentrations below. The stations between indicate a methane plume centered at 40-60 m and stations 32 and 33 indicate another plume at 110 m water depth. While the shelf cross-section shows variable depth profiles, the depth profiles of the section crossing the Isfjorden entrance were found to be more consistent. Methane concentration increased from 10 nM to 15 nM from the surface to 70 m. Below methane concentrations reached 25 nM forming a broad plume in 80-220 m water depth, which decreased to 9 nM towards the seafloor.

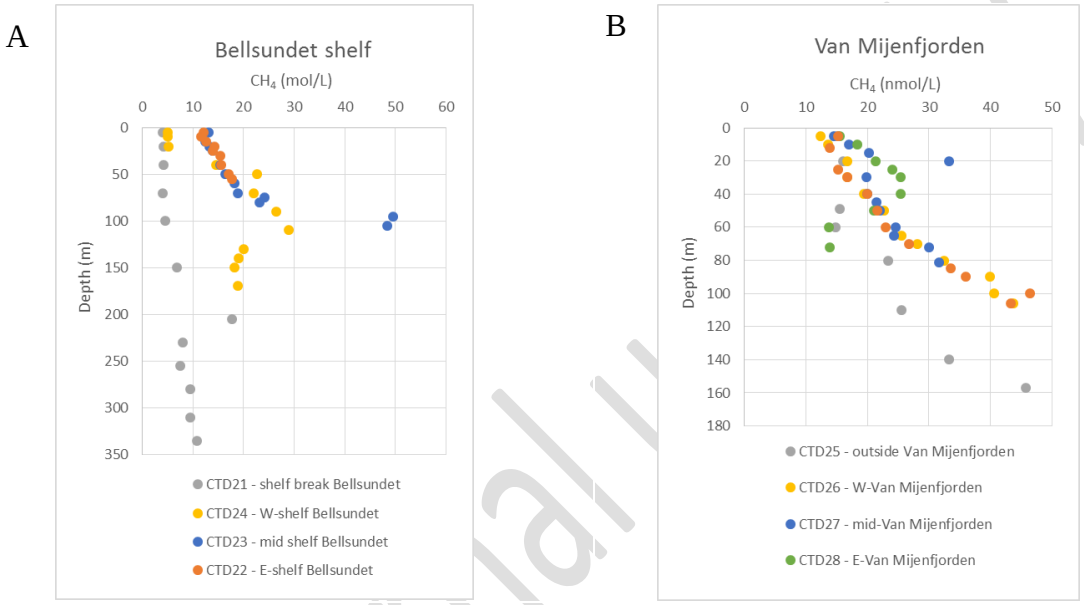

Fig. 23: Methane concentrations in the water above the shelf of Bellsundet (A) and in Van Mijenfjorden (B). The left plot shows depth profiles taken from west to east across the shelf and the right plot shows profiles sampled also from west to east in the fjord.

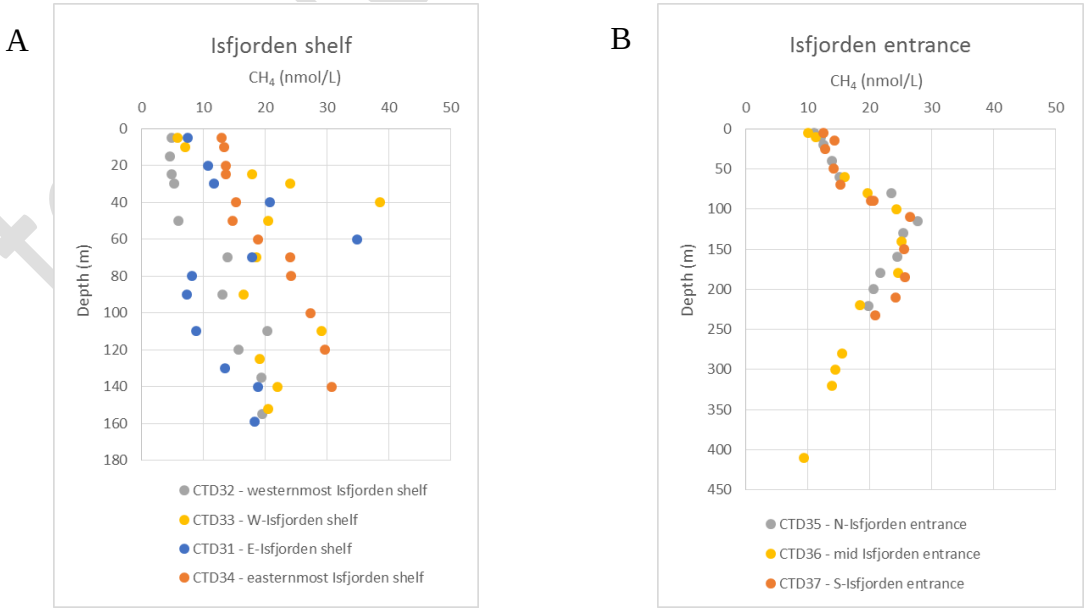

Fig. 24: Methane concentrations in the water across the shelf south of Isfjordrenna (left) and across the entrance of Isfjorden (right).

Billefjorden: Methane concentrations were lower in the fjord than outside of the fjord (Fig. 25). We speculate that the depth profile in Billefjorden is influenced by degradation of phytoplankton bloom material in 20-40 m water depth and degradation of organic matter in the sediments in the near-bottom sample. In contrast, the elevated methane concentrations outside of Billefjorden were due to methane seepage as gas flares were observed in the vicinity of the station.

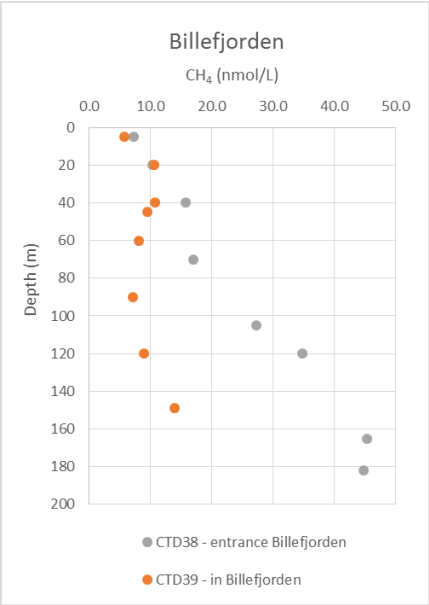

Fig. 25: Methane concentrations in the water outside and in Billefjorden.

4.2.2 Underwater Mass Spectrometer

(T. Gentz)

A novel Underwater Mass Spectrometer (UWMS) was used to quantify the dissolved methane concentration in high temporal and spatial resolution in the water column above gas seep areas. Both areas, Storfjorden and Hornsund, were the instrument was deployed, are located on the Spitsbergen shelf in depth of 60 m and 100 m, respectively. To determine the coordinates and depth of the UWMS during deployment the on board GAPS-system was used.

Technical Description

Main components of the UWMS are the vacuum system (turbo and roughing pump), the Membrane Inlet System (MIS) and the Mass Spectrometer unit (Fig. 26). Within the MIS (Fig. 27A and B) gases are extracted from ambient seawater and transferred into the high vacuum section of the mass spectrometer unit. For this purpose a tubular PDMS membrane is applied (Fig. 27A).

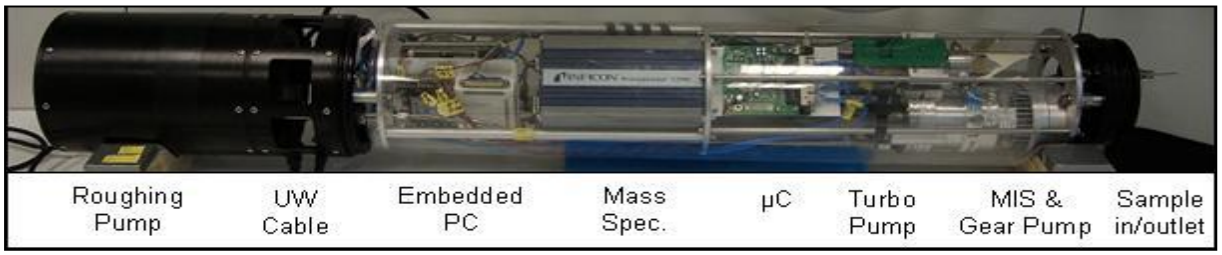

Fig. 26: Main components of the UWMS System for in situ gas analysis (up to an Atomic Mass Unit of 200) in water depths of up to 200 m.

An underwater peristaltic pump (Fig. 27C), which is robust and provides a very accurate volume flow adjustable over a wide range, pumps sea water through the membrane inlet system along the outside of the tubular membrane. Through the tubular PDMS membrane (Fig. 27A), gases are permeating from the dissolved phase into the high vacuum section of the mass spectrometer.

Generally, the membrane inlet interface is one of the crucial parts of underwater gas analyzers, whether solid state detectors, optical sensors or mass spectrometry is applied. Essentially for reproducible gas permeation through membranes is the temperature as well as the hydrodynamic regime in the close vicinity of the membrane. Therefore, the MIS designed for the UWMS is fully controlled with respect to temperature (we operate the MIS at 35°C) and the volume flow of sea water along the membrane.

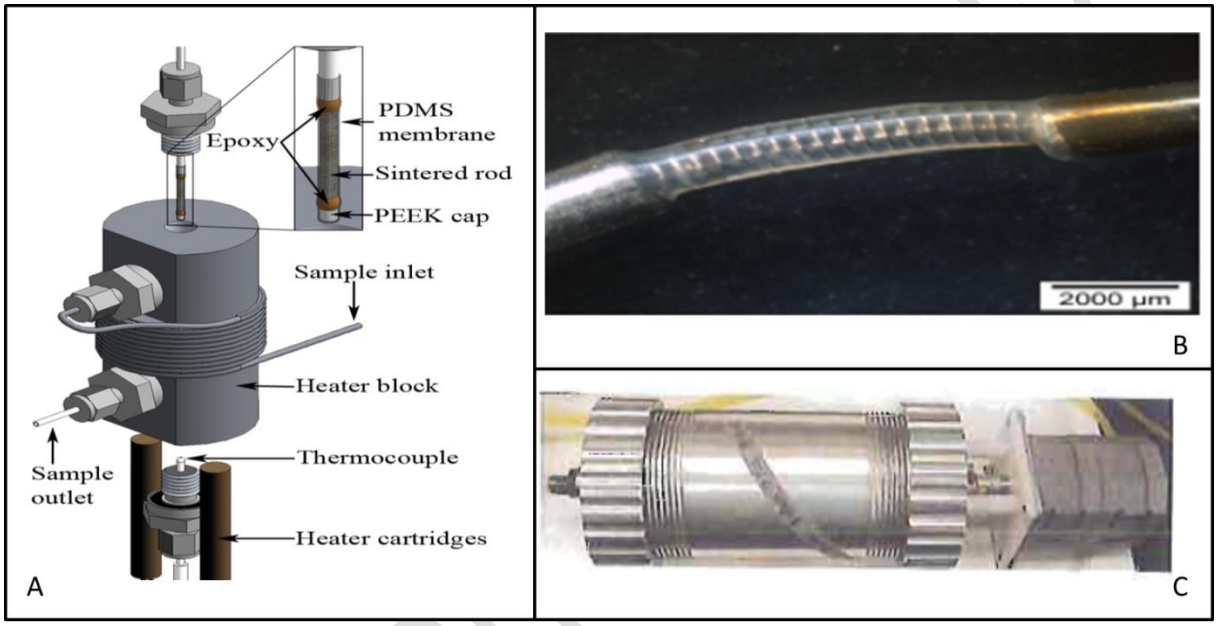

Fig. 27: The membrane inlet system (A, B) and the underwater peristaltic pump (C).

Another important issue is the response time of a sensor. Most "physical sensors" for e.g. temperature or pressure are responding fast (within seconds). Unfortunately, most chemical sensors require to reach a state of equilibrium (e.g. methods based on adsorption, colorimetry, or mass transfer across membranes) which is often rather slow. In contrast, the permeation of gases through the membrane inlet system of the UWMS is a uni-directional process; the gas of interest, e.g. CH_4, is permeating into the high vacuum section of the mass spectrometers and back diffusion does not occur. Consequently, the response times of the UWMS is less than 20 – 45 sec (t_{90}-t_{10}).

Performance and Results

We performed five deployments of each ~2 hours during the cruise HE449. The deployed system consisted of the UWMS, two underwater batteries from Deepsea®, and a GAPS system for detailed information of the x, y and z positioning in relation to the ship (Fig. 28). For the quality control of the data an onboard calibration of the UWMS was applied prior and subsequent to the deployments.

During the first deployment in Storfjorden on the 9th of August 2015, methane concentrations along two grids were mapped by towing the instrument with 1-2 knots ship speed in 60 m and 25 m water depth. Although small gas flares were detected with hydroacoustic instruments in this area, no significant variations in the concentration of methane were detected at both depths.

Another transect of ~2 hours was conducted across a gas seep area at the Hornsund shelf in 50 m – 90 m water depth on the 11th of August 2015 (Fig. 29). The depth was variable due to necessary ship speed adjustments; either the UWMS rose when the ship went faster or dropped when the ship went slower. During the 2 hours deployment more than 2500 data points were recorded by the UWMS (every 1.6 m). At greater depth and in the surrounding of gas flares, steep gradients of the dissolved methane concentration up to 435 nM were detected by the UWMS (Fig. 29). For a detailed map the acquired methane concentration need to be merged with the data set by GAPS for especially depth correction. During recovery of the mass spectrometer, the frame banged against the ship's side, which resulted in a failure of the ion source and power supply.

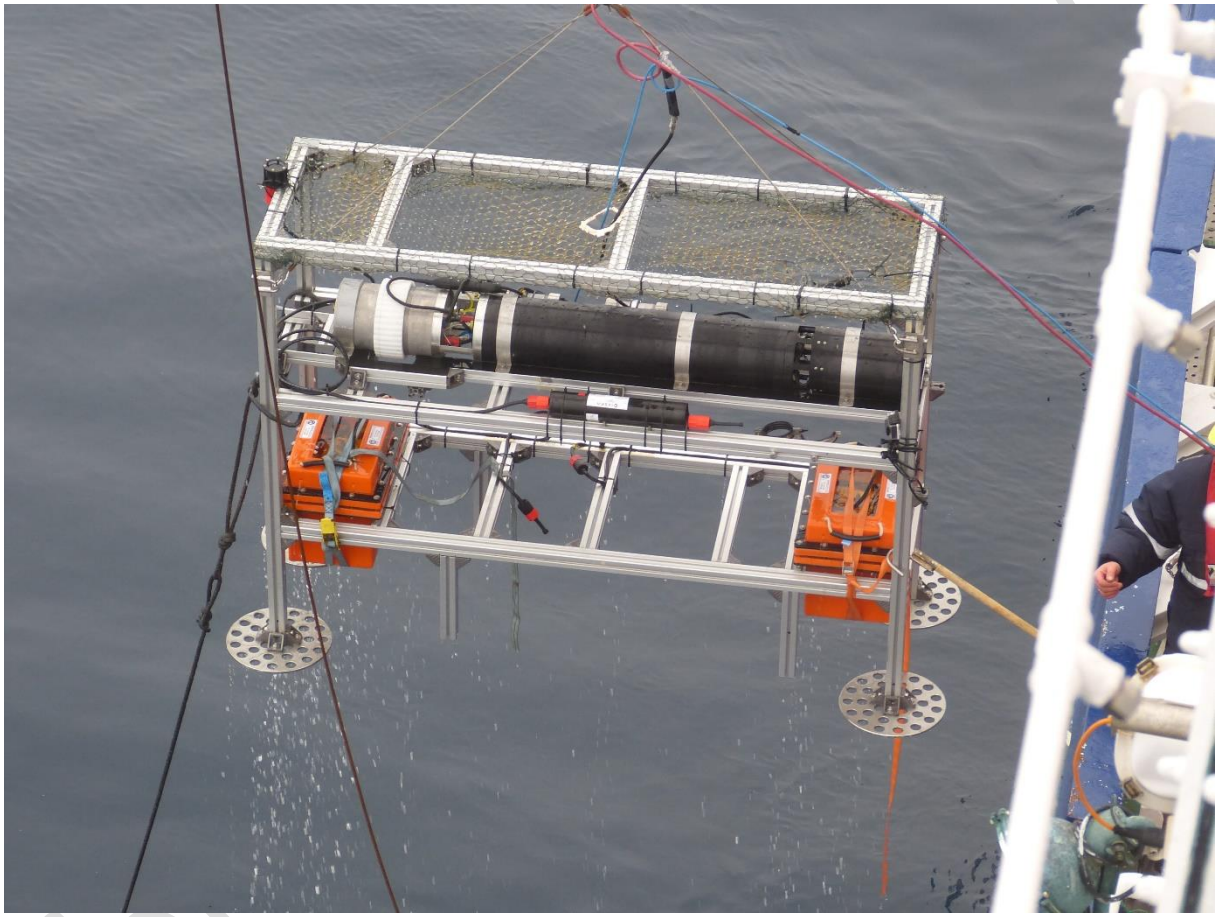

Fig. 28: Deployment of the UWMS at the HE449.

On the 12th of August, two more transects across the gas seep area of Hornsund were planned. The first one in 25 m depth was operated by external (cable) power supply. The results show now significant variations above the flares. The second run was performed using batteries as power supply. Due to the accident the day before, a constant power supply was not given and the instrument turned off. Therefore, no data were acquired.

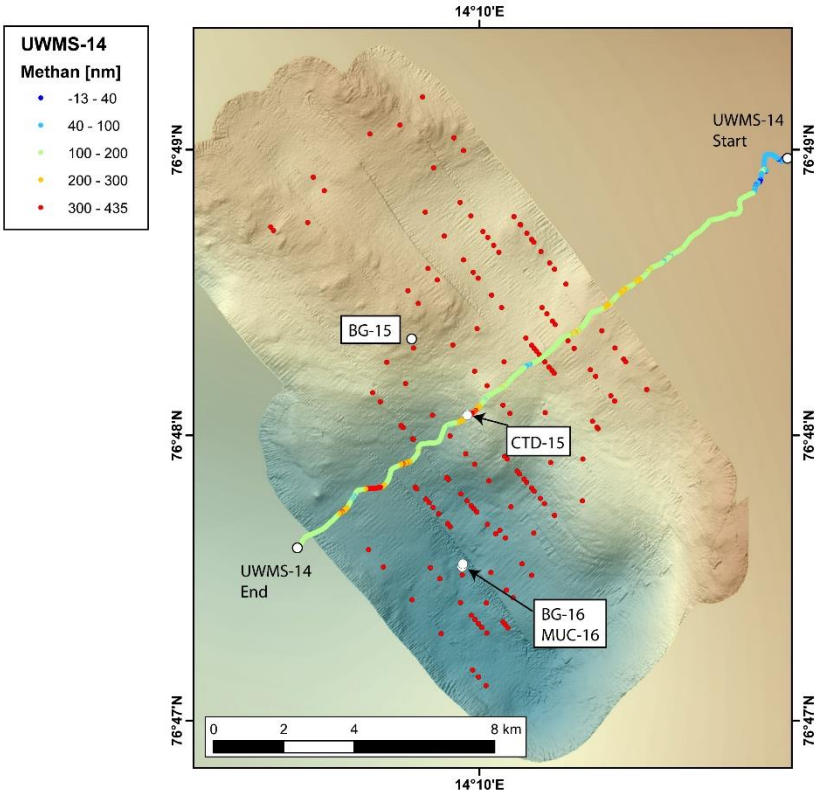

Fig. 29: Methane concentration in nM at the Hornsund gas seep area (11.08.2015). Preliminary data, which are not corrected by depth yet.

4.3 Methane Oxidation Rate Measurements and Experiments

(I. Bussmann)

The consumption or oxidation of methane through methanotrophic bacteria is an important process in the water column and oxic sediment surfaces. Methane oxidation (MOX) is the only biological filter that is able to reduce the amount of methane released by pockmarks and flares into the water column.

Methane oxidation was measured with tritiated methane. The ratio of tracer injected and the consequent production of water provides an estimation of the activity of methanotrophs. We took triplicate samples for methane oxidation rates at most stations from four different water depths (CTD 1 - 7, 9, 10, 12, 13, 15, 17, 18, 21- 28, 35 – 39); in total we took 477 samples. Most samples were analyzed on board, however, very low activities have to be verified in the home laboratory. We also measured MOX in the water overlaying sediment cores sampled by the Multicorer (MUC 1, 2, 3, 5, 9, 10), as well as in the surface sediment (by diluting the sediment 1:100 with water). In addition, we filtered the water samples for DNA-extraction in the home laboratory, which can be used for quantification of methanotrophic bacteria with qPCR. Besides the activity measurements it is important to know which factors affect this activity. Therefore, we performed four experiments to assess the influence of temperature and substrate (methane) concentration on the methane oxidation rate. Experiment I was performed with surface water from CTD-2, experiment II with bottom water from CTD-10, experiment III with bottom water from CTD-33 and experiment IV with surface water from CTD-37.

First results show rather low activity in surface and intermediate waters. However, towards the seafloor MOX increased substantially, mainly due to increased methane concentrations near the seafloor. This pattern was most obvious at the Hornsund transect and at a lower level also at the Storfjorden transect (Fig. 30).

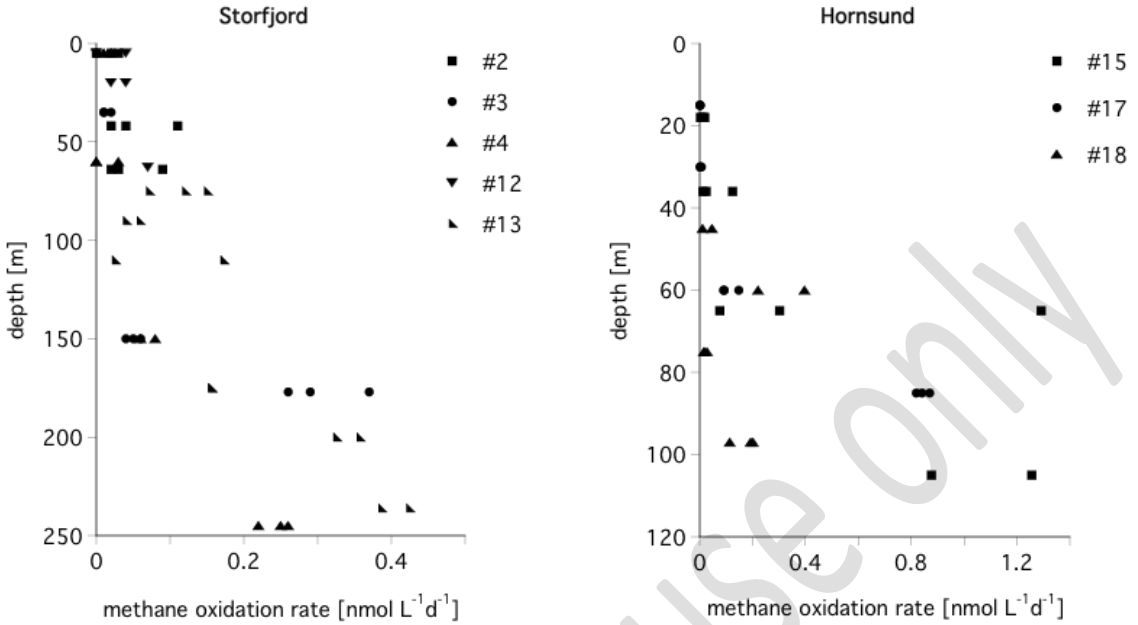

Fig. 30: Methane oxidation rates measured in the water column of Storfjorden and Hornsund.

At the Hornsund flare area we followed the water masses northward with the currents and tried to sample the same water masses. As can be seen in Figure 31 we found elevated methane oxidation rates in the bottom water near the flare. Within approx. 10 km the rates stayed at a similar level, however, at a distance of approx. 26 km activities in the bottom water had decreased.

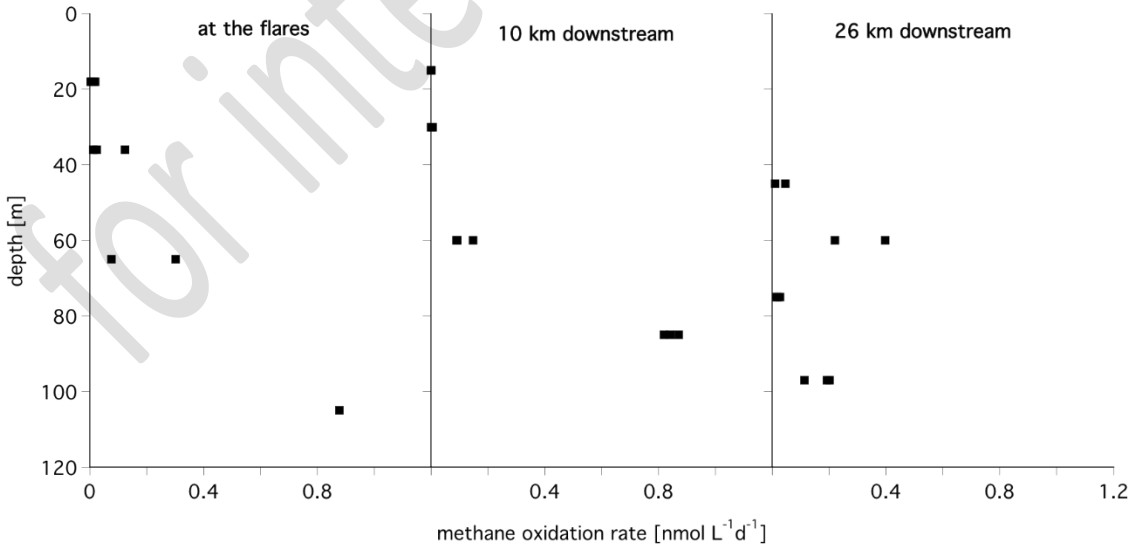

Fig. 31: Methane oxidation rates measured down-current from the Hornsund seeps.

Our experiments revealed a strong dependence of the MOXrate on temperature (Fig. 32). However, already at 20°C activity seemed to level off, indicating a psychrotolerant methanotrophic population. The kinetic experiments suggest two populations of methanotrophs, one adapted to low methane

concentrations and the other adapted to high methane concentrations. But this has to be verified in the home laboratory.

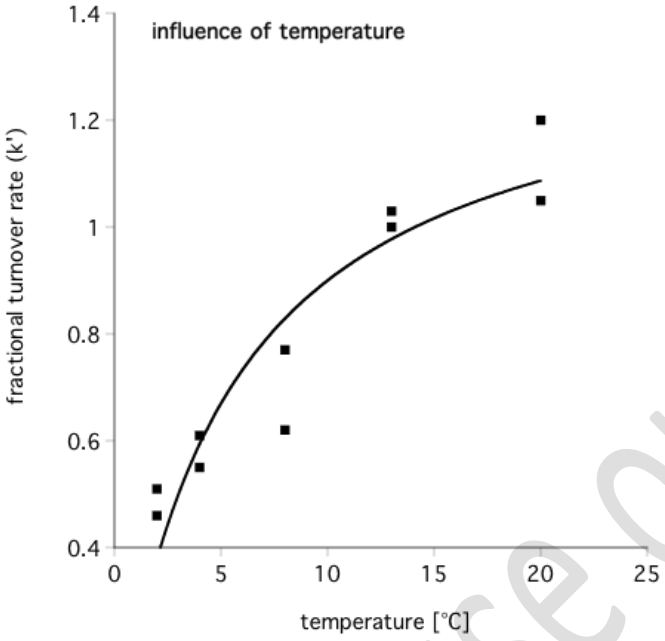

Fig. 32: The fractional turnover rate (k'), i.e., the ratio of converted and injected tracer per unit time, versus incubation temperature.

4.4 Biomarker Studies and Incubation Experiments

(N. Goldenstein)

The organic geochemical study of the water column was based on the usage of in-situ pumps, which were correlated with CTD-profiles and samples derived from Niskin bottles. Four different types of samples were taken from the Niskin bottles immediately after recovery:

- *Sample 1:* For determination of NH_4^+ concentrations 80 mL of seawater were filled into brown-glass bottles and right away measured on board, with the method by Holmes et al. (1999) using a Turner Designs Trilogy Laboratory Fluorometer equipped with the Turner Designs CDOM/NH4 Module (P/N:7200-041). In addition, 10 mL of seawater were filled into clean falcon tubes and immediately used for on board determination of NO_2 concentrations, in triplicate, using diazo-colorimetry (Strickland and Parsons, 1972) with photometric detection by the Turner Designs Nitrate/Nitrite Module (P/N: 7200-074) in the Trilogy Laboratory Fluorometer.
- *Sample 2:* 70 mL of water were filled into sterile falcon tubes and stored frozen for shore based investigation of stable inorganic nutrients (e.g. PO_4, NO_3).
- *Sample 3:* 15 mL of water were chemically fixed using a 4 % Paraformaldehyde solution and stored at -20°C for shore-based determination of microbial cell concentrations.
- *Sample 4:* For determination of mRNA-based microbial activities 2-3 L of water were sterile filtered through a 3 µm pre-filter followed by a 0.1 µm filter. The filters were thereafter immediately treated with 2 mL Quiagen RNA later reagent and stored frozen at -20 °C.

- *Sample 5:* Samples for shore based determination of DIC/DOC concentrations and isotopic composition were taken in 2 mL glass vials, which were filled headspace free and stored frozen at -20 °C.
- *Sample 6:* Large volume water samples (9 x 10 L) were filled into 20 L glass schott bottles for on board incubation experiments with different types of substrates.

A tool string equipped with up to four in-situ pumps (ISP) was deployed in the water column for several hours to filter large volumes of water at selected water depths. Deployment ISP returned samples of particulate matter on glass fiber filters through which up to 750 L of sea water had been pumped. In order to separate different size fractions, the following filters were combined: GF/D (Whatman, 142 mm Φ, pore size ~2.7 µm), GF/F (Whatman, 142 mm Φ, pore size 0.7 µm) and GF 75 (Whatman, 142 mm Φ, pore size 0.3 µm). Samples were stored at -80°C and will be used for shore based molecular and carbon isotopic analysis of microbial membrane lipids as well as DNA-based phylogenetic analyses. In total, the water column was investigated and sampled for organic geochemical investigations at eight sites. An overview on water samples taken by Niskin bottles, particulate matter samples filtered by ISP deployment and preserved subsamples is given in Table 3.

Table 3: Overview on correlated CTD and ISP samples for organic and inorganic geochemical as well as microbiological analyses taken from the water column during HE449.

CTD-Cast	GeoB	Latitude N	Longitude E	Water depth [mbsl]	Bottle #	Depth [mbsl]	Sample					
							1	2	3	4	5	6
CTD-8	20108_1	76° 52.88	014° 37.25	138.6	3, 6, 9, 12	120, 75, 30, 5	x	x	x	x	x	
CTD-10-1	20110_1	77° 03.16	013° 22.40	438	3	340	x	x	x	x	x	
CTD-10-1	20110_1	77° 03.16	013° 22.40	438	8	80	x	x	x		x	
CTD-10-1	20110_1	77° 03.16	013° 22.40	438	10	30	x	x	x		x	
CTD-10-1	20110_1	77° 03.16	013° 22.40	438	12	5	x	x	x		x	
CTD-10-2	20110_2	77° 03.10	013° 22.71	443.5	1-12	80				x		x
CTD-10-3	20110_3	77° 03.08	013° 22.50	445.7	1-12	30				x		x
CTD-10-4	20110_4	77° 03.12	013° 22.95	441.6	1-12	5				x		x
CTD-12	20112_1	76° 40.81	018° 49.48	62.8	1, 6, 10	55, 20, 5					x	
CTD-13	20113_1	76° 38.88	018° 03.60	240.5	2, 3, 4, 8	236, 200, 175, 75					x	
CTD-25	20125_1	77° 38.63	014° 14.22	159.4	3, 5, 10, 12	140, 110, 20, 5	x	x	x	x	x	
CTD-29-1	20129_1	77° 45.07	015° 01.36	108.7	3, 5, 20, 12	80, 65, 20, 5	x	x	x	x	x	
CTD-29-2	20129_3	77° 45.08	015° 01.38	108.6	1-12	65						x
CTD-29-3	20129_4	77° 45.07	015° 01.16	107.6	1-12	20						x
CTD-29-4	20129_5	77° 45.09	015° 01.09	108.2	1-12	5						x
CTD-38	20138_1	78° 25.01	015° 58.41	186.4	3, 7, 10, 12	165, 70, 20, 5	x	x	x	x	x	
CTD-39	20139_1	78° 35.71	016° 31.01	157.8	3, 8, 10, 12	120, 40, 20, 5	x	x	x	x	x	
ISP-Cast	**GeoB**	**Latitude N**	**Longitude E**	**Water depth [mbsl]**	**Pump**	**Depth [mbsl]**	**Volume [L]**					
ISP-1	20108_2	76° 53.10	014° 37.45	126.3	Ginger	5	197.34					
					Fred	30	579.03					
					Norbert	75	587.76					
					Jochen	120	513.2					
ISP-2	20110_5	77° 03.01	013° 22.73	444.7	Ginger	5	201.74					
					Fred	30	289.75					
					Norbert	80	627.73.					
					Jochen	340	749.16					
ISP-3	20112_3	76° 40.77	018° 49.62	64.1	Norbert	20	108.6					
					Jochen	50	526.52					
ISP-4	20113_2	76° 38.92	018° 03.66	240.8	Norbert	30	325					
					Fred	185	608.8					
					Jochen	225	396.94					
ISP-5	20125_2	77° 38.67	014° 14.26	159.2	Ginger	5	173.26					
					Fred	20	391.94					
					Norbert	110	802.6					
					Jochen	140	634.13					

ISP-6	20129_2	77° 45.09	015° 01.46	109.5	Ginger	5	124.71
					Fred	20	219.74
					Jochen	65	391.32
					Norbert	80	418.4
ISP-7	20138_2	78° 25.00	015° 58.57	186.5	Ginger	5	127.49
					Fred	20	242.03
					Jochen	60	394.72
					Norbert	165	637.68
ISP-8	20139_2	78° 35.94	016° 31.85	155.3	Ginger	5	69.45
					Fred	20	322.64
					Jochen	40	502.36
					Norbert	120	614.86

Incubation experiments

For determination of Thaum- and Euryarchaeal activity associated with different water masses, large volume water samples (10 L) were filled into 20 L glass schott bottles for on board incubation experiments with different types of substrates. For each experiment 3 different water depths were sampled in triplicate. Each of the three bottles with water from a distinct water depth was amended with a different substrate. For each water depth the first bottle was treated with 0.296 MBq $^{14}C_3$-Leucine, to the second bottle 1.23 MBq ^{14}C-Bicarbonate was added and the third bottle was incubated as a control without any additional substrate. Incorporation of substrates into total biomass was monitored on board by daily subsampling of 10 mL from each bottle and filtration of the material on 0.1 µm poresize Durapore membrane filters (Merck Millipore Ltd) and subsequent rinsing of extracellular radioactive material from the filters with 10 mL PBS:MilliQ (v:v; 10:90). The ^{14}C content of the material on the filters was then measured, by addition of a liquid scintillation counting cocktail (Ultima Gold, Perkin Elmer), with a Hidex liquid scintillation counter, counting for 15 minutes per sample. The experiments were harvested after 5 days of incubation by filtration on polyethersulfone (PES) membranefilters (Sartorius Stedim Biotech; pore size 0.1 µm), which were immediately stored frozen at -80°C for shore based analysis of specific uptake into archaeal biomarker lipids. A schematic of the setup for each water depth can be seen in Figure 33.

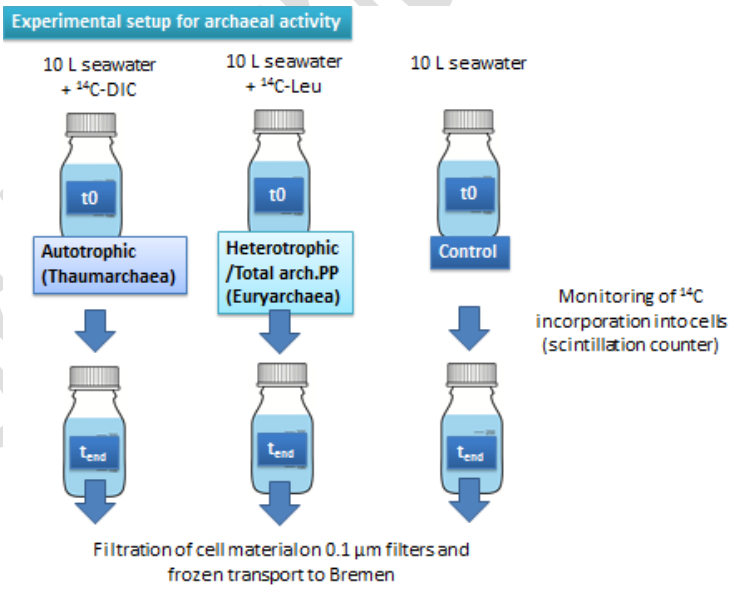

Fig. 33: Scheme of experimental setup for radiotracer incubation experiments.

The measurements of intermediate time-points during the experiments are displayed in Figures 34 and 35. These show good incorporation of $^{14}C_3$-Leucine derived ^{14}C into total biomass for both experiments, with maximum counts of 7408 and 5449 for the first (Exp. 1) and second experiment (Exp. 2), respectively. ^{14}C-Bicarbonate incorporation was, as expected, much lower and showed maximum counts of 54 for Exp. 1 and 45 for Exp. 2. The controls as natural background signal stayed

at around 30 counts throughout the two experiments. Nitrite concentrations increased in Exp. 1 by about 20 µM, while there was no detectable increase during the incubation of Exp. 2. Differences between the two experiments were also observable between individual depths, since, for Exp. 1 leucine incorporation was highest for the sample from 30 m water depth, whereas, for Exp. 2 highest counts were observable for the 5 m water depth sample. Differences in bicarbonate incorporation were not as distinct between individual depths, as were nitrite contents in the distinct water samples.

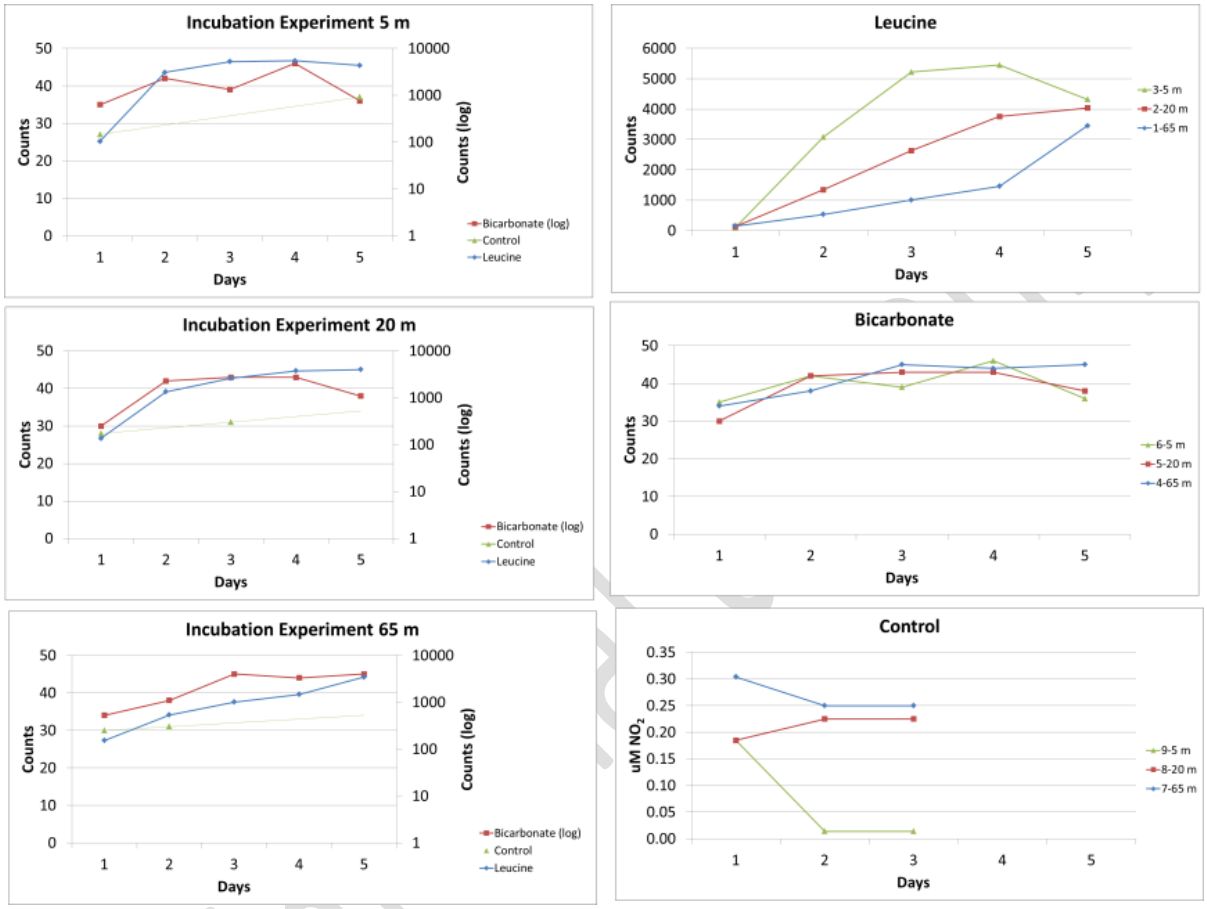

Fig. 34: On board measurements of ^{14}C incorporation into total biomass and nitrite production in the control for the first experiment.

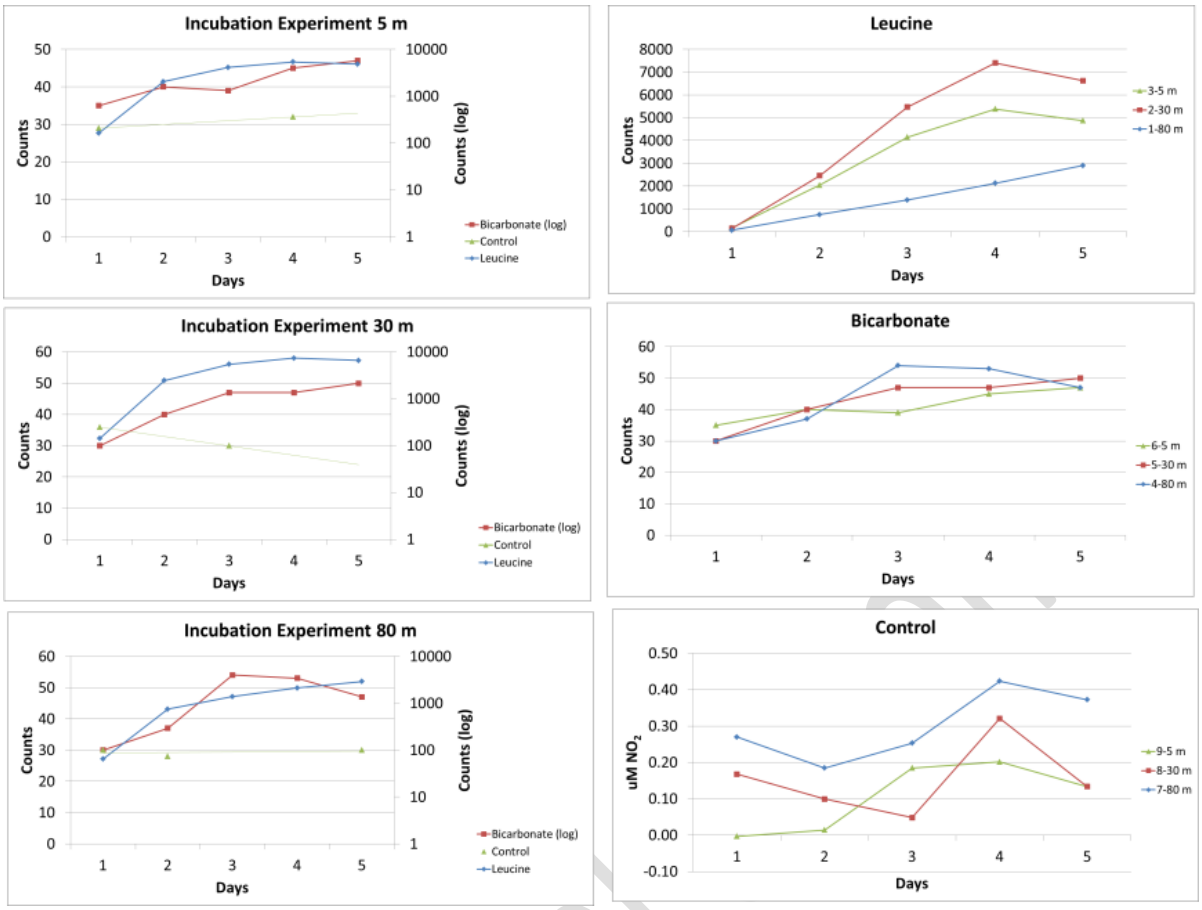

Fig. 35: On board measurements of ^{14}C incorporation into total biomass and nitrite production in the control for the second experiment.

5 Seafloor Sampling

(A. Lichtschlag, I. Bussmann, N. Goldenstein)

To address the depositional and biogeochemical processes in the sediments, especially their potential of methane oxidation, sediment samples for geochemical and biological analyses were taken off the southern and west coast of Svalbard. Oxygen and pH profiles were measured in the retrieved sediment cores. This was done at different locations inside and outside (shelf) different fjords (Hornsund, Storfjorden, Bellsund, Van Mijenfjorden, Billefjorden, Table 4). Sediments were obtained with a Multicorer (MUC) (Fig. 36A) to collect approximately the upper 20-40 cm of the seafloor sediments (Fig. 36B, C). From each station one sediment core was used for pore-water extraction (5.1), one core for oxygen uptake measurements (5.2), one core was sampled for geochemical analyses (5.3) and another core for biomarker analyses (5.4).

Table 4: Overview of sampling locations (MUCs).

Event	GeoB St. No.	Location Name	Latitude N	Longitude E	Water Depth (m)
MUC-1_1 MUC-1_2	20105-2 20105-3	Hornsund Shelf	76° 52.82 76° 52.83	014° 37.12 014° 37.29	137.5 138
MUC-2_1 MUC-2_2	20110-6 20110-7	N-Hornsund Basin	77° 03.20 77° 03.10	013° 22.08 013° 22.55	441.6 443.8
MUC-3_1 MUC-3_2	20111-2 20111-3	Storfjorden - West	76° 38.90 76° 38.89	018° 03.76 018° 03.73	242.3 242.2
MUC-4_1 MUC-4_2 (gravel, no samples taken)	20112-6 20112-7	Storfjorden - Ridge	76° 40.7s5 76° 40.88	018° 49.65 018° 49.95	65 61.2
MUC-5	20116-2	Hornsund Flare area	76° 47.54	014° 09.73	127.2
MUC-6_1 MUC-6_2	20125-3 20125-4	Bellsund	77° 38.66 77° 38.63	014° 13.98 014° 14.12	158.7 159.1
MUC-7_1 MUC-7_2 MUC-7_3	20129-6 20129-7 20129-8	Van Mijenfjorden	77° 45.08 77° 45.08 77° 45.10	015° 01.58 015° 01.38 015° 01.52	108.3 108.3 109
MUC-8	20130-3	Van Mijenfjorden	77° 45.15	014° 48.50	109.8
MUC-9_1	20138-3	Billefjorden Entrance	78° 24.98	015° 58.40	186.8
MUC-10_1	20139-3	Billefjorden	78° 35.69	016° 30.40	162.9

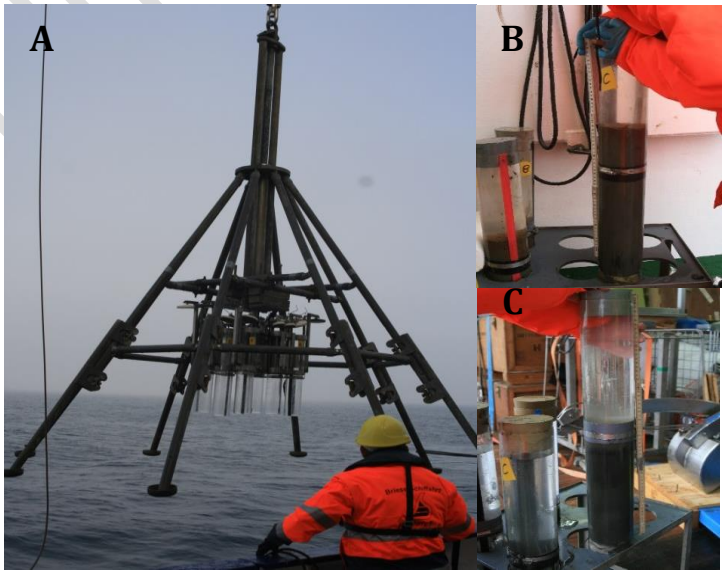

Fig. 36: MUC sampling (A) and 2 examples of retrieved sediments (B, C).

5.1 Pore Water and Element Sampling

Immediately after retrieval, one MUC sediment core was transported into a controlled temperature (CT) room cooled to 6.5 °C. Pore-water was extracted from sediments directly with Rhizons (Rhizon CSS: length 5 cm, pore diameter 0.2 µm; Rhizosphere Research Products, Wageningen, Netherlands) inserted though pre-drilled holes in the MUC liners and connected to a syringe on which a small under-pressure was applied. For each MUC station samples were collected at 1 cm intervals the first 10 cm and at 2 cm intervals below. Aliquots of pore-water were collected for cations (2 mL), DIC / $\delta^{13}C_{DIC}$ (2 mL), nutrients (2 mL), and total alkalinity (0.5 mL).

Total alkalinity was determined on board by titration against 0.0004 mol L^{-1} HCl using a mixture of methyl red and methylene blue as an indicator. Analyses were calibrated against the IAPSO seawater standard. The cation samples were acidified (5 µL of conc. suprapure HNO_3) for later analyses by ICP-MS/ICP-OES. DIC and $\delta^{13}C_{DIC}$ samples were poisoned with saturated $HgCl_2$ (5 µL) to prevent further microbial turnover. Remaining pore-water was frozen at -20 °C for nutrient analyses.

5.2 Oxygen Uptake

Oxygen measurements were performed on retrieved MUCs to determine diffusive oxygen uptake and oxygen penetration depth in the sediments. The oxygen concentration at the sediment-water interface and surface layers of the sediment were access by using needle-type fiber-optical oxygen microsensors (OXR50-OI, PyroScience©). Oxygen penetration depth was in general less than 1 cm. The measurements were performed in 100 µm resolution and a total length of up to 2 centimeters. An example of an oxygen profile from measurements in MUCs can be found in Figure 37.

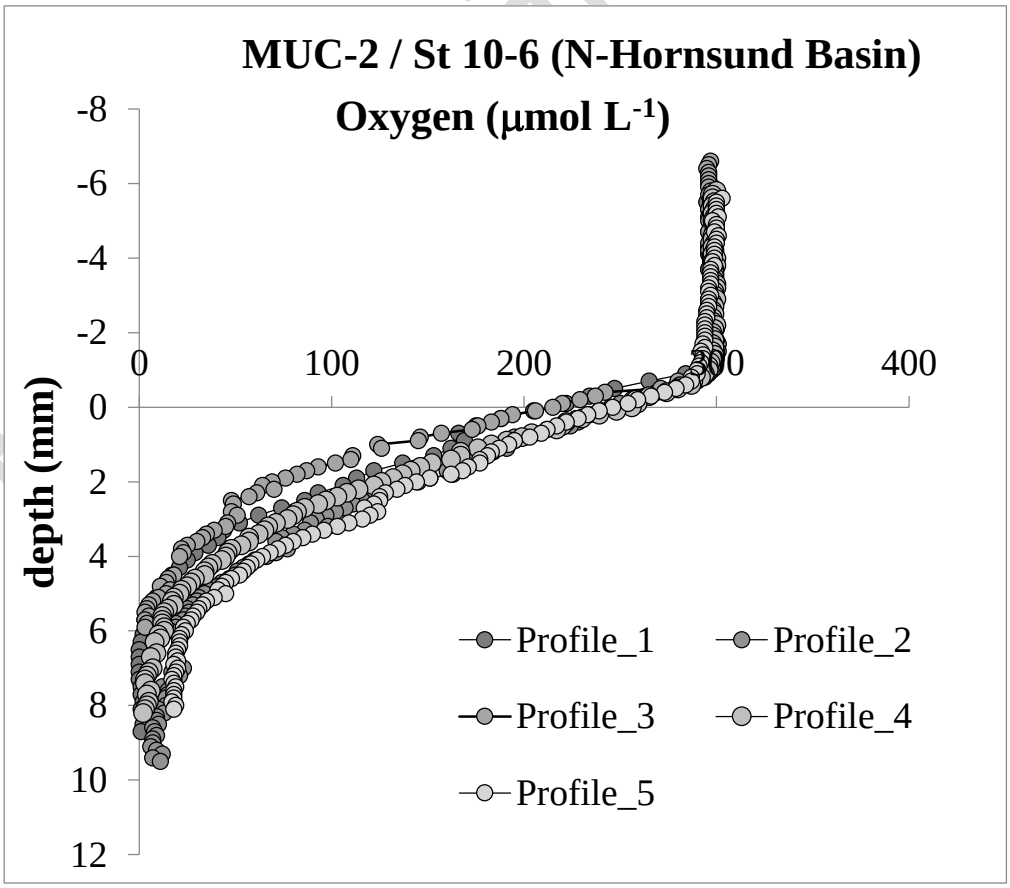

Fig. 37: Oxygen concentration profiles measured in sediments retrieved with the MUC.

5.3 Sediment Sampling

An additional MUC sediment core was taken und cut into 1 cm sections the upper 10 cm and 2 cm sections below. A subsample of these sediments was frozen into a plastic bag for solid phase metals and CNS (carbon, nitrogen, sulphur) analysis at -20°C and another subsample was placed in a pre-weighed pot for a measurement of porosity and sedimentation rates, and a measurement of pH was made on these samples. To determine the methane concentration in the sediment exactly 3 mL of sediments was placed in glass vials filled with 5 mL 1M NaOH, immediately crimped sealed, placed on a shaker overnight and the methane concentrations were measured on board with a Agilent 6890N GC.

From the sediment surface (3 x 1 mL) and from the overlaying water, samples were taken for later DNA analyses and for immediate determination of the methane oxidation rate. This was done at all MUC stations except MUC 7. First results indicate that the fractional turnover-rate of the methane oxidation increases by one order of magnitude from surface sediment towards the overlying water and towards the water column.

In addition to MUC samples, some grab samples were retrieved to test if sediments are suitable for MUC sampling; grabs were not subsampled or used for further analyses.

5.4 Biomarker Sampling

To be able to correlate biomarker abundances with geochemical measurements from the sediment cores, at each station, one MUC sediment core was sliced in 1 cm sections for the top 10 cm and in 2 cm sections for the rest of the core below. The individual sections were placed in sample containers and stored at -80°C for transport and subsequent shore based organic geochemical as well as phylogenetic analyses.

6 Hydroacoustic Work

(M. Römer, S. Gaide, N. Brückner, E. Falck)

In total, 46 surveys for hydroacoustic mapping have been performed during HE449. The surveys were consecutively numbered but do not correspond to individual days. A new survey number was given when interrupted by station work and/or a different purpose for mapping was followed.

Data was acquired simultaneously with different ship-mounted echosounders, which are described in the following subchapters: multibeam echosounder EM710 (6.1), fishechosounder EK60 (6.2), subbottom profiler SES2000 (6.3) and ADCP (6.4). Depending on the purpose and cruise planning, the vessel speed was adjusted. During transit, data was also recorded with up to 10-12 knots, which resulted reduced data quality but depending on the weather condition and sea state, the data was still useful and in most cases even sufficient for flare mapping. However, when time allowed, the speed was reduced for detailed mapping to 5-6 knots to ensure best results.

Four roughly defined geographical areas were mapped (Storfjorden, Hornsund, Bellsund and Isfjorden) and shown in different colours in Figure 38 and Table 5 showing a summary of the hydroacoustic surveys, which are described further in the subchapters.

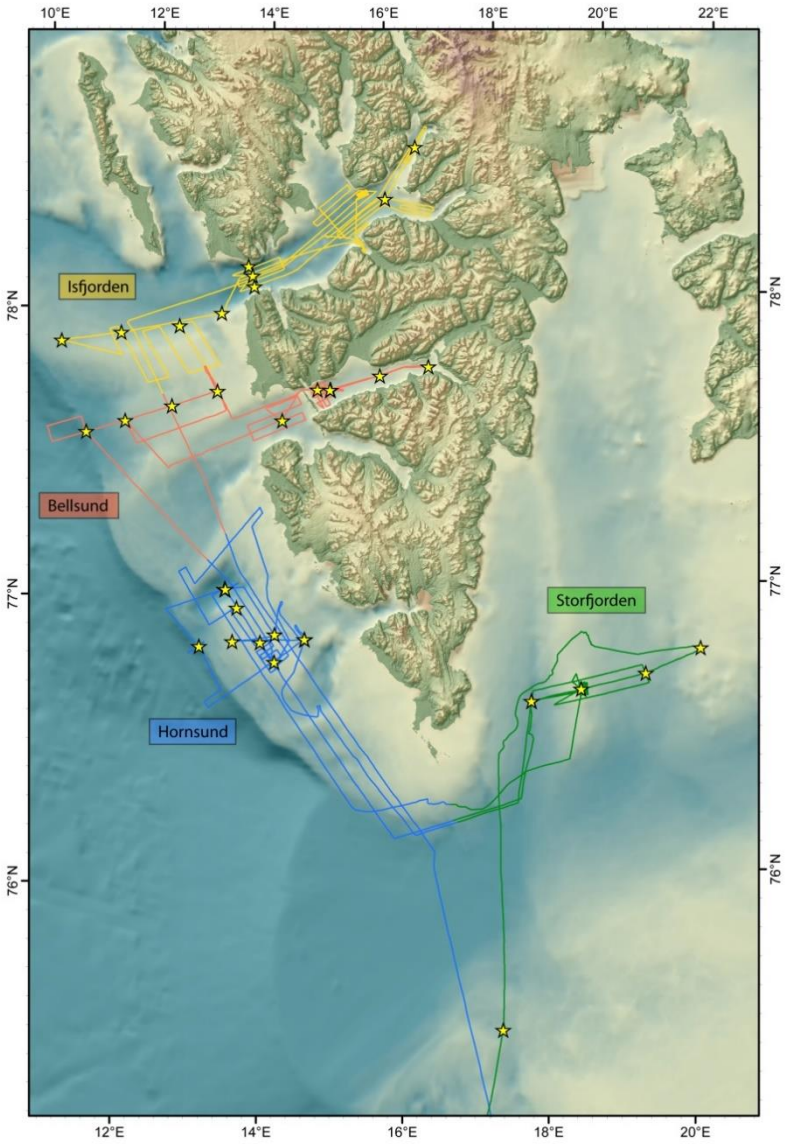

Fig. 38: Overview of the hydroacoustic surveys acquired during HE449 grouped in four areas illustrated in different colours. Stations are shown as stars.

Table 5: Hydroacoustic survey list during HE449. The colours agree with the different geographical areas shown in Figure 38.

Survey	Speed	Purpose	Findings
1	10 kn	Transit	9 Flares
2	10 kn and slower	Was planned as transit to ADCP Transect, but had to be replanned due to ice conditions	Numerous flares mainly distributed along the N-S ridge
3	5 kn	From East to West across Storfjorden	Numerous flares mainly distributed along the N-S ridge
4	10 kn	Transit from Storfjorden to Hornsund	Several flares northwest of the Storfjorden fan on the SW area of Svalbard
5	10 kn	Transit between the two CTD-Stations, filling two hours, searching for an entrance through ice to the Hornsund (without success)	No flares, but need to be checked
6	5 kn	Transit between the two CTD-Stations, filling 2,5 hours, moving slowly instead of surveying another line	No flares
7	10 kn	Straight line back to Station 5 (now 8), not enough time to move slowly	No flares
8	6 kn	Long line across the shelf down to 1000 m water depth	Flare area in ~100 m depth detected
9	6 kn	Mapping along the shelf break	No flares
10	5 / 10 kn	Mapping the flare area	Huge amount of strong flares clustering in groups
11	10 kn	Transit from Hornsund area to Storfjorden	Two anomalies in EK60, need to be checked in EM710
12	5 km	Mapping flares in an area of 4 x 5 km	Lots of flares, all relatively weak, locations do not correspond to those detected during Survey 03
13	8 kn	Line between Station West of the ridge to the flare area	Probably some weak flares, need to be checked
14	1-2 kn	Recording during UWMS deployment	3-4 flares detected, but weak and not visible in UWMS measurement
15	6 kn	Mapping shallowest point of the ridge, and two long W-E lines over the ridge	Many small and weak flares
16	8 kn	Line between mapped flare area and Station 13, West of the Ridge	Some weak flares
17	10 kn	Transit from Storfjorden to Hornsund	Anomalies in EK60, need to be checked in EM710
18	6 kn	Flare mapping at the Hornsund Flare area	A few further flares detected around the main flare area
19	1.5 kn	During UWMS deployments (two times the same track line)	Numerous strong flare clusters along the track for the two UWMS deployments
20	0 - 10 kn	During CTD, BG and MUC deployments in the main flare fields and short transit to the next CTD northwest of it	Intensive flare observations during the station work
21	6 kn	Transit between two CTD-Stations, parallel line	Check for flares in EM710, but nothing in EK60

22	6 kn	Nightsurvey searching for flares	Several flares, south and north of the deep basin and on the ridge between the deep basin and the Bellsund trough
23	1.5 kn	UWMS deployments 3 and 4	Very strong flare clusters at same locations as already known
24	10 kn	Transit from Hornsund Flare area to first CTD station in front of Bellsund, with one last line parallel at the Hornsund shelf and crossing the northern deep basin	Several flares at the Hornsund shelf and also flare clusters south and north of the deep basin
25	6 kn	Long transects across the shelf in front of Bellsund	No flares
26	6 kn	Along the transect on the shelf between Stations 22 and 23	No flares
27	6 kn	Along the transect on the shelf between Stations 23 and 24	An relatively strong flare cluster detected close to St. 23
28	10 kn	From the shelf to the entrance of Bellsund	Some small anomalies in EK60, which need to be checked in EM710
29	6 kn	Flare survey within Bellsund	No flares
30	Changing	During the day transits from station to station through the Van-Mijenfjorden from W to E	One flare close to St. 26
31	10 kn	From the easternmost station in the Van Mijenfjorden to the westernmost	Two flares recorded
32	6 kn	Mapping grid of 3 lines covering the area behind the island in the VanMijenfiorden	A few weak flares around St. 26 and 30
33	6 kn	Additional line within the grid of Survey 32, to fill time between the two close stations	No flare, only an anomaly in EK60 need to be checked
34	10 kn	Transit from Van Mijenfjorden to Isfjorden	No flares, but nice backscatter features
35	6 kn	Transects crossing elevation height and small trench	Flares along the nothern wall of the trench
36	6 kn	Transits between stations	Several weak flares
37	10 kn	From St. 34 to Longyearbyen	Occasional weak flares
38	6 kn	Isfjorden mound structure	Several flares in the surrounding area of the mound structure
39	6 kn	Transects at the entrance of the Isfjorden	Several flares at the eastern slope of a basin
40	6 kn	Transit between stations	No flares
41	10 kn	Transit from Isfjorden to Sassenfjorden	Occasional weak flares
42	6 kn	Mapping of the Sassenfjorden	No flares at the Sassenfjorden, but flares on the transit to station 38
43	6 kn	Transit between stations	Pockmarks but no obvious flare
44	6 kn	Mapping of the Billefjorden	No flares
45	6 kn	Mapping of flare area between Adventfjorden and Sassenfjorden	Clustering of flares
46	10-12 kn	Transit from Longyearbyen to end of working area, along additional lines for flare mapping	Further confirmation of flares at the known areas

6.1 Multibeam Echosounder EM710

6.1.1 Multibeam Bathymetry

(S. Gaide)

The hull-mounted 1-by-2 degree multibeam echosounder (MBES) EM710 from MARITIME KONGSBERG on R/V HEINCKE was used to conduct bathymetric surveys and to visualize the water column. The EM710 operates with 200 beams at sonar frequencies between 70 and 100 kHz. Though the maximum limit is at a water depth of 2000 m, the best performance can be observed at depths less than 1000 m. Since one of the main objectives during surveying time was to detect gas emissions, the ping mode of the EM710 was set manually from shallow to very shallow depths to have a high resolution image of the water column at all times. For the reduction of noise that influences the outer beams, the extent of the swath was mainly set to 60° by 60° degrees. Though the sea state was very good, interferences coming from the SES2000 and the ADCP that were recorded at the same time, are clearly visible in the bathymetry and especially in the water column data. The multibeam processing was carried out by using the open-source software package MB-System 5.5.2252 with the newly implemented version of GMT 5.1.2 (Caress and Chayes, 1996). For this purpose the KONGSBERG .all RAW format had to be converted into the editable .m59 format. Manual line-by-line cleaning of the swath soundings has been done during the cruise with the 3-D editor mbeditviz. The bathymetry and the backscatter data was then gridded by using mbgrid. Even though SVPs were directly implanted during the cruise at some surveys a manual correction had to be applied in MB-system by using mbset due to the quick velocity changes that occur in the fjord areas (see chapter 6.1.2 Sound Velocity).

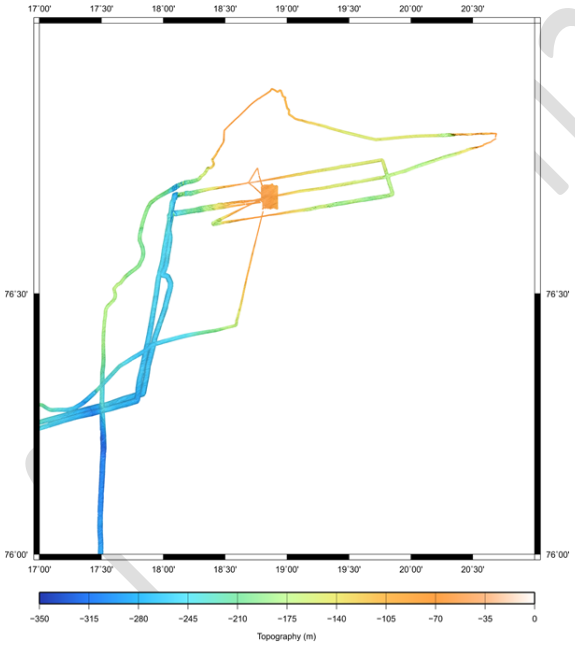

Fig. 39: Bathymetry data of the Storfjorden area.

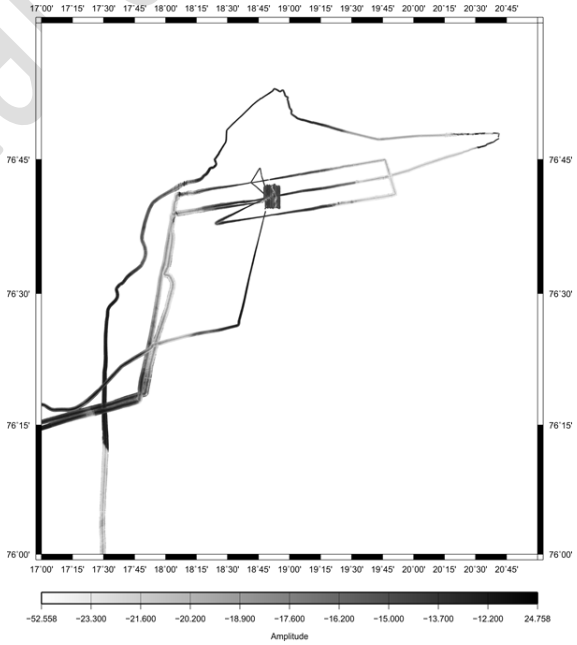

Fig. 40: Backscatter data of the Storfjorden area.

Storfjorden

The bathymetry of the Storfjorden area (Fig. 39) mainly consists of an elevated high in the centre and a ~ 70 m high ridge at the western shelf of Svalbard. Various iceberg scars are prominent throughout the area with a general NE/SW elongation. The backscatter image (Fig. 40) shows abrupt changes between low and high backscatter especially near fault zones and at higher depths.

Hornsund

The bathymetry of the Hornsund area (Fig. 41) displays the shelf in front of entrance to the Hornsundfjorden. The area is relatively flat with the exception of one deeper part in the western part of the area. The area has predominantly a high backscatter with low backscatter patches at the Hornsund flare area (Fig. 42) and a general low backscatter at higher depths.

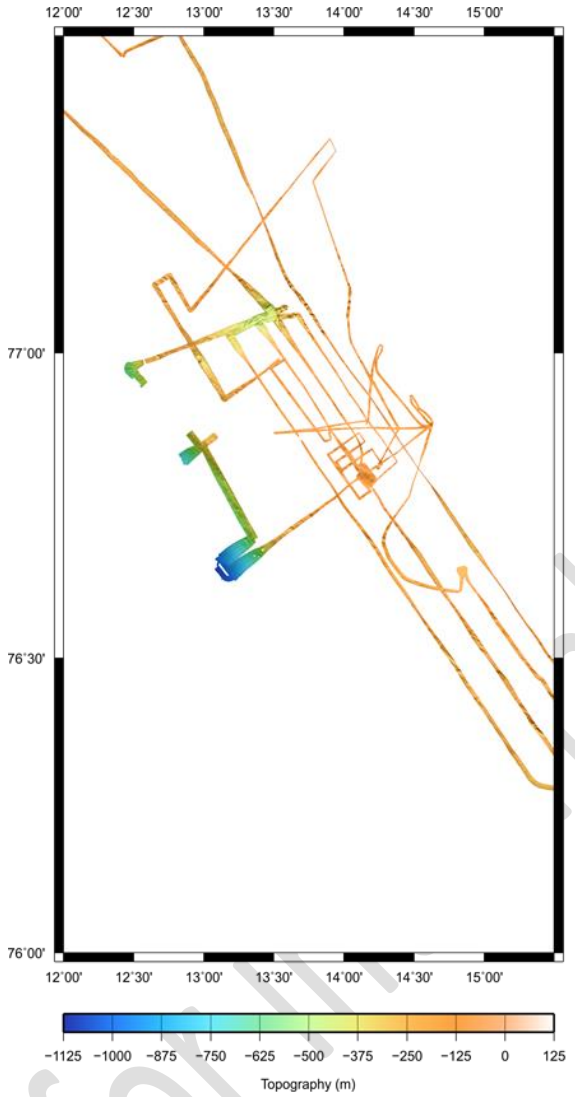

Fig. 41: Bathymetry of the data acquired on the shelf close to Hornsund.

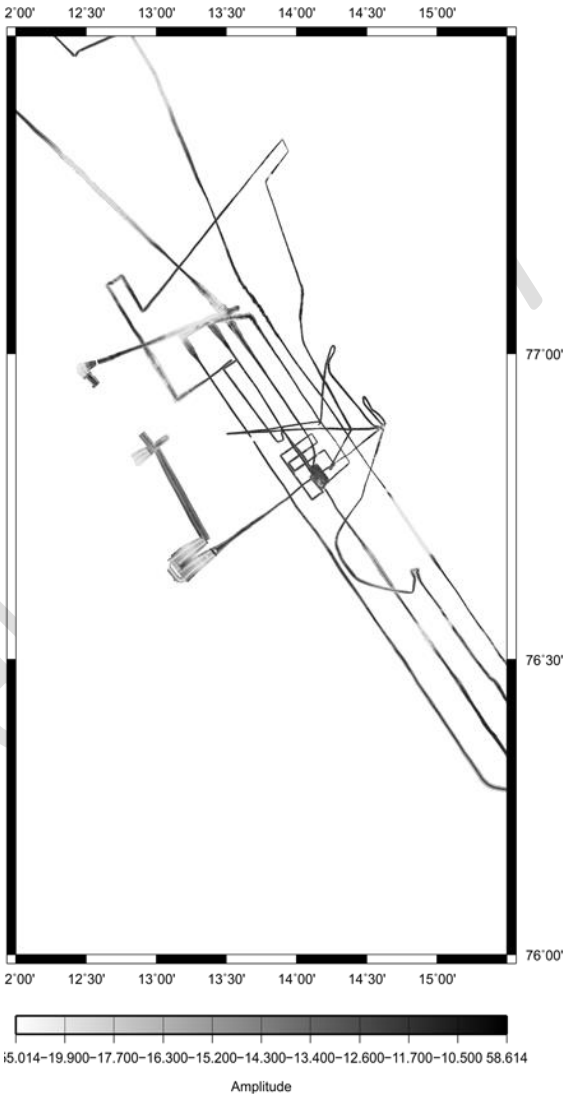

Fig. 42: Backscatter of the data acquired on the shelf close to Hornsund.

Bellsund

The bathymetry at the Bellsund is also relatively flat with iceberg scars along the slope (Fig. 43). A few pockmarks are visible, especially in the Van Mijenfjorden, at the researched flare site. The backscatter of the Bellsund is like at the Hornsund generally high, with the exception of lower backscatter patches in the north (Fig. 44), while the backscatter in Van Mijenfjorden is mostly low.

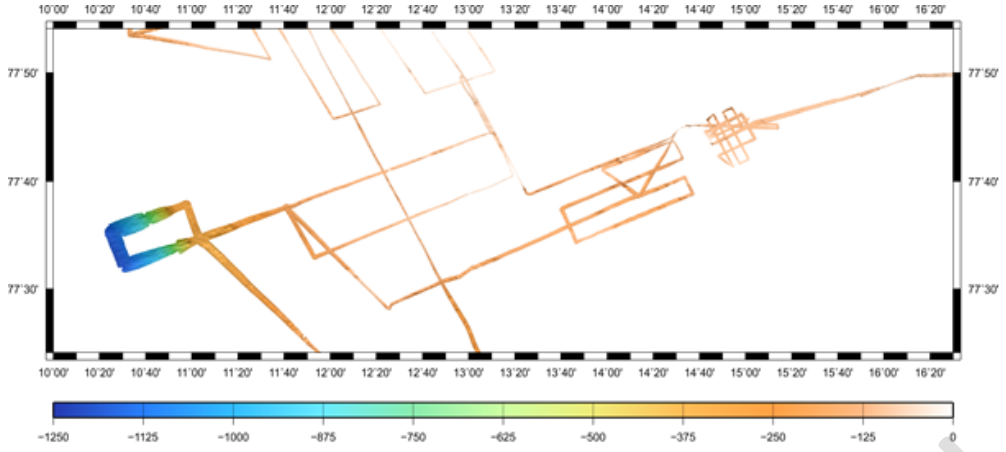

Fig. 43: Bathymetry data of the Bellsund area including the Van Mijenfjorden.

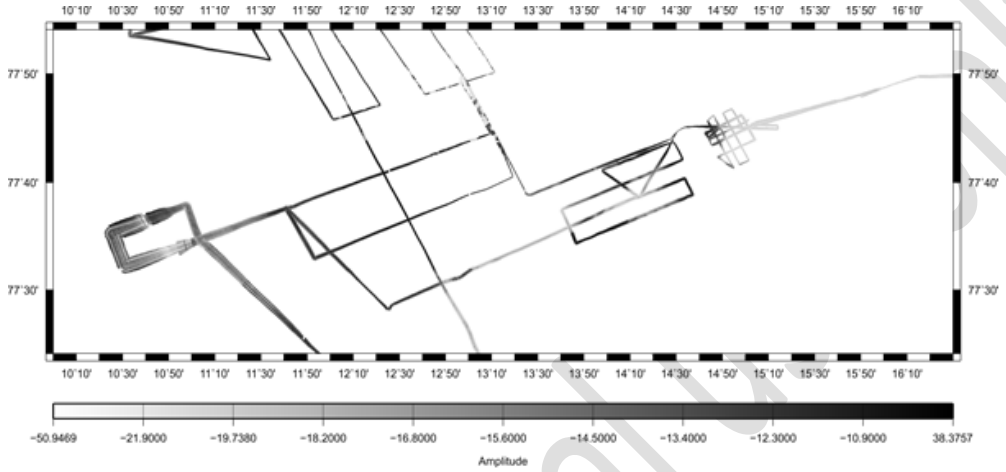

Fig. 44: Backscatter data of the Bellsund area.

Isfjorden

The bathymetry of the Isfjorden is in contrast to other research areas relatively diverse, with ridges in the north and deeper areas in the south (Fig. 45). Pockmarks occur along the outer and inner fjord especially at the northern part of the fjord. Also the backscatter changes inside the Isfjorden (Fig. 46), with high backscatter in the north and low backscatter in the south. Quick changes in backscatter occur mostly along the northern rim of the deeper parts of the fjord.

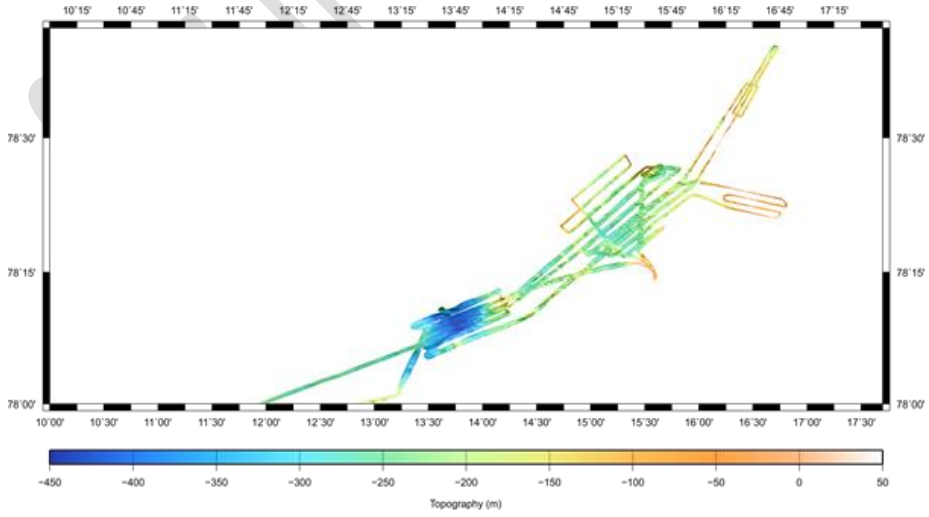

Fig. 45: Overview of the bathymetric data acquired in the Isfjorden area.

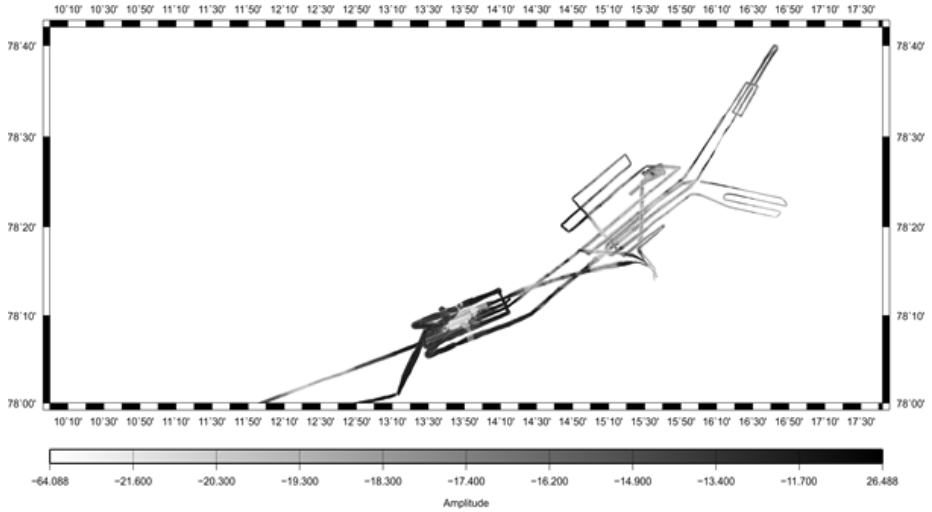

Fig. 46: Overview of the backscatter data acquired in the Isfjorden area.

6.1.2 Sound Velocity

(N. Brückner)

In order to guarantee high quality bathymetric maps, obtaining accurate sound velocity profiles (SVP) is essential. On board of the R/V HEINCKE, SVPs can be obtained by deploying the Sound Velocity Probe (see Fig. 47) or calculating them from available CTD data.

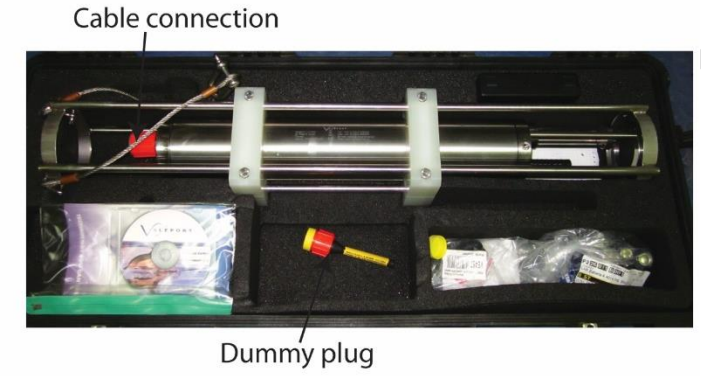

Fig. 47: Image of the sound velocity probe on R/V HEINCKE.

The first station of the cruise was used for a CTD-SVP correlation showing equivalent values (Fig. 48). Thus, it was decided to acquire all SVP through manually calculating profiles derived from conductivity, temperature and depth values by using the UNESCO-formula (Wong and Zhu, 1995). This proved to be a time-saving approach, because no extra instrument had to be deployed at each station.

$$c(S,T,P) = C_W(T,P) + A(T,P)\cdot S + B(T,P)\cdot S^{3/2} + D(T,P)\cdot S^2 \quad (7)$$

With the parameters C_W, A, B, D coming from a series expansion which is dependent on the temperature, pressure and the specific coefficients C_{ij}, A_{ij}, B_{ij} and D_{ij}.

$$\begin{aligned} C_W(T,P) = {} & (C_{00} + C_{01}\cdot T + C_{02}\cdot T^2 + C_{03}\cdot T^3 + C_{04}\cdot T^4 + C_{05}\cdot T^5) \\ & + (C_{10} + C_{11}\cdot T + C_{12}\cdot T^2 + C_{13}\cdot T^3 + C_{14}\cdot T^4)\cdot P \\ & + (C_{20} + C_{21}\cdot T + C_{22}\cdot T^2 + C_{23}\cdot T^3 + C_{24}\cdot T^4)\cdot P^2 + (C_{30} \\ & + C_{31}\cdot T + C_{32}\cdot T^2)\cdot P^3 \end{aligned} \quad (8)$$

$$A(T,P) = (A_{00} + A_{01}\cdot T + A_{02}\cdot T^2 + A_{03}\cdot T^3 + A_{04}\cdot T^4 + A_{05}\cdot T^5) + (A_{10} + A_{11}\cdot T + A_{12}\cdot T^2 + A_{13}\cdot T^3 + A_{14}\cdot T^4)\cdot P + (A_{20} + A_{21}\cdot T + A_{22}\cdot T^2 + A_{23}\cdot T^3 + A_{24}\cdot T^4)\cdot P^2 + (A_{30} + A_{31}\cdot T + A_{32}\cdot T^2)\cdot P^3 \quad (9)$$

$$B(T,P) = B_{00} + B_{01}\cdot T + (B_{10} + B_{11}\cdot T)\cdot P \quad (10)$$

$$D(T,P) = D_{00} + D_{10}\cdot P \quad (11)$$

Where T is the temperature [°C], S is the salinity [ ] and P is the pressure [bar].
The formulas (8), (9), (10) and (11) will be completed with the following coefficients.

$C_{00} = 1402.388$
$C_{01} = 5.03830$
$C_{02} = -5.81090 \cdot 10^{-2}$
$C_{03} = 3.3432 \cdot 10^{-4}$
$C_{04} = -1.47797 \cdot 10^{-6}$
$C_{05} = 3.1419 \cdot 10^{-9}$
$C_{10} = 0.153536$
$C_{11} = 6.8999 \cdot 10^{-4}$
$C_{12} = -8.1829 \cdot 10^{-6}$
$C_{13} = 1.3632 \cdot 10^{-7}$
$C_{14} = -6.1260 \cdot 10^{-10}$
$C_{20} = 3.1260 \cdot 10^{-5}$
$C_{21} = -1.7111 \cdot 10^{-6}$
$C_{22} = 2.5986 \cdot 10^{-8}$
$C_{23} = -2.5353 \cdot 10^{-10}$
$C_{24} = 1.0415 \cdot 10^{-12}$
$C_{30} = -9.7729 \cdot 10^{-9}$
$C_{31} = 3.8513 \cdot 10^{-10}$
$C_{32} = -2.3653 \cdot 10^{-12}$
$A_{00} = 1.389$
$A_{01} = -1.262 \cdot 10^{-2}$
$A_{02} = 7.166 \cdot 10^{-5}$
$A_{03} = 2.008 \cdot 10^{-6}$
$A_{04} = -3.21 \cdot 10^{-8}$
$A_{10} = 9.4742 \cdot 10^{-5}$
$A_{11} = -1.2583 \cdot 10^{-5}$
$A_{12} = -6.4928 \cdot 10^{-8}$
$A_{13} = 1.0515 \cdot 10^{-8}$
$A_{14} = -2.0142 \cdot 10^{-10}$
$A_{20} = -3.9064 \cdot 10^{-7}$
$A_{21} = 9.1061 \cdot 10^{-9}$
$A_{22} = -1.6009 \cdot 10^{-10}$
$A_{23} = 7.994 \cdot 10^{-12}$
$A_{30} = 1.100 \cdot 10^{-10}$
$A_{31} = 6.651 \cdot 10^{-12}$
$A_{32} = -3.391 \cdot 10^{-13}$
$B_{00} = -1.922 \cdot 10^{-2}$
$B_{01} = -4.42 \cdot 10^{-5}$
$B_{10} = 7.3637 \cdot 10^{-5}$
$B_{11} = 1.7959 \cdot 10^{-7}$
$D_{00} = 1.727 \cdot 10^{-3}$
$D_{10} = -7.9836 \cdot 10^{-6}$

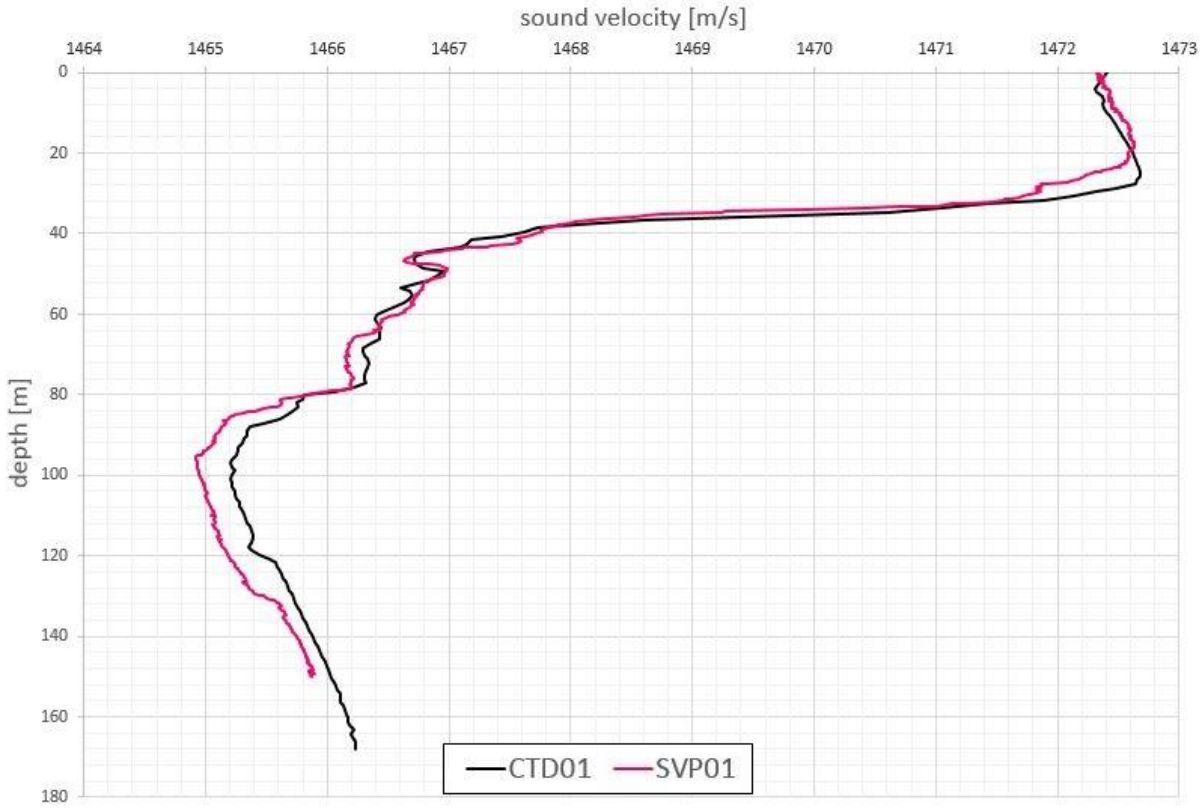

Fig. 48: Correlation of CTD and SVP measurement at the first station.

Values from Sound Velocity Profiles in the working area of HE449 range from 1440 to 1485 m s^{-1}. However, significant changes between specific subareas (Storfjorden, Hornsund, Isfjorden, Isfjorden Shelf, Bellsund, Van Mijenfjorden) were documented. Profiles in Storfjorden showed the slowest sound velocities whereas Bellsund and Hornsund exhibit the highest sound velocity values. Interestingly, narrower fjords like the Van Mijen (CTDs 26-30), Sassenfjorden (38) and Billefjorden (39) each showed a rapid sound velocity decline in the first 60 m which indicates oceanographic separation between the shelf and the fjords.

Calculated SVP were applied either during on-line acquisition by importing them into SIS or during processing in MB-System. SVP-correction highly improved data quality (Fig. 49).

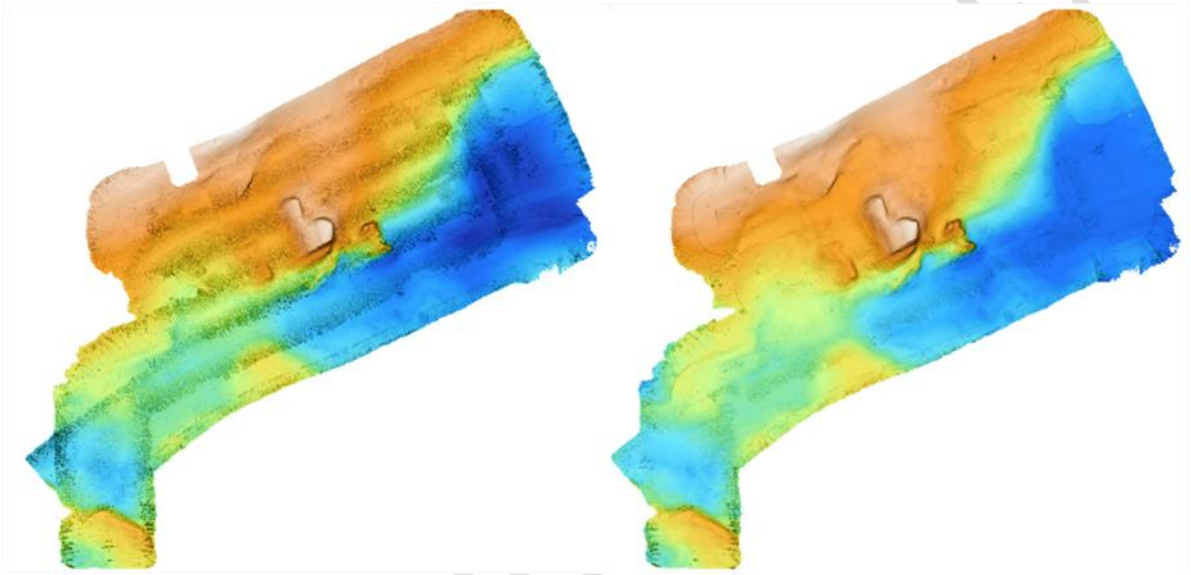

Fig. 49: Example of successful SVP correction. Left: Uncorrected data. Right: Sound velocity corrected data. Especially the outer beams exhibit a smaller bending, leading to an overall smoother surface.

6.1.3 Flare Imaging with EM710

(M. Römer)

Additionally to seafloor mapping, the multibeam Kongsberg EM710 allows to record water column features. Gas emissions become visible as flares, similar to flare observations with the single beam echosounder EK60. The advantage of flare mapping with EM710 is the three dimensional view as an entire volume is mapped with the fan and not only flares exactly below the vessel are recorded. Positioning the sources of flares is, therefore, a lot more precise.

During HE449 the water column data was not implemented in the *.all files produced by SIS but saved individually as *.wcd files. Both is possible, but files become very large when saved together and quick bathymetry processing is a lot easier and faster if the water column information is already stored in a separate file.

For visualization the software package IVS Fledermaus was used, which enables a three dimensional view of the data. In a first step, the FM Midwater tool is needed to open the *.wcd sonar file and convert it to a *.gwc file, which can be displayed in the software. Afterwards the entire three dimensional fan can be exported as an *.sd file and opened with Fledermaus, where it can be replayed

in 3D, for instance, together with the underlying bathymetry. When scrolling through the fan view, source locations of appearing flares can be picked directly with the geo-picking tool. As a last step, the positions have been exported as a table to be displayed in GIS maps for further planning.

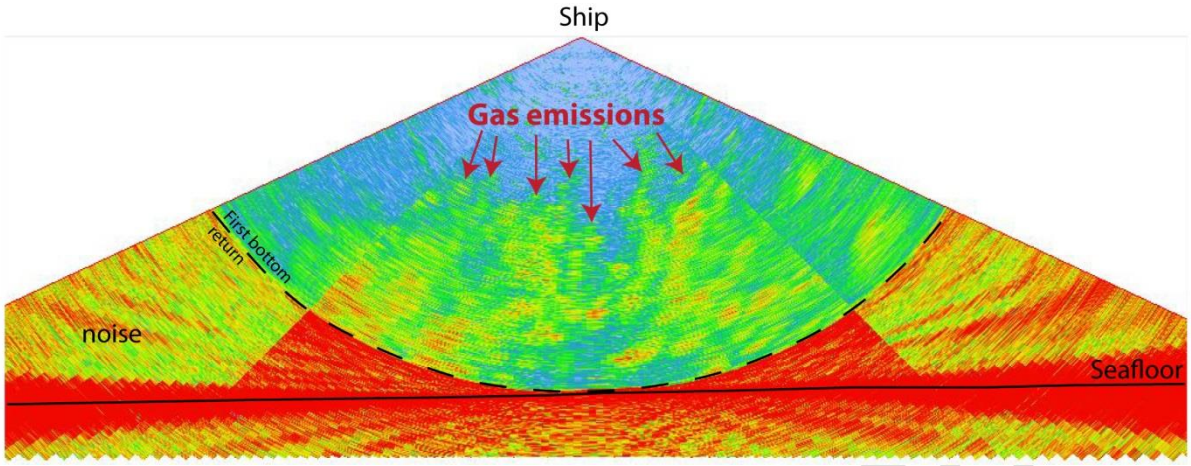

Fig. 50: Example of flares visible in the fan view during recording in FMMidwater tool. Numerous backscatter anomalies in the water column indicate gas emissions. The example was taken from data recorded in the Hornsund flare area.

It is also possible to extract only the anomalies within the fans that make up the flares. For this, the clippings have to be set in FM Midwater in the way that more or less only the flares are still visible and as export option 'export ASCII' has to be chosen. The text file has to be opened as ungridded data within the DMagic tool of the Fledermaus package and converted to a *.pfm file, which again can be imported into the 3D Fledermaus. The single points can now still be edited and flares cleaned manually. The results can be visualized in combination with bathymetric data, tracks or further geographic information available (Fig. 51).

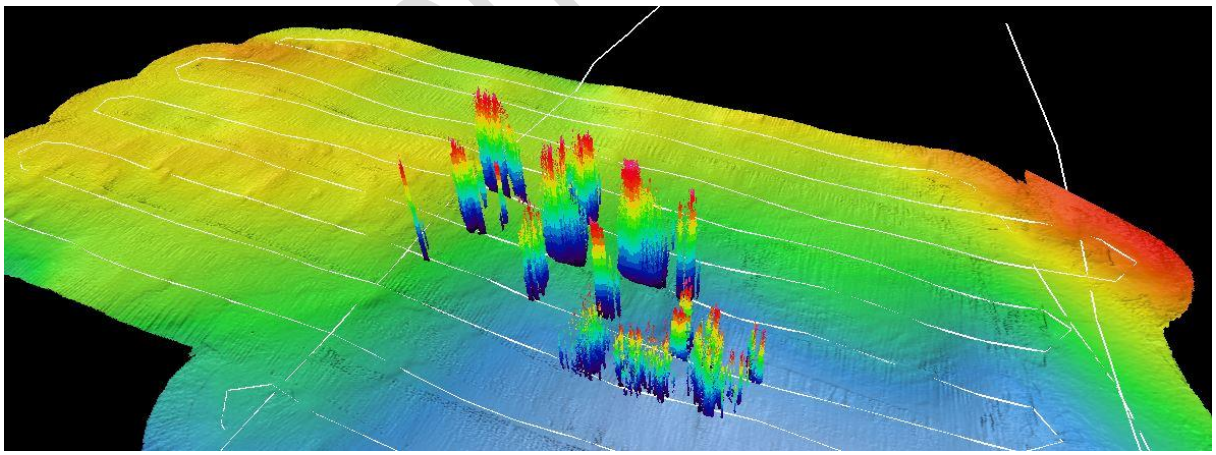

Fig. 51: Extracted flares in the Hornsund area. This area is the most intense gas emission site detected during HE449. Flares occurred in clusters and often reach through the entire water column up to the surface.

Only part of the data could be processed during the cruise and need to be analyzed carefully afterwards. However, a first plot of the flare distribution found is given in Figure 52, whereas white points indicate the online observations of flare locations, which need to be confirmed during the post-processing. Flares have been detected in all four geographically separated areas, both on the shelf and within the two surveyed fjord systems Isfjorden and Van Mijenfjorden.

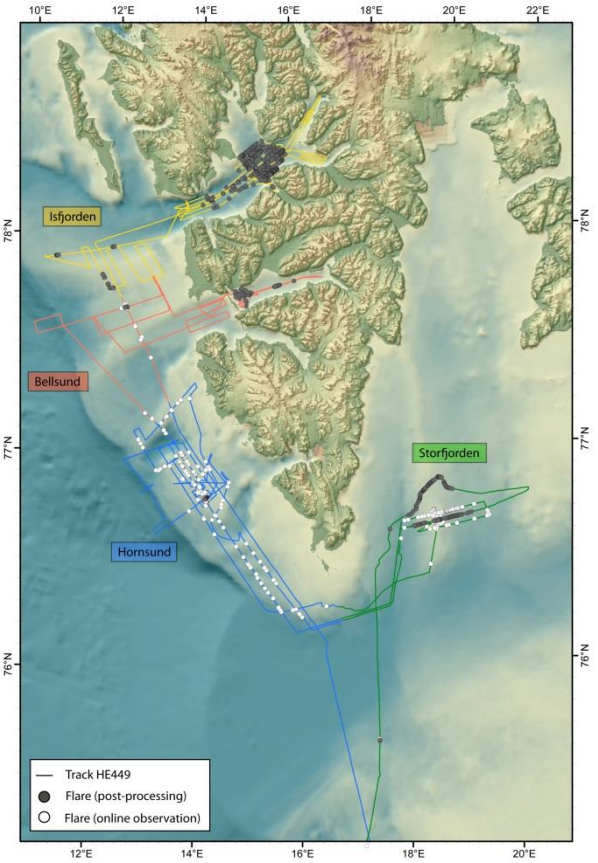

Fig. 52: Map of the flare distribution as detected during HE449 by recording the water column information with the multibeam system EM710.

6.2 Fishechosounder EK60

(M. Römer)

The EK60 system is a split beam scientific echosounder, giving measures of echo strengths of targets within the insonified volume of the beam. The data were visualized using the ER60 software. The footprint of this echosounder is approximately 12% of the water depth. Four frequencies are available: 38 kHz, 70 kHz, 120 kHz, and 200 kHz. However, due to the resonance frequency of gas bubbles rising in the water, the best performance is achieved with 38 kHz. Therefore, only the 38 kHz frequency was recorded during HE449. Electrical power was set to 1000 W, with a pulse duration of 256 µs, a sample interval of 64 µs and a band width of 3.68 kHz. The depth range and the color bar had to be adjusted during the cruise according to the survey area and condition. RAW data were stored with a file size of 100 MB for every *.raw file, in addition, *.idx and *.bot files created. The RAW data folder has a total size of 68.8 GB with 706 *.raw files.

The EK60 recorded data during the entire cruise within the permitted work area without any exception, during surveys, transit, and station work. The system did not have any problems and was running permanently. The range was generally set correctly and no data gap occurred during HE449. The echograms were mirrored to the main work area in the back of the bridge as well as to the dry lab on the main deck. Watch keepers permanently observed the online screen and took screenshots of flares or other interesting features in the water column. Post-processing was not done during the cruise. Flare locations were added online by the watch keeper into the software Global Mapper in a layer called “OnlineObservations”, which was at the end of the cruise exported as shapefile and

implemented into the final GIS project. First analyses of exact flare locations were, however, done with the more precise EM710 records as described in the respective chapter.

Nevertheless, the screenshots of the echograms allow for a rough classification of flare intensities. We defined five main flare areas: (1) Storfjorden flare area, (2) Hornsund flare area, (3) Van Mijenfjorden flare area, (4) Isfjorden mouth flare area, (5) Inner Isfjorden flare area. The most intense flare clusters have been observed in the Hornsund flare area, whereas all other flare areas show only weak flares, often only pulsing bubble bursts. Flares in the Isfjorden flare area are also relatively intense and rising high through the water column but occur in a small area and not in large clusters as in the Hornsund flare area.

(1) **Storfjorden flare area:** Huge amount of weak flares, in a wide area, but mainly distributed along a N-S directed ridge in 60 to 120 m water depth. Only few flares are continuous bubble streams rising more than 50 m high.
(2) **Hornsund flare area:** Numerous clusters of very intense flares rising high up in the water column from about 80 to 100 m water depth sometimes even to the surface.
(3) **Van Mijenfjorden flare area:** Few very weak flares just behind the sill forming the boundary of the fjord to the Bellsund in ~100 m water depth.
(4) **Isfjorden mouth flare area:** Few but intense flares east of the deep depression at the entrance of the fjord in around 150 m water depth.
(5) **Inner Isfjorden flare area:** Large area with numerous flares, however, all very weak in intensity and situated in 150 to even 250 m water depth.

(1) Storfjorden flare area

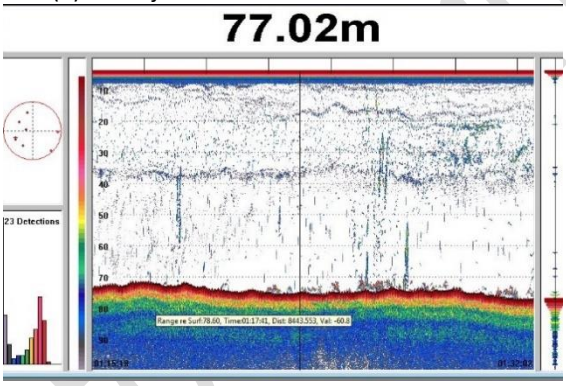

(2) Hornsund flare area

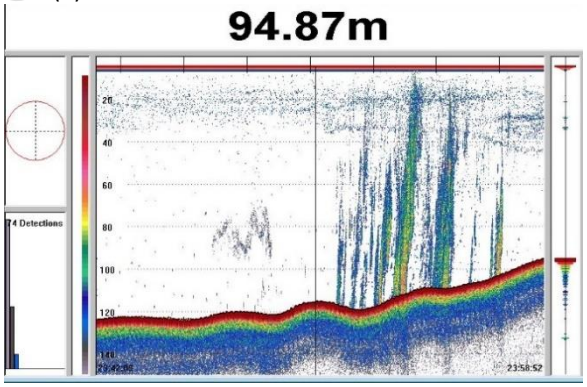

(3) Van Mijenfjorden flare area

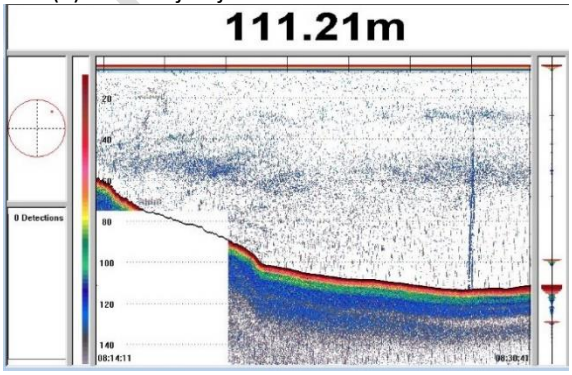

(4) Isfjorden mouth flare area

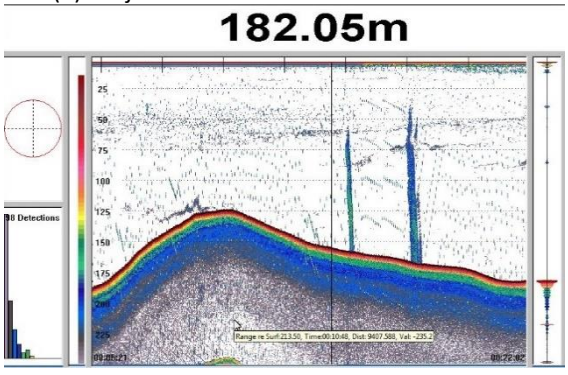

(5) Inner Isfjorden flare area

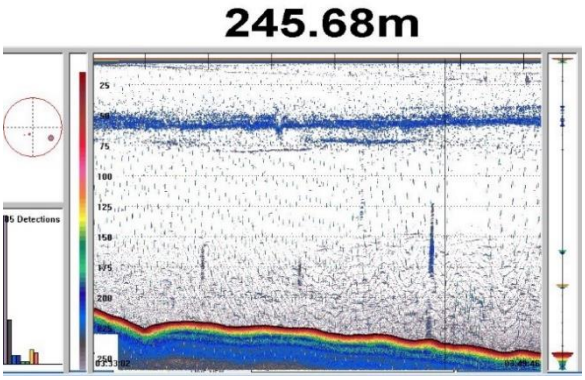

Fig. 53: Examples of the five defined flare areas as recorded with the fishechosounder EK60.

6.3 Subbottom Profiler

(N. Brückner)

Visualizing sub-seafloor structures was done with the sediment echosounder *Innomar* SES-2000 medium, which is permanently installed on R/V HEINCKE. Using the parametric effect, a narrow-beam arrangement is achieved suitable for penetrating the seafloor. For further information refer to *https://spaces.awi.de/confluence/display/HEdevices/Sedimentecholot*.

The SES 2000 sediment echosounder was intended to determine suitable locations for Van Veen grab and Multicorer deployment as well as to visualize acoustic blankening associated with fluid migrations within sediments. Additionally, fault structures acting as a potential pathway for vertical fluid migration were analyzed.

The system was running continuously and only turned off during detailed mapping of gas emission sites to achieve less acoustic interference in the water column. Acquired data was stored in *.ses and *.raw-formatted files and replayed with the program ISE, which is available on board. Here, post-acquisition parameters can be changed to obtain better signal-to-noise ratios and enhance data quality.

Table 6: SES2000 System settings during cruise HE449.

Depth	Detection Sensitivity LF Detection Sensitivity HF	40% 40%
Gain	LF HF	2-20 (depending on depth) 20-60 (depending on depth)
Process	Stacking Smoothing Soft TVG	1 1 0.0
Range	Length	40 m
Threshold	LF-Mode LF Min Level LF SRange HF-Mode HF Min Level HF SRange	LOG 1 1 LOG 8 8
Transmit	LF-Frequency LF-Pulses	8 kHz 1

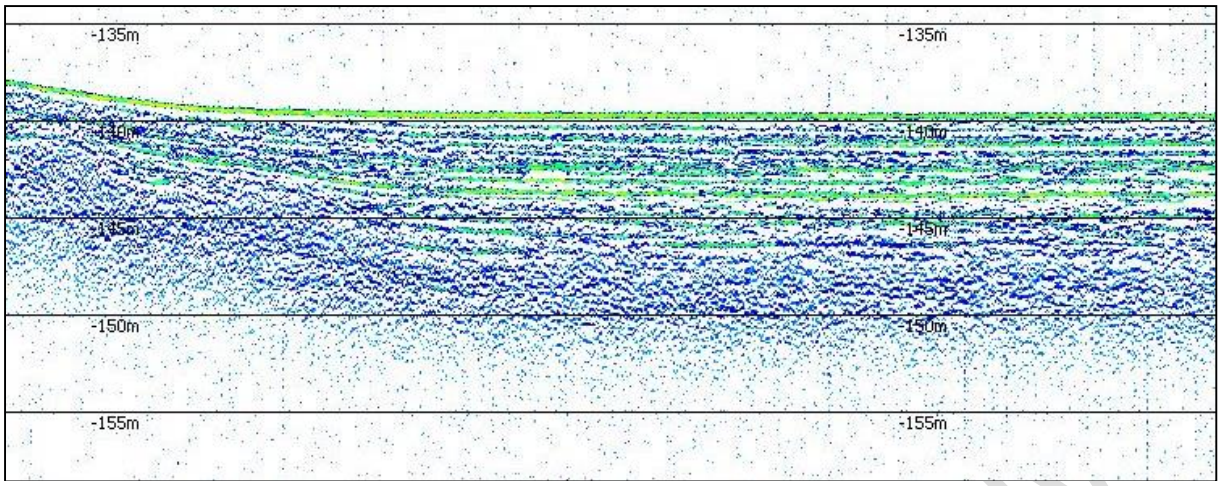

Fig. 54: Screenshot of the SES-replay program ISE2000. Sediment Echo Sounder data is displayed showing the subbottom information for the multicorer location at station 05 (GeoB 20105-2). The image shows well layered sediments for good MUC-recovery rates.

6.4 ADCP

(E. Falck)

The Teledyne RDInstruments Ocean Surveyor vessel mounted Acoustic Doppler Current Profiler (ADCP) was used for current measurements during the cruise. The ADCP uses the Doppler Shift of an acoustic signal to calculate current velocities. The ADCP emits a sound signal with a certain frequency which is reflected from particles like algae or sediments. The backscattered signal is Doppler shifted and the change in frequency is an injective function of the velocity of the particles that are assumed to move with the current. Therefore the current velocity can be calculated from the change in frequency. The velocity is calculated using four different beams which allows to resolve the three dimensional structure of the current. The technical specifications of the ADCP in the long range mode with a frequency of 150 kHz are given in Table 7.

Table 7: Instrument specification for the Ocean Surveyor ADCP.

Depth resolution (bin size)	8 m
Maximum range	400 m
Velocity accuracy	±1% ±0.5 cm s^{-1}
Velocity range	-5 m s^{-1} to 9 m s^{-1}

The data received from the ADCP along the distances indicated in Table 8 were collected with the Vessel-Mount Data Acquisition System (VMDAS) software. The WinADCP software was used to process the data. The east and north components were calculated by subtracting the ships velocity from the measured velocities. A percentage maid good value (PG4) was used to evaluate the quality of the data. The PG4 value is the percentage of data passed various internal error thresholds (Teledyne RD Instruments, 2014). Time averaging of the data was applied for short term averaging (STA) and long term averaging (LTA), every 1 and 5 minutes, respectively. From the WinADCP export options the east (u) and north (v) velocity and PG4, together with the navigation data (east (u), north (v), Latitude/Longitude) was exported as Matlab files (.mat) for all the STA and LTA files. To plot the data different Matlab scripts were used.

Table 8: The ADCP log from the cruise.

Project	*HE449*
Cruise ID	*HE449*
Vessel	*Heincke*
Period	*01.08 – 22.08 2015*

ADCP CRUISE LOG

Date Start	UTC Time Start	Latitude	Longitude	File	Date Stop	UTC Time Stop	Latitude	Longitude	File Number	COMMENT
04.08	14:06	75°7.92N	17°5.04E	1	05.08	14:50	76°38.81N	18°3.24E	001_000005	Config: Setup 04082015_1400
05.08	14:55	76°38.81N	18°3.24E	2	06.08	07.49	76°52.88N	14°36.87	002_000004	Without bottom track from CTD4 to CTD5
06.08	07:58	76°53.29N	14°31.85E	3	07.08	17:48	77°3.22N	13°21.82E	004_000002	With bottom track from CTD5
09.08	08:13	76°39.97N	18°28.21E	5	11.08	05:54	76°49.02N	14°14.74E	005_0000010	With bottom track
11.08	07:46	76°47.63N	14°07.07E	6					006_000001	
12.08	11:01	76°48.42N	14°06.79E	7	17.08	06:11	78°16.9N	13°37.74E	007_0000027	
17.08	06:12	78°16.9N	13°37.74E	8	17.08	10:28	78°6.57N	13°44.16E	008_000001	Isfjorden mouth
17.08	10:30	78°6.56N	13°44.15E	9	18.08	11:46	78°35.68E	16°30.44E	009_000006	Isfjorden mouth - Billefjorden

As an example File 8 (Table 8), which is the data collected across the mouth of Isfjorden on the 17. August, is shown in Figure 55 and Figure 56. Figure 55 shows a stick plot of the currents at three different depth levels, 20, 124, and 204 m, where the speed is proportional to the length of the arrow, and the arrow indicates the direction of the current. At the southern side of the fjord the current direction is mainly into Isfjorden while at the northern side is northwesterly, indicating an outflow from the fjord.

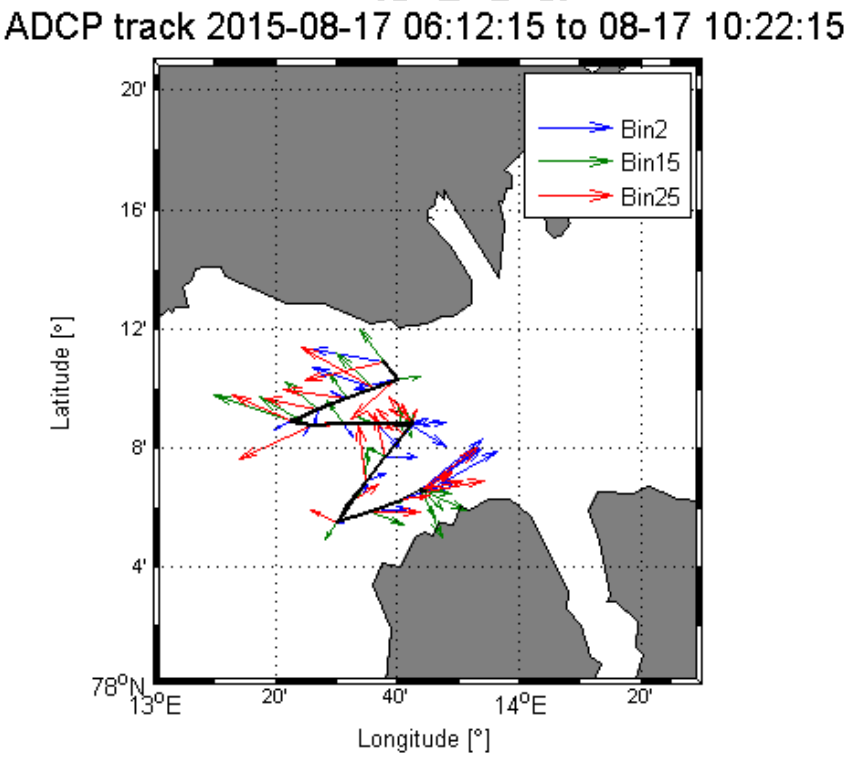

Fig. 55: Stick plot of the currents in the mouth of Isfjorden at three different depth levels using the LTA (long term average) file. Bin 2 (blue) is at 20 m, Bin 15 (green) is at 124 m, and Bin 25 is at 204 m. The black line shows the ship track.

Figure 56 shows the east and north component of the currents in the mouth of Isfjorden from 20 to 200 m. The east component (Fig. 56 left) which shows the current perpendicular to the transect across the mouth of Isfjorden also shows an inflow in the southern part (positive values) and an outflow in the northern part (negative values). The velocities are mostly between 0 and 10 m s^{-1}, but also higher velocities up to 25 m s^{-1} are seen. There was also a strong northerly component (positive in Fig. 56 right) at the time of measurements as can also be visualized in the stick plots (Fig. 55).

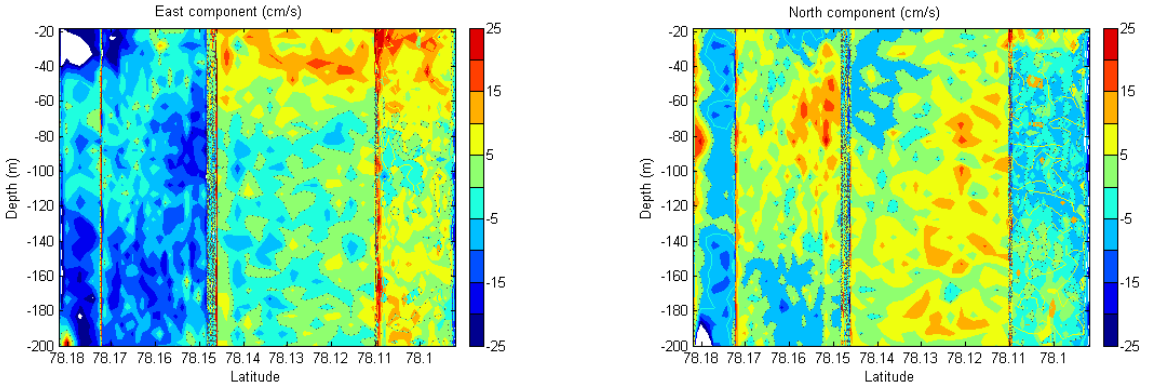

Fig. 56: The east and north components of the current across the mouth of Isfjorden. The STA (short term average) file was used, and only measurements with a PG value above 98% were used, measurements with a PG < 98% are shown as white areas.

7 Data and Sample Storage and Availability

A one-page cruise summary report was submitted at the end of the cruise to AWI. The Norwegian authorities will receive this extended report latest in February 2016 and published data and scientific publications will be made available to the Research in Svalbard database (RiS ID 10158).

The station list, CTD-data, and the raw hydroacoustic data were copied on hard disks at the end of the cruise and will be handed over to PANGAEA. It is planned to make available all the results of the cruise as scientific publications. Upon publication, all the data (raw and processed) is planned to be submitted to PANGAEA. All data and samples will be available in three years upon request.

This cruise report will be published as part of the “Berichte aus dem MARUM und dem Fachbereich Geowissenschaften der Universität Bremen” (available online at: https://www.marum.de/en/Berichte_aus_dem_MARUM_und_dem_Fachbereich_Geowissenschaften_der_Universitaet_Bremen.html).

In order to protect the valuable results obtained during the cruise, this report will be freely accessible in three years.

8 References

Caress, D. W. and Chayes, D. N. (1996) Improved processing of Hydrosweep DS multibeam data on the R/V Maurice Ewing, Mar. Geophys. Res., 18, 631-650.

Clark, J. F., Leifer, I., Washburn, L., and Luyendyk, B. P. (2003) Compositional changes in natural gas bubble plumes: observations from the Coal Oil Point marine hydrocarbon seep field, Geo-Mar. Lett., 23, 187-193.

Damm, E., Mackensen, A., Budeus, G., Faber, E., and Hanfland, C. (2005) Pathways of methane in seawater: Plume spreading in an Arctic shelf environment (SW-Spitsbergen), Cont. Shelf Res., 25, 1453-1472.

Dumestre, J. F., Guezennec, J., Galy-Lacaux, C., Delmas, R., Richard, S., and Labroue, L. (1999) Influence of light intensity on methanotrophic bacterial activity in Petit Saut Reservoir, French Guiana, Appl Environ Microb, 65, 534-539.

Elsaied, H. E., Hayashi, T., and Naganuma, T. (2004) Molecular analysis of deep-sea hydrothermal vent aerobic methanotrophs by targeting genes of 16S rRNA and particulatemethane monooxygenase, Mar. Biotechnol., 6, 503–509.

Elvevold, S., Dallmann, W., and Blomeier, D. (2007) Geology of Svalbard, Grafisk Nord AS.

Gentz, T. and Schlüter, M. (2012) Underwater cryotrap-membrane inlet system (CT-MIS) for improved in situ analysis of gases, Limnol. Oceanogr.: Methods, 10, 317-328.

Greinert, J. and McGinnis, D. F. (2009) Single bubble dissolution model - The graphical user interface SiBu-GUI, Environ. Model. Softw., 24, 1012-1013.

Heintz, M., Mau, S., and Valentine, D. L. (2012) Physical control on methanotrophic potential in waters of the Santa Monica Basin, Southern California, Limnol. Oceanogr., 57, 420-432.

Holmes, A. J., Roslev, P., McDonald, I. R., Iversen, N. and Henriksen, B. J. (1999) A simple and precise method for measuring ammonium in marine and freshwater ecosystems, Can. J. Fish. Aquat. Sci. 56, 1801-180.

IPCC: Climate Change 2007 – The Physical Science Basis – Contribution of Working Group I to the Fourth Assessment Report of the Intergovernmental Panel on Climate Change (2007) Cambridge University Press, Cambridge, 996 pp.

Lammers, S. and Suess, E. (1994) An improved head-space analysis method for methane in seawater, Mar. Chem., 47, 115-125.

Largier, J. L. (2003) Considerations in estimating larval dispersal distances from oceanographic data, Ecol. Appl., 13, S71-S89.

Lidstrom, M. E. (1988) Isolation and characterization of marine methanotrophs, Antonie Van Leeuwenhoek J. Microbiol., 54, 189–199.

Mau, S., Heintz, M. B., and Valentine, D. L. (2011) Quantification of CH4 loss and transport in dissolved plumes of the Santa Barbara Channel, California, Cont. Shelf Res., 32, 110-120.

Mau, S., Valentine, D. L., Clark, J. F., Reed, J., Camilli, R., and Washburn, L. (2007) Dissolved methane distributions and air-sea flux in the plume of a massive seep field, Coal Oil Point, California, Geophys. Res. Lett., 34, L22603.

Moussard, H., Stralis-Pavese, N., Bodrossy, L., Neufeld, J. D., Murrell, J. C. (2009) Identification of active methylotrophic bacteria inhabiting surface sediment of a marine estuary, Environ. Microbiol. Rep. 1, 425–433.

Reeburgh, W. S. (2007) Oceanic Methane Biogeochemistry, Chem. Rev., 107, 486-513.

Rehder, G. (1999) Quellen und Senken marinen Methans zwischen Schelf und offenem Ozean, GEOMAR, Kiel, 161 pp.

Roy, S., Hovland, M., Noormets, R., and Olaussen, S. (2015) Seepage in Isfjorden and its tributary fjords, West Spitsbergen, Marine Geology, 363, 146–159.

Rudd, J. W. M. and Hamilton, R. D. (1975) Factors controlling rates of methane oxidation and the distribution of the methane oxidizers in a small stratified lake, Arch Hydrobiol, 75, 522-538.

Sahling, H., Römer, M., Pape, T., Bergès, B., dos Santos Fereirra, C., Boelmann, J., Geprägs, P., Tomczyk, M., Nowald, N., Dimmler, W., Schroedter, L., Glockzin, M., and Bohrmann, G. (2014)

Gas emissions at the continental margin west of Svalbard: mapping, sampling, and quantification, Biogeosciences, 11, 6029–6046.

Saloranta, T. M., and Svendsen, H. (2001) Across the Arctic front west of Spitsbergen: high-resolution CTD sections from 1998-2000, Polar Research, 20, 177-184.

Schmitt, M., Faber, E., Botz, R., Stoffers, P. (1991) Extraction of methane from seawater using ultrasonic vacuum degassing. Analytical Chemistry 63, 529-532.

Sieburth, J. M., Johnson, P. W., Eberhardt, M. A., Sieracki, M. E., Lidstrom, M., and Laux, D. (1987) The first methaneoxidizing bacterium from the upper mixing layer of the deep ocean—Methylomonas Pelagica sp. nov., Curr. Microbiol., 14, 285–293.

Strickland, J. D. H. and Parsons, T. R. (1972) A practical handbook of seawater analysis. Second Edition, Bulletin 167. Fisheries Research Board of Canada, Ottawa.

Tavormina, P. L., Ussler III, W., and Orphan, V. J. (2008) Planktonic and sediment-associated aerobic methanotrophs in two seep systems along the North American Margin, Appl. Environ. Microbiol., 74, 3985-3995.

Valentine, D. L. (2011) Emerging topics in marine methane biogeochemistry, Annu. Rev. Mar. Sci., 3, 147-171.

Wankel, S. D., Huang, Y., Gupta, M., Provencal, R., Leen, J. B., Fahrland, A., Vidoudez, C., and Girguis, P. R. (2013) Characterizing the distribution of methane sources and cycling in the deep sea via in situ stable isotope analysis, Environ Sci Technol, 47, 1478−1486.

Ward, B. B., Kilpatrick, K. A., Wopat, A. E., Minnich, E. C., and Lidstrom, M. E. (1989) Methane oxidation in Saanich inlet during summer stratification, Cont. Shelf Res., 9, 65-75.

Wasmund, K., Kurtboke, D. I., Burns, K. A., and Bourne, D. G. (2009) Microbial diversity in sediments associated with a shallow methane seep in the tropical Timor Sea of Australia reveals a novel aerobic methanotroph diversity, FEMS Microbiol. Ecol., 68, 142–151.

Wiesenburg, D. A. and Guinasso, J. N. L. (1979) Equilibrium solubilities of methane, carbon monoxide, and hydrogen in water and sea water, J. Chem. Eng. Data, 24, 356-360.

Wong, G. S .K. and Zhu, S. (1995) Speed of sound in seawater as a function of salinity, temperature and pressure. J. Acoust. Soc. Am. 97(3) pp 1732-1736.

9 Appendix: Station List

Heincke HE449

Station list

				Time (UTC)			Begin / on seafloor		End / off seafloor				
Date	Station	GeoB	Instrument	Location								Water	Recovery
2015	No.	St. No.	No.		Begin	on seafloor	off seafloor	End	Latitude N	Longitude E	Water depth (m)	Latitude N	Longitude E	(m)	Remarks
04.08.	1-1	20101-1	CTD-1	South of Svalbard	16:22	16:27	16:27	16:43	75° 30.35	017° 25.95	166	75° 30.50	017° 26.96	168	Mini-CTD (background)
04.08.	1-2	20101-2	SVP-1	South of Svalbard	16:45			16:55	75° 30.57	017° 27.12	167	75° 30.67	017° 27.24	168	Sound profile to 150 m water depth (for calibration)
05.08.	2	20102-1	CTD-2	Storfjorden - East	08:17	08:25	08:25	08:31	76° 47.44	020° 41.11	64	76° 47.34	020° 41.32	61	Mini-CTD
05.08.	3	20103-1	CTD-3	Storfjorden - Mid	10:02	10:08	10:08	10:19	76° 43.20	019° 48.79	177	76° 43.20	019° 50.02	174	Mini-CTD
05.08.	4	20104-1	CTD-4	Storfjorden - West	14:39	14:45	14:45	15:00	76° 38.88	018° 03.90	255	76° 38.79	018° 03.21	241	Mini-CTD
06.08.	5-1	20105-1	CTD-5	Hornsund Shelf	06:15	06:21	06:21	06:35	76° 52.82	014° 37.38	138	76° 52.93	014° 37.24	138	Mini-CTD
06.08.	5-2	20105-2	MUC-1_1	Hornsund Shelf		06:54	06:54		76° 52.82	014° 37.12	138				Not properly closed, 6 core tubes, but empty
06.08.	5-3	20105-3	MUC-1_2	Hornsund Shelf		07:30	07:30		76° 52.83	014° 37.29	138				4 cores recovered
06.08.	6	20106-1	CTD-6	Hornsund Shelf	10:00	10:06	10:06	10:18	76° 53.26	014° 09.47	75	76° 53.39	014° 09.88	79	
06.08.	7	20107-1	CTD-7	Hornsund Shelf	12:30	12:33	12:33	12:48	76° 52.22	013° 30.59	112	76° 52.28	013° 31.31	109	
06.08.	8-1	20108-1	CTD-8	Hornsund Shelf	14:25	14:28	14:28	14:40	76° 52.88	014° 37.25	139	76° 53.01	014° 37.45	134	Location of Station 8 is same as Station 5
06.08.	8-2	20108-2	ISP-1	Hornsund Shelf	14:54	15:13	15:13	21:53	76° 53.10	014° 37.45	126	76° 53.01	014° 37.62	130	
07.08.	9	20109-1	CTD-9	Hornsund Shelf break	06:06	06:16	06:16	06:35	76° 51.02	013° 00.04	323	76° 51.03	012° 58.79	362	
07.08.	10-1	20110-1	CTD-10_1	N-Hornsund Basin	11:00	11:12	11:12	11:33	77° 03.16	013° 22.40	438	77° 03.13	013° 22.73	441	Maxi-CTD in deepest part of the basin, First cast
07.08.	10-2	20110-2	CTD-10_2	N-Hornsund Basin	12:13	12:29	12:29	12:40	77° 03.10	013° 22.71	444	77° 03.02	013° 22.80	444	Maxi-CTD in deepest part of the basin, Second cast
07.08.	10-3	20110-3	CTD-10_3	N-Hornsund Basin	13:04	13:06	13:06	13:10	77° 03.08	013° 22.50	446	77° 03.08	013° 22.62	445	Maxi-CTD in deepest part of the basin, Third cast
07.08.	10-4	20110-4	CTD-10_4	N-Hornsund Basin	13:30	13:34	13:34	13:34	77° 03.12	013° 22.95	442	77° 03.11	013° 22.99	442	Maxi-CTD in deepest part of the basin, Fourth cast
07.08.	10-5	20110-5	ISP-2	N-Hornsund Basin	14:01			14:08	77° 03.01	013° 22.73	445	77° 03.01	013° 22.55	443	Same station, 6 hour deployment
08.08.	10-6	20110-6	MUC-2_1	N-Hornsund Basin	06:23				77° 03.20	013° 22.08	442				3 cores recovered, 2 core liners lost
08.08.	10-7	20110-7	MUC-2_2	N-Hornsund Basin	07:10				77° 03.10	013° 22.55	444				One core recovered
09.08.	11-1	20111-1	BG-1	Storfjorden - West	06:06				76° 38.88	018° 03.71	242				same station as GeoB20104, about 20 cm sediment, at bottom lots of worms/worm tubes
09.08.	11-2	20111-2	MUC-3_1	Storfjorden - West	06:33				76° 38.90	018° 03.76	242				3 core liners full
09.08.	11-3	20111-3	MUC-3_2	Storfjorden - West	07:12				76° 38.89	018° 03.73	242				3 core liners full
09.08.	12-1	20112-1	CTD-12	Storfjorden - Ridge	09:12	09:16	09:16	09:34	76° 40.81	018° 49.48	63	76° 40.75	018° 49.60	64	
09.08.	12-2	20112-2	UWMS-1	Storfjorden - Ridge	09:55			16:27	76° 40.71	018° 49.58	63	76° 40.78	018° 49.63	63	
09.08.	12-3	20112-3	ISP-3	Storfjorden - Ridge	16:36			21:24	76° 40.77	018° 49.62	64				
10.08.	12-4	20112-4	BG-2_1	Storfjorden - Ridge	06:08				76° 40.75	018° 49.67	65				not triggered
10.08.	12-5	20112-5	BG-2_1	Storfjorden - Ridge	06:13				76° 40.75	018° 49.66	64				gravel layer 5-10 cm, soft sediment below
10.08.	12-6	20112-6	MUC-4_1	Storfjorden - Ridge	06:30				76° 40.75	018° 49.65	65				4 core liners filled, but very short and only gravel, not used, no water above
10.08.	12-7	20112-7	MUC-4_2	Storfjorden - Ridge	06:42				76° 40.88	018° 49.95	61				2 core liners filled, but very short and only gravel, not used, no water above
10.08.	13-1	20113-1	CTD-13	Storfjorden - West	08:56	09:02	09:02:00	09:19	76° 38.88	018° 03.60	241	76° 38.89	018° 03.66	241	
10.08.	13-2	20113-2	ISP-4	Storfjorden - West	09:49			16:11	76° 38.92	018° 03.66	241	76° 38.88	018° 03.79	246	
11.08.	14-1	20114-1	UWMS-2	Hornsund Flare area	06:07			07:59	76° 48.95	014° 14.36	75	76° 48.06	014° 09.45	108	First transect over seep area. Towed in 80-90 m water depth
11.08.	15-1	20115-1	CTD-15	Hornsund Flare area	08:12	08:49	08:49	08:52	76° 48.06	014° 09.73	107	76° 48.12	014° 09.49	106	
11.08.	15-2	20115-2	BG-3_1	Hornsund Flare area	09:08				76° 48.11	014° 09.57	105				not triggered
11.08.	15-3	20115-3	BG-3_2	Hornsund Flare area	09:16				76° 48.33	014° 08.88	93				gravel, some sediment
11.08.	16-1	20116-1	BG-4	Hornsund Flare area	10:51				76° 47.55	014° 09.74	127				Within low backscatter patch, sampled soft sediments, sulfidic, black (reduced)
11.08.	16-2	20116-2	MUC-5	Hornsund Flare area	10:51				76° 47.54	014° 09.73	127				Within low backscatter patch, successfully taken 4 cores
11.08.	17-1	20117-1	CTD-17	Hornsund Shelf	13:05	13:08	13:08	13:21	76° 52.18	013° 56.23	87	76° 52.19	013° 56.29	87	
11.08.	18-1	20118-1	CTD-18	Hornsund Shelf	16:01	16:06	16:06	16:14	76° 59.30	013° 33.81	100	76° 59.32	013° 33.05	99	
12.08.	19-1	20119-1	UWMS-3	Hornsund Flare area	06:09			08:06	76° 48.96	014° 14.62	70	76° 47.30	014° 05.12	94	Second transect over seep area. 25 m below sealevel
12.08.	20-1	20120-1	UWMS-4	Hornsund Flare area	09:04			10:48	76° 49.19	014° 14.68	80	76° 47.66	014° 07.04	117	Third transect over seep area. Just above the seafloor
12.08.	21-1	20121-1	CTD-21	Bellsund shelf	17:19	17:27	17:27	17:48	77° 34.79	011° 03.43	338	77° 34.79	011° 03.35	340	
13.08.	22-1	20122-1	CTD-22	Bellsund shelf	05:59	06:02	06:02	06:12	77° 44.51	013° 09.85	57	77° 44.50	013° 09.81	57	
13.08.	23-1	20123-1	CTD-23	Bellsund shelf	07:57	08:03	08:03	08:15	77° 41.09	012° 25.97	106	77° 41.05	012° 25.53	107	
13.08.	24-1	20124-1	CTD-24	Bellsund shelf	10:09	10:14	10:14	10:26	77° 37.59	011° 40.79	174	77° 37.67	011° 40.81	172	
13.08.	25-1	20125-1	CTD-25	Bellsund	14:30	14:39	14:39	14:48	77° 38.63	014° 14.22	159	77° 38.64	014° 14.36	160	
13.08.	25-2	20125-2	ISP-5	Bellsund	15:00			21:57	77° 38.67	014° 14.26	159	77° 38.66	014° 13.95	160	
14.08.	25-3	20125-3	MUC-6_1	Bellsund	06:11				77° 38.66	014° 13.98	159				
14.08.	25-4	20125-4	MUC-6_2	Bellsund	06:39				77° 38.63	014° 14.12	159				
14.08.	26	20126-1	CTD-26	Van Mijenfjorden	10:01	10:05	10:05	10:24	77° 45.09	015° 01.54	110	77° 45.03	015° 00.90	108	
14.08.	27	20127-1	CTD-27	Van Mijenfjorden	11:42	11:48	11:48	11:55	77° 47.99	015° 50.25	83	77° 47.91	015° 50.24	84	
14.08.	28	20128-1	CTD-28	Van Mijenfjorden	13:57	14:02	14:02	14:12	77° 49.74	016° 38.53	73	77° 49.74	016° 38.45	73	

Appendix: Station List continued

Heincke HE449				Station list											
				Time (UTC)				Begin / on seafloor			End / off seafloor				
Date	Station	GeoB	Instrument	Location		on	off		Latitude	Longitude	Water	Latitude	Longitude	Water	Recovery
2015	No.	St. No.	No.		Begin	seafloor	seafloor	End	N	E	depth (m)	N	E	(m)	Remarks
14.08.	29-1	20129-1	CTD-29_1	Van Mijenfjorden	16:26	16:33	16:33	16:40	77° 45.07	015° 01.36	109	77° 45.05	015° 01.31	108	
14.08.	29-2	20129-2	ISP-6	Van Mijenfjorden	16:53			23:29	77° 45.09	015° 01.46	110	77° 45.00	015° 00.78	109	
15.08.	29-3	20129-3	CTD-29_2	Van Mijenfjorden	06:04	06:13	06:13	06:16	77° 45.08	015° 01.38	109	77° 45.09	015° 01.35	109	
15.08.	29-4	20129-4	CTD-29_3	Van Mijenfjorden	06:33	06:36	06:36	06:37	77° 45.07	015° 01.16	108	77° 45.04	015° 01.19	107	
15.08.	29-5	20129-5	CTD-29_4	Van Mijenfjorden	07:05	07:05	07:05	07:09	77° 45.09	015° 01.09	108	77° 45.13	015° 01.09	109	
15.08.	29-6	20129-6	MUC-7_1	Van Mijenfjorden	07:24				77° 45.08	015° 01.58	108				
15.08.	29-7	20129-7	MUC-7_2	Van Mijenfjorden	07:56				77° 45.08	015° 01.38	108				
15.08.	29-8	20129-8	MUC-7_3	Van Mijenfjorden	08:28				77° 45.10	015° 01.52	109				
15.08.	30-1	20130-1	CTD-30	Van Mijenfjorden	10:00	10:16	10:16	10:18	77° 45.16	014° 48.67	109	77° 45.14	014° 48.36	110	
15.08.	30-2	20130-2	BG-5	Van Mijenfjorden	10:27				77° 45.17	014° 48.36	110				
15.08.	30-3	20130-3	MUC-8	Van Mijenfjorden	10:49				77° 45.15	014° 48.50	110				
15.08.	31-1	20131-1	CTD-31	Isfjorden shelf	15:18	15:20	15:20	15:37	77° 57.91	012° 30.30	162	77° 57.90	012° 30.20	161	
16.08.	32-1	20132-1	CTD-32	Isfjorden shelf	06:02	06:07	06:07	06:20	77° 53.46	010° 33.22	152	77° 53.55	010° 34.04	150	
16.08.	33-1	20133-1	CTD-33	Isfjorden shelf	08:07	08:12	08:12	08:24	77° 55.96	011° 32.00	155	77° 55.95	011° 32.84	159	
16.08.	34-1	20134-1	CTD-34	Isfjorden shelf	10:47	10:51	10:51	11:02	78° 00.91	013° 12.07	131	78° 00.98	013° 12.98	152	
17.08.	35-1	20135-1	CTD-35	Isfjorden Entrance	05:59	06:05	06:05	06:18	78° 10.83	013° 37.97	232	78° 10.91	013° 37.68	208	
17.08.	36-1	20136-1	CTD-36	Isfjorden Entrance	08:01	08:16	08:16	08:33	78° 08.85	013° 42.25	418	78° 08.90	013° 42.46	420	
17.08.	37-1	20137-1	CTD-37	Isfjorden Entrance	10:18	10:26	10:26	10:36	78° 06.61	013° 44.21	241	78° 06.55	013° 44.04	247	
17.08.	38-1	20138-1	CTD-38	Billefjorden Entrance	13:53	14:00	14:00	14:11	78° 25.01	015° 58.41	186	78° 25.00	015° 58.61	187	
17.08.	38-2	20138-2	ISP-7	Billefjorden Entrance	14:16				78° 25.00	015° 58.57	187	78° 25.11	015° 57.90	183	~6 hour deployment
18.08.	38-3	20138-3	MUC-9	Billefjorden Entrance	06:05				78° 24.98	015° 58.40	187				
18.08.	39-1	20139-1	CTD-39	Billefjorden	08:34	08:39	08:39	08:50	78° 35.71	016° 31.01	158	78° 35.64	016° 30.90	155	
18.08.	39-2	20139-2	ISP-8	Billefjorden	09:00			13:36	78° 35.94	016° 31.85	155	78° 35.69	016° 30.30	163	
18.08.	39-3	20139-3	MUC-10	Billefjorden	13:44				78° 35.69	016° 30.40	163				

CTD CTD-Rosette
MUC Multicorer
UWMS Underwater mass spectrometer
ISP In situ pumps
BG Grab sampler
SVP Sound velocity probe